JAERI-M
86-136

ANALYSIS OF THE SPERTIII E-CORE EXPERIMENT USING THE EUREKA-2 CODE

September 1986

Taikan HARAMI, Mutsumi UEMURA* and
Nobuaki OHNISHI

日本原子力研究所
Japan Atomic Energy Research Institute

JAERI-Mレポートは，日本原子力研究所が不定期に公刊している研究報告書です。
入手の問合わせは，日本原子力研究所技術情報部情報資料課（〒319-11茨城県那珂郡東海村）あて，お申しこしください。なお，このほかに財団法人原子力弘済会資料センター（〒319-11 茨城県那珂郡東海村日本原子力研究所内）で複写による実費頒布をおこなっております。

JAERI-M reports are issued irregularly.
Inquiries about availability of the reports should be addressed to Information Division Department of Technical Information, Japan Atomic Energy Research Institute, Tokai-mura, Naka-gun, Ibaraki-ken 319-11, Japan.

編集兼発行　日本原子力研究所
印　　刷　いばらき印刷㈱

JAERI-M 86-136

Analysis of the SPERT III E-Core Experiment using the EUREKA-2 Code

Taikan HARAMI†, Mutsumi UEMURA* and Nobuaki OHNISHI

Department of Research Reactor Operation

Tokai Research Establishment
Japan Atomic Energy Research Institute
Tokai-mura, Naka-gun, Ibaraki-ken

(Received August 22, 1986)

EUREKA-2, a coupled nuclear thermal hydrodynamic kinetic code, was adapted for the testing of models and methods. Code evaluations were made with the reactivity addition experiments of the SPERT III E-Core, a slightly enriched oxide core. The code was tested for non damaging power excursions including a wide range of initial operating conditions, such as cold-startup, hot-startup, hot-standby and operating-power initial conditions. Comparisons resulted in a good agreement within the experimental errors between calculated and experimental power, energy, reactivity and clad surface temperature.

Keywords: EUREKA-2 Code, Reactivity Addition Experiment, SPERT III E-Core, Clad Surface Temperature, Reactor Kinetics

---

† Department of Reactor Safety Research

* On leave from Computer Services Corp.

JAERI－M 86－136

EUREKA－2コードによるSPERT Ⅲ・E一炉心実験の解析

日本原子力研究所東海研究所研究炉管理部
原見　太幹[+]・植村　　睦[*]・大西　信秋

（1986年8月22日受理）

核熱水力結合動特性解析コードEUREKA－2の解析の妥当性を評価するため，低濃縮酸化ウランを使用したSPERT Ⅲ－E炉心における反応度添加実験の解析を行った。SPERT Ⅲ・E炉心で行われた低温大気圧実験，高温実験及びホットスタンバイ出力実験の広範囲に及ぶ初期運転状態における暴走出力実験を解析した。解析の結果，EUREKA－2による計算結果と実験値は最大暴走出力，暴走エネルギー，フィードバック反応度及び被覆管表面温度のデータについて実験誤差範囲内でよい一致を示した。

東海研究所：〒319－11 茨城県那珂郡東海村白方字白根2－4
＋ 原子炉安全工学部リスク評価解析研究室
＊ コンピューターサービス（株）

Contents

目　　次

1. Introduction

Reactor safety is generally assessed on the basis of calculation models that predict the courses and consequences of postulated reactor accidents. The accuracy of these predictions can be determined only by comparison with experimental data.

The EUREKA-2 code[1] was adapted for the testing of models and methods. Comparisons were made with the experimental results from the SPERT III E-Core reactivity accident tests[2].

The EUREKA-2 code is an extension of the EUREKA code[3], originally developed for the analysis of neutronic, thermal and hydrodynamic transient behaviors in a water cooled reactor. The EUREKA-2 code can provide a coupled thermal hydraulic and point kinetics capability with reactivity feedback and a voiding model that estimates the voiding produced by subcooled boiling.

The SPERT III E-Core experiments cover a wide range of initial conditions, typical for PWR, such as cold-startup, hot-startup, hot-standby and operating-power initial conditions. These initial system conditions are defined as tabulated below. The excursions result from

Accident Conditions	Coolant Inlet Temperature (°F)	System Pressure (psig)	Average Coolant Flow Rate (fps)	Initial Reactor Power (MW)
Cold Startup	70	Atm	0	5×10^{-5}
Hot Startup	260	1500	2.4 to 22	5×10^{-5}
	500	1500	4.8 to 24	5×10^{-5}
Hot Standby	500	1500	14	1
Operating Power	500	1500	14	20

rapid reactivity insertions ranging from 0.5 to 1.3 $.

The kinetic behavior of the E-core has been discussed by evaluating the codes, PARET[4] and IREKIN[5]. In the IREKIN code, only Doppler reactivity feedback is taken into account. IREKIN prediction were up to 30% larger than the experimental results for the cold-startup reactivity tests, but were 40 to 60% larger than experimental values for all the hot-startup reactivity accident tests. The PARET code calculates the

coupled thermal, hydrodynamic and nuclear response of the reactor, and all the known major reactivity feedback mechanisms are accounted for. PARET predictions were within 30% of the experimental results for all accident conditions tested. The EUREKA-2 code has similar capabilities of calculation to the PARET code.

The EUREKA-code has analyzed a few tests of the SPERT III-E Core (one cold-statup, three hot start-up, one hot-standby and one operating-power tests)[3]. The EUREKA-2 code was evaluated using the experimental data of the 66 power excursions including the cold-startup, hot-startup, hot-standby and operating-power tests.

The description of the EUREKA-2 code will be given in Sec. 2. The brief description of the SPERT III-E Core will be presented in Sec. 3. The comparisons of calculation with the experiment will be described in Sec. 4.

2. EUREKA-2 Description

The EUREKA-2 code provides a coupled thermal, hydrodynamic and point kinetics capability[1], and evaluates a reactivity addition transient. The core can be represented by several regions in the code. Each region may have different power generation, coolant mass flow rate and hydraulic parameters. The reactor power can be calculated from the reactor point kinetics equations with reactivity feedback (Sec. 2.1). Feedback reactivity include Doppler, void, moderator temperature and fuel rod expansion effects (Sec. 2.2). The EUREKA-2 code cover both geometries of pin- and plate-type fuels. The heat conduction model is based on the method of the one-dimensional time dependent heat conduction equations (Sec. 2.3) In order to transfer heat from a conductor into a cooling fluid, heat transfer correlations are utilized and shown in Sec. 2.5. The hydrodynamic solution in the code is based on the mass, momentum and energy conservation equation assumed to contain one-dimensional homogeneous fluid with the vapor and liquid phases in thermodynamic equilibrium (Sec. 2.6). In addition, the EUREKA-2 code has prompt moderator heating effect (Sec. 2.7) and subcooled void model (Sec. 2.8).

coupled thermal, hydrodynamic and nuclear response of the reactor, and all the known major reactivity feedback mechanisms are accounted for. PARET predictions were within 30% of the experimental results for all accident conditions tested. The EUREKA-2 code has similar capabilities of calculation to the PARET code.

The EUREKA-code has analyzed a few tests of the SPERT III-E Core (one cold-statup, three hot start-up, one hot-standby and one operating-power tests)[3]. The EUREKA-2 code was evaluated using the experimental data of the 66 power excursions including the cold-startup, hot-startup, hot-standby and operating-power tests.

The description of the EUREKA-2 code will be given in Sec. 2. The brief description of the SPERT III-E Core will be presented in Sec. 3. The comparisons of calculation with the experiment will be described in Sec. 4.

2. EUREKA-2 Description

The EUREKA-2 code provides a coupled thermal, hydrodynamic and point kinetics capability[1], and evaluates a reactivity addition transient. The core can be represented by several regions in the code. Each region may have different power generation, coolant mass flow rate and hydraulic parameters. The reactor power can be calculated from the reactor point kinetics equations with reactivity feedback (Sec. 2.1). Feedback reactivity include Doppler, void, moderator temperature and fuel rod expansion effects (Sec. 2.2). The EUREKA-2 code cover both geometries of pin- and plate-type fuels. The heat conduction model is based on the method of the one-dimensional time dependent heat conduction equations (Sec. 2.3) In order to transfer heat from a conductor into a cooling fluid, heat transfer correlations are utilized and shown in Sec. 2.5. The hydrodynamic solution in the code is based on the mass, momentum and energy conservation equation assumed to contain one-dimensional homogeneous fluid with the vapor and liquid phases in thermodynamic equilibrium (Sec. 2.6). In addition, the EUREKA-2 code has prompt moderator heating effect (Sec. 2.7) and subcooled void model (Sec. 2.8).

2.1 Reactor Kinetics Model

The normalized reactor power can be calculated from the reactor point kinetics equations, which include delayed neutron data of 6 groups.

$$\frac{dn}{dt} = \frac{\beta}{\ell}(R - 1)\, n + \sum_{i=1}^{6} \lambda_i C_i + s \tag{2-1}$$

$$\frac{dC_i}{dt} + \lambda_i C_i = \frac{\beta_i}{\ell} n \tag{2-2}$$

$$\beta = \sum_{i=1}^{6} \beta_i \tag{2-3}$$

where

n = normalized reactor power

β = effective delayed neutron fraction

ℓ = prompt neutron lifetime (sec^{-1})

R = total reactivity normalized to the delayed neutron fraction ($)

λ_i = decay constant of delayed neutron group i (sec^{-1})

C_i = concentration of delayed neutron group i

S = neutron source

β_i = effective fraction for delayed neutron group i

A Runge-Kutta method is used for the solution of the point kinetics equations. Table 2.1 shows delayed neutron constants.

Radioactive decay terms are calculated by the following equations.

$$\frac{d\gamma_i}{dt} + \lambda_i \gamma_j = E_j n \tag{2-4}$$

where

γ_j = concentration of decay heat group j

λ_j = decay constant of decay heat group j (sec^{-1})

E_j = yield fraction of decay heat group j

Table 2.2 shows the constants used in the radioactive decay equations.

The total power in a region is the sum of the direct fission power and the radioactive decay power. The total power, P, is

$$P = nE_f + \sum_{i=1}^{11} \lambda_i \gamma_i \tag{2-5}$$

where E_f = fraction of power produced at steady state conditions by fission.

Table 2.1 Delayed Neutron Constants

group	β_i/β	λ_i (sec^{-1})
1	0.038	0.0127
2	0.213	0.0317
3	0.188	0.115
4	0.407	0.311
5	0.128	1.40
6	0.026	3.87

Table 2.2 Radioactive Decay Constants

group	E_j	λ_i (sec^{-1})
1	0.00299	1.772×10^{0}
2	0.00825	5.774×10^{-1}
3	0.01550	6.743×10^{-2}
4	0.01935	6.214×10^{-3}
5	0.01165	4.739×10^{-4}
6	0.00645	4.810×10^{-5}
7	0.00231	5.344×10^{-6}
8	0.00164	5.726×10^{-7}
9	0.00085	1.036×10^{-8}
10	0.00043	2.959×10^{-9}
11	0.00057	7.585×10^{-10}

2.2 Feedback Model

Contributions to the reactivity include a time-dependent inserted reactivity and individual reactivities due to feedback effects in each core region. Feedback reactivities contain Doppler, void, moderator temperature and fuel rod expansion effects. The feedback reactivity is calculated from

$$R(t) = R_0 + \{R_{exp}(t) - R_{exp}(0)\} + \{\sum_i R^i(t) - \sum_i R^i(0)\} \tag{2-6}$$

$$R^i(t) = W_D^i R_D(\bar{T}_F{}^i(t)) + W_V{}^i R_V(\alpha_V{}^i(t))$$

$$+ W_{WT}{}^i R_{WT}(\bar{T}_W{}^i(t) + W_E{}^i \cdot \lambda_C{}^i (\frac{V_F}{V_M})^i \cdot \bar{T}_C{}^i(t) \tag{2-7}$$

where

R = total reactivity normalized to the delayed neutron fraction ($)

R_0 = initial reactivity ($)

R_{exp} = explicit time dependent reactivity ($)

R^i = feedback reactivity from core region i ($)

$W_D{}^i$ = weighting factor for Doppler feedback of core region i

R_D = Reactivity as a function of average fuel temperature in entire core ($)

$\bar{T}_F{}^i$ = average fuel temperature of core region i (°C)

$W_V{}^i$ = weighting factor for void feedback of core region i

R_V = Reactivity as a function of void fraction in entire core ($)

$\alpha_{WT}{}^i$ = void fraction of core region i

$W_{WT}{}^i$ = weighting factor for coolant temperature feedback of core region i

R_{WT} = Reactivity as a function of coolant temperature in entire core ($)

$\bar{T}_W{}^i$ = average coolant temperature of core region i (°C)

$W_E{}^i$ = weighting factor given by fitting coefficients multiplied $W_V{}^i$ or $W_{WT}{}^i$

$\lambda_C{}^i$ = linear expansion coefficient of cladding material of core region i (1/°C)

$(\frac{V_F}{V_M})^i$ = volume ratio of fuel to moderator in core region i

$\bar{T}_C{}^i$ = average cladding temperature of core region i (°C)

Weighting factors W_D^i, W_V^i, W_{WT}^i and W_E^i are specified by importance distributions in the core. Feedback reactivities R_D, R_V and R_{WT} are fitting coefficients given in EUREKA-2 as input data.

2.3 Heat Transfer

The heat conductor consists of clad, gap and fuel with heat generation. A part of generated heat is utilized to heat moderator directly. The rest of internally generated heat in the fuel is transported in the conductor. A conductor geometry is cylindrical or rectangular. Cylindrical geometry is used in describing the radial cross section of a pin-type fuel, and rectangular in describing a plate-type fuel. We show heat conductor reactions and nodarizations in Fig. 2.1. Typical nodalizations are

1) Cylindrical type conductor

region 1　fuel
region 2　gap
region 3　clad

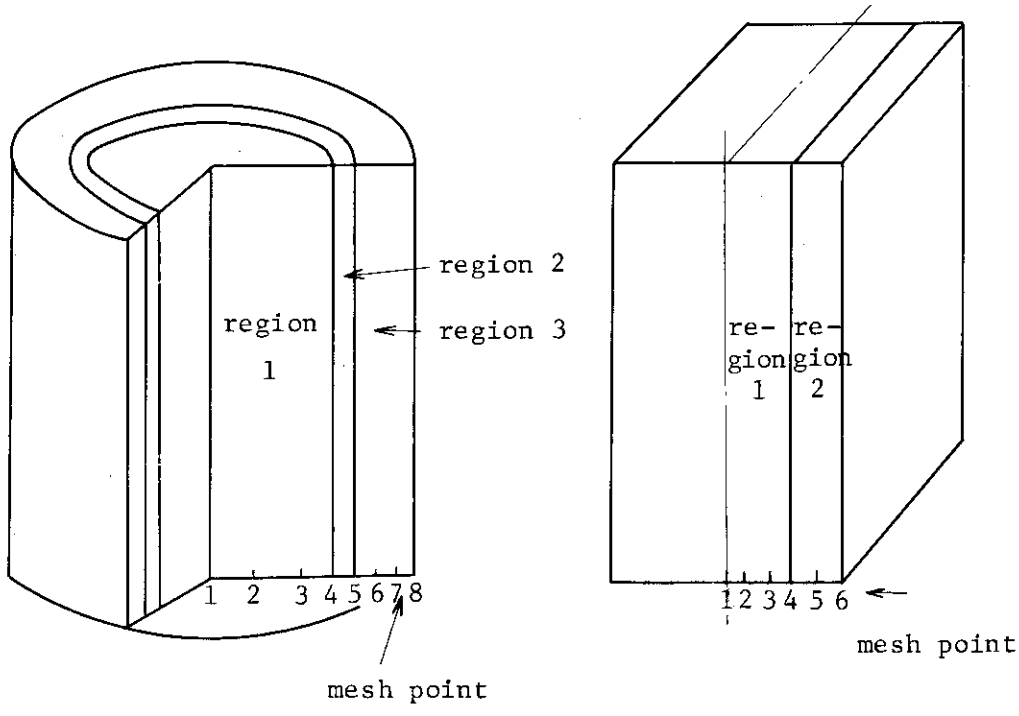

1) cylindrical　　2) rectangular

Fig. 2.1　Heat Conductor Sections and Nodalization

2) Rectangular type conductor

region 1 fuel

region 2 clad

Temperature-dependent thermal properties are used in the conduction calculations as input data. The thermal properties consist of thermal conductivity (kcal/m·hr·°C), volumetric heat capacity (kcal/m^3·°C) and linear expansion coefficient (1/°C).

The heat conduction model is based on the one-dimensional time dependent or steady state heat conduction. The basic conduction equation is solved numerically for incremental volumes within a conductor. The heat balance equation is:

$$V_n C_n \frac{dT_n}{dt} = Q_n + \left(Ak \frac{dT}{dX}\right)_r - \left(Ak \frac{dT}{dX}\right)_\ell \qquad (2\text{-}8)$$

where

n = number of incremental volume

V_n = incremental volume (m^3)

C_n = volumetric heat capacity (kcal/m^3·°C)

T_n = temperature at node n (°C)

t = time (sec)

Q_n = internal heat generation rate (kcal/sec)

A = heat transfer area (m^2)

k = thermal conductivity (kcal/m·sec·°C)

X = radial distance (m)

ℓ = subscript for left side

r = subscript for right side

2.4 Gap Conductance

The gap conductance can be expressed as the sum of gas conductance and conductance due to radiation across the gap.

$$h = h_{gas} + h_{rad} \qquad (2\text{-}9)$$

where

h = gap conductance (kcal/m^2·hr·°C)

h_{gas} = conductance through gas in the gap (kcal/m^2·hr· °C)

h_{rod} = conductance due to radiation across the gap (kcal/m^2·hr·°C)

h_{gas} is predicted by the following equation.

$$h_{gas} = k(\bar{T}_g(t))/\Delta x(t) \qquad \text{for} \quad \Delta x(t) > R_0 \qquad (2\text{-}10)$$

$$h_{gas} = k(\bar{T}_g(t))/R_0 \qquad \text{for} \quad \Delta x(t) < R_0 \qquad (2\text{-}11)$$

where

$\Delta x(t)$ = gap thickness at time t (m)

R_0 = roughness factor (m)

$\bar{T}_g$ = average gap temperature (°C)

k = conductance of gas in the gap (kcal/m·hr·°C)

The radiation heat transfer is determined by using the heat transfer equation of the radiation gray body.

$$q_{rod} = A_F F_{12}(E_1 - E_2) \qquad (2\text{-}12)$$

where

$$F_{12} = \left[\frac{1}{\varepsilon_F} + \frac{A_F}{A_C}\left(\frac{1}{\varepsilon_C} - 1\right)\right]^{-1}$$

$E_1 = 4.88\ (T_F/100)^4$

$E_2 = 4.88\ (T_C/100)^4$

F,C = subscript for outer surface of fuel pellet and inner surface of cladding, respectively

ε = emissivity

A = area (m^2)

T = temperature (°C)

2.5 Clad Surface Heat Transfer Correlation

The heat transfer correlations used in the EUREKA-2 code are listed in Table 2.3 and Table 2.4. The criteria of high mass flux or low mass flux is determined by mass flux as the following.

$g > 271$ kg/m^2・sec : high mass flux

$g < 14$ kg/m^2・sec : low mass flux

Between high mass flux and low mass flux ($14 < g < 271$ kg/m^2・sec) the continuity of heat flux is kept by taking higher heat flux.

The DNB heat flux correlations utilized are tabulated in Table 2.5. The linear interpolation related to mass flux is taken for the range of $271 < g \leq 1360$ kg/m^2・sec.

Table 2.3 Name List of Heat Transfer Correlations used in EUREKA-2

Regime	High Mass Flux	Low Mass Flux
Forced Convection (subcooled)	Diffus-Boelter	—
Natural Convection (subcooled)	—	Ostrache
Subcooled Nucleate Boiling	Modified Chen	—
Nucleate Boiling	Chen	Nishikawa-Yamagata
Transition Boiling	Modified Tong-Young	—
Film Boiling	Condie-Bengston	—
Natural Convection (Dryout)	—	Ohnishi-Tanzawa

Table 2.4 Heat Transfer Correlations in EUREKA-2

Mode No.	Heat Transfer Correlation	Mode No.	Heat Transfer Correlation
1	Dittus-Boelter $h = 0.023 \frac{k}{D_e} Pr^{0.4} Re^{0.8}$	1	Ostrache $h = \frac{k}{L} N_U$
2	Chen $h = h_{min} + h_{max}$ $h_{min} = 0.00122 \left(\frac{k_f^{0.79} C_{pf}^{0.45} \rho_f^{0.49} g_c^{0.25}}{\sigma^{0.5} \mu_f^{0.29} h_{fg}^{0.24} \rho_g^{0.24}}\right) \times \Delta T_{sat}^{0.24} \Delta P^{0.75} \cdot S$ $h_{max} = 0.023 \frac{k_f}{D_e} Pr_f^{0.4} Re_f^{0.8} F$	2	Nishikawa and Yamagata $q_{NB} = 19550 P_{sat}^{12} \Delta T_{sat}^{3}$
3	Modified Tong-Young $q = q_{TB} + q_{FB}$ $q_{TB} = q_{DNB} e^{-\phi}$ $\phi = \frac{0.001 \cdot Xe^{0.66}}{\left(\frac{q}{G \cdot h_{fg}}\right)\left(\frac{4}{D_e}\right)} \cdot \left(\frac{\Delta T_{sat}}{100}\right)^{1+0.0016 \Delta T_{sat}}$	6	Ohnishi and Tanzawa $h = h_0(1+f(v)\Delta T_{sub})$ $h_0 = 0.62 \left[\frac{k_g^3 h_{fg} \rho_g (\rho_f - \rho_g) g_c}{\mu_g \cdot 2\pi \sqrt{\frac{\sigma}{\rho_f - \rho_g}}} \Delta T_{sat}\right]^{0.25}$ $f(v) = 0.025+0.01(v-1.0)$, $v>1.0$ $f(v) = 0.025$, $v \leq 1.0$
6	Condie-Bengston $q = q_{TB} + q_{FB}$ $q_{FB} = h \Delta T_{sat}$ $h = [0.04487 k_g^{0.4376} Pr_g^{2.3070} \times Re_g^{0.6004+0.2456 \ell n(1+Xe)}] / [D_e^{0.7842} (1+Xe)^{2.59028}]$	2	Modified Chen $F = 1$ and $q = h_{min} \Delta T_{sat} + h_{max} (T_w - T_f)$

(note) Mode numbers identify the correlations to be used in the code and printed out.

Nomenclature

Cp	Specific heat at constant pressure (Btu/ft^3·hr)
D_e	Wetted equivalent diameter (ft)
F	Reynolds number Coefficient (note 1)
G	Mass flux (ℓb_m/ft^2·hr)
g_c	Gravitational conversion factor (ℓb_m·ft/ℓb_f·sec^2)
h	Heat transfer coefficient (Btu/ft^2·hr·°F)
h_{fg}	Heat of vaporization (Btu/ℓb_m)
S	Coefficient (note 2)
T_f	Fluid temperature (°F)
T_w	Wall temperature (°F)
ΔT_{sat}	$T_w - T_s$ (°F)
ΔT_{sub}	$T_s - T_{subcool}$ (°F)
Xe	Equilibrium quality
μ	Viscosity (ℓb_m/ft hr)
k	Thermal conductivity (Btu/ft·hr·°F)
L	Length of heat transfer surface (ft)
Nu	Nusselt number
Pr	Prandtl number
P_{sat}	Saturation pressure (ℓb_f/ft^2)
ΔP	Vapor pressure difference corresponding to ΔT_{sat} (ℓb_f/ft^2)
q	Heat flux (Btu/ft^2·hr)
Re	Reynolds number
ρ	Density (ℓb_m/ft^2)
σ	Surface tension (ℓb_f/ft)
Subscript	
DNB	Departure from nucleate boiling
f	Saturation
FB	Film boiling
g	Saturated vapor
NB	Nucleate boiling
TB	Transition boiling

(note 1) determined from $\left(\frac{X_e}{1-X_e}\right)^{0.9}\left(\frac{\rho_f}{\rho_g}\right)^{0.5}\left(\frac{\mu_g}{\mu_f}\right)^{0.1}$

(note 2) determined from $Re_f \cdot F^{1.25}$

Table 2.5 DNB Heat Flux

I. $g > 1360 kg/m^3 \cdot sec$

1. Subcooled DNB correlation: Tong W - 3 correlation

$$q_{w-3} \times 10^{-6} = \prod_{i=1} C_i$$

$$C_1 = (2.002 - 0.0004302P) + (0.1722 - 0.0000984P) \times \exp\{(18.177 - 0.004129P)Xe\}$$

$$C_2 = (0.1484 - 1.596Xe + 0.1729Xe|Xe|)G \times 10^{6} + 1.037$$

$$C_3 = 1.157 - 0.869Xe$$

$$C_4 = 0.2664 + 0.8357e^{-37.81De}$$

$$C_5 = 0.8258 + 0.000794(h_f - h_{in})$$

2. Saturated DNB correlation: Hsu and Beckener modified W - 3 correlation

1) $\alpha \geq 0.96$

Dryout

2) $\alpha < 0.96$

$$q_{DNB} = q_{dry} + \sqrt{1.76\ (0.96 - \alpha)} \cdot q_{w-3}\Big|_{\substack{Xe = 0 \\ C_5 = 0.8258}}$$

a) $Re > 2000$

q_{dry} = higher flux between Rohsenow-Choi and NSRR's experimental correlation.

(note 1) Rohsenow-Choi

$$q = \frac{4K}{D_e} (T_w - T_f)$$

(note 2) $q_{w-3}\Big|_{\substack{Xe=0 \\ C_5=0.8258}}$ corresponds to Tong w-3 correlation with quality = 0 and subcooling = 0.

II. $g < 271\ kg/m^2 \cdot sec$

1. Subcooled DNB correlation: Zuber correlation and Kutateladze's modification

$$q_{NDB} = q_{Zuber}\,|_{\alpha=0} \times \{1.0 + 0.065(\frac{\rho_f}{\rho_g})^{0.8}\ \frac{C_{p\ell}\cdot\Delta T_{sub}}{h_{fg}}\}$$

$q_{Zuber}\,|_{\alpha=0}$ is modified Zuber correlation with $\alpha=0$.

2. Saturated DNB correlation: Modified Zuber correlation

$$q_{Zuber} = 0.13 h_{fg}\cdot\rho_g^{0.5}[\sigma(\rho_f-\rho_g)g\cdot g_c]^{0.25}[\frac{\rho_f}{\rho_f+\rho_g}]^{0.5} \times (0.96-\alpha)$$

where

g = gravitational acceleration (ft/sec^2)

h_{in} = inlet enthalpy of subcooled water ($Btu/\ell b_m$)

P = node pressure ($\ell b_f/ft^2$)

α = void fraction

2.6 Coolant Thermohydrodynamics

The fluid equations are derived with the one-dimensional homogeneous conservation equations for fluid mass, energy and momentum. These equations are as follows:

1) fluid mass equation

$$A \frac{\partial \rho}{\partial t} = - \frac{\partial W}{\partial X} \tag{2-13}$$

2) fluid energy equation

$$A \frac{\partial (\rho \cdot e)}{\partial t} = - \frac{\partial}{\partial X} [W(h + \frac{1}{2} V^2 + \phi)] + q_w \frac{\partial A_w}{\partial X} \tag{2-14}$$

3) fluid momentum equation

$$A \frac{\partial (\rho \cdot V)}{\partial t} = - \frac{\partial (V \cdot W)}{X} + A \frac{\partial P}{\partial X} - \rho g A \frac{\partial Z}{\partial X} - \frac{\partial F_K}{\partial X} \tag{2-15}$$

where

A = flow area (m^2)
A_w = wall area for heat transfer (m^2)
e = total fluid specific energy ($u + \frac{1}{2} V^2 + \phi$) ($m^2/sec^2$)
F_K = frictional force ($kg \cdot m/sec^2$)
g = gravitational acceleration (m/sec^2)
h = fluid enthalpy ($u + P/\rho$) (m^2/sec^2)
P = thermodynamic pressure ($kg/m \cdot sec^2$)
q_w = wall heat flux (kg/sec^3)
t = time (sec)
μ = fluid specific internal energy (m^2/sec^2)
V = fluid velocity (m/sec)
W = mass flow rate (kg/sec)
X = path length coordinate value (m)
Z = elevation coordinate value (m)
ρ = fluid density (kg/m^3)
ϕ = gravity potential function (m^2/sec^2)

To obtain mass, energy, momentum values, the conservation equations are intergrated over defined control volumes. The resulting set of simultaneous

equations is linearlized and advanced for a small time increment by a fully implicit numerical technique.

2.7 Prompt Moderator Heating Effect (PMH effect)

The code can provide the option to transfer energy directly from a conductor to neighbor coolant fluid (moderator). The prompt moderator heating energy is calculated as follows:

$$Q_{PMH} = Q_{frac} \times P_t \times Q_{PMH\ frac} \times P_0 \times \frac{\rho}{\rho_0} \qquad (2\text{-}16)$$

where

Q_{PMH} = energy used for prompt moderator heating (MW)
Q_{frac} = fraction of total reactor power generated in the core conductor
P_t = normalized power
$Q_{PMH\ frac}$ = fraction of Q_{frac} utilized for PMH
P_0 = total initial reactor power (MW)
ρ/ρ_0 = ratio of coolant density to initial coolant density

This fraction of the energy produced by a given core conduction is subtracted from total reactor power to get the internal heat source used in the conduction solution. The heat source for the conduction solution is therefore given as follows:

$$Q = Q_{frac} \times P_t \times P_0 - Q_{PMH} \qquad (2\text{-}17)$$

2.8 Subcooled Void Model

Reactivity feedback phenomena in the moderator can include the effects of any vapor volume produced during subcooled boiling. The equation for the vapor volume fraction is

$$\frac{dR}{dt} + \frac{R}{\tau} = \lambda\ Kq' \qquad (2\text{-}18)$$

where

R = volume fraction of vapor in coolant channel
τ = bubble collapse life time (sec)

λ = fraction of surface heat flux utilized in producing vapor

q' = surface heat flux (kcal/m^2·sec)

K = convertion factor (m^2/kcal)

t = time (sec)

The parameters, τ and λ are given as input data. Vapor transport is neglected in the equation. The solution of equation (2-17) is

$$R = R_o e^{-t/\tau} + \lambda K q' \tau (1 - e^{-t/\tau}) \qquad (2\text{-}19)$$

where

R_o = the value of R at the beginning of a time step.

3. SPERT III E-Core Description

A brief description of the general features of the SPERT III reactor facility is presented in this section[2]. The SPERT III reactor facility contains nuclear and hydraulic equipments that characterizes a conventional, pressurized-water reactor. The primary system is comprised of a reactor vessel, pressurizer vessel, and two coolant loops as shown in Figure 3.1. The reactor vessel and primary coolant system are designed for maximum operating pressures and temperatures of 170 kg/cm^2g (2500 psi) and 343°C (650°F), respectively. Each of the primary coolant loops consists of two canned rotor pumps operating in parallel. The total flow capability of both loops is 76 m^3/min (20,000 gpm), which corresponds to velocities in the E-CORE fuel channels of 7.2 m/sec (24 f/sec). A cutaway view of the SPERT III reactor pressure vessel is shown in Figure 3.2. Its inside diameter is 48 inches and its overall length is 23 feet 9 inches. After entering the vessel bottom tee, the coolant flows upward through the core, reverses direction, and flows downward through the thermal shields leaving the vessel near the bottom.

The cross section for the E-core is illustrated in Figure 3.3. The E-core fuel is comprised of 4.8%-enriched UO_2 fuel rods restrained in stainless steel fuel assembly cans, which are shown in Figure 3.4. The maximum number of E-core fuel assemblies that can be loaded in the core is 68. The UO_2 fuel, in the form of 0.42-inch diameter pellets, is contained in 40.8 inch long, 0.466-inch outside diameter Type 348 stainless steel tubes that have a wall thickness of 0.020 inch. There is a 0.003-inch radial, helium-filled gap between the fuel pellets and the cladding. Each of the fuel rods has an active length of 38.3 inches and contains 38.5 grams of U-235. As shown in Figure 3.4, the majority of the fuel rods are restrained in 48 3-by 3-inch square assembly cans that contain 25 rods in a 5 by 5 rectangular array. There are 12 smaller 2.5-by 2.5-inch square fuel assembly cans, each containing 16 fuel rods arranged in a 4 by 4 rectangular array. Four of the 16-rod assemblies surround the centrally located transient rod guide, and the remaining eight 16-rod assemblies form fuel followers of the eight E-core control rods. The cruciform-shaped transient rod used for initiating reactor power excursions is located at the core center.

A summary of static nuclear characteristics of the E-core is presented in Table 3.1[8].

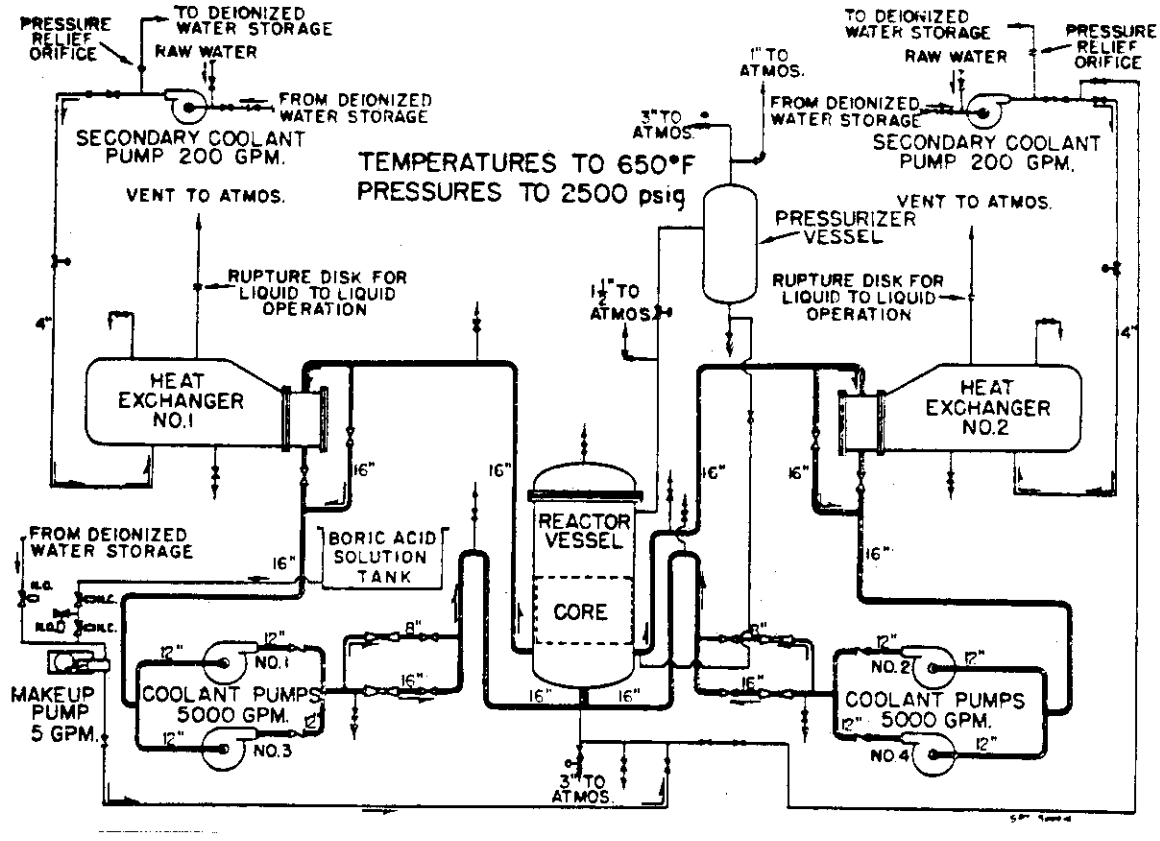

Fig. 3.1 Spert III process flow diagram

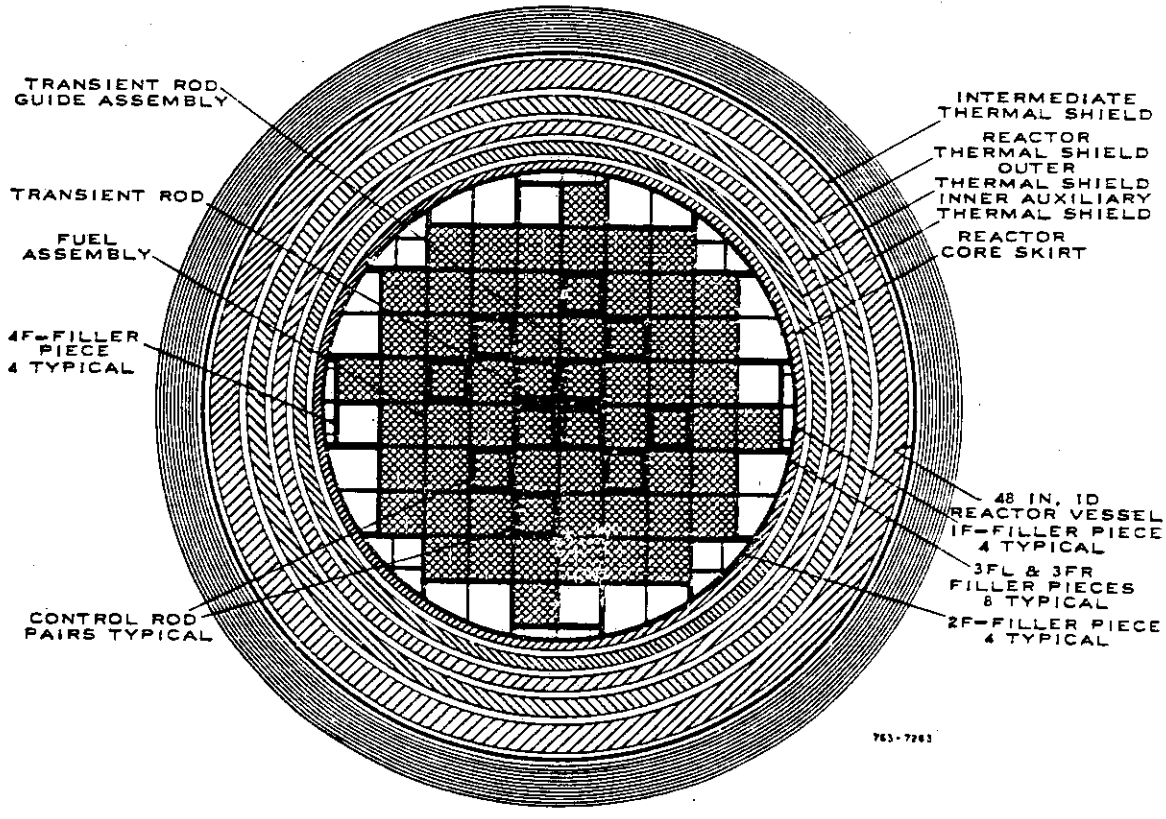

Fig. 3.3 E-core cross section (64-assembly loading)

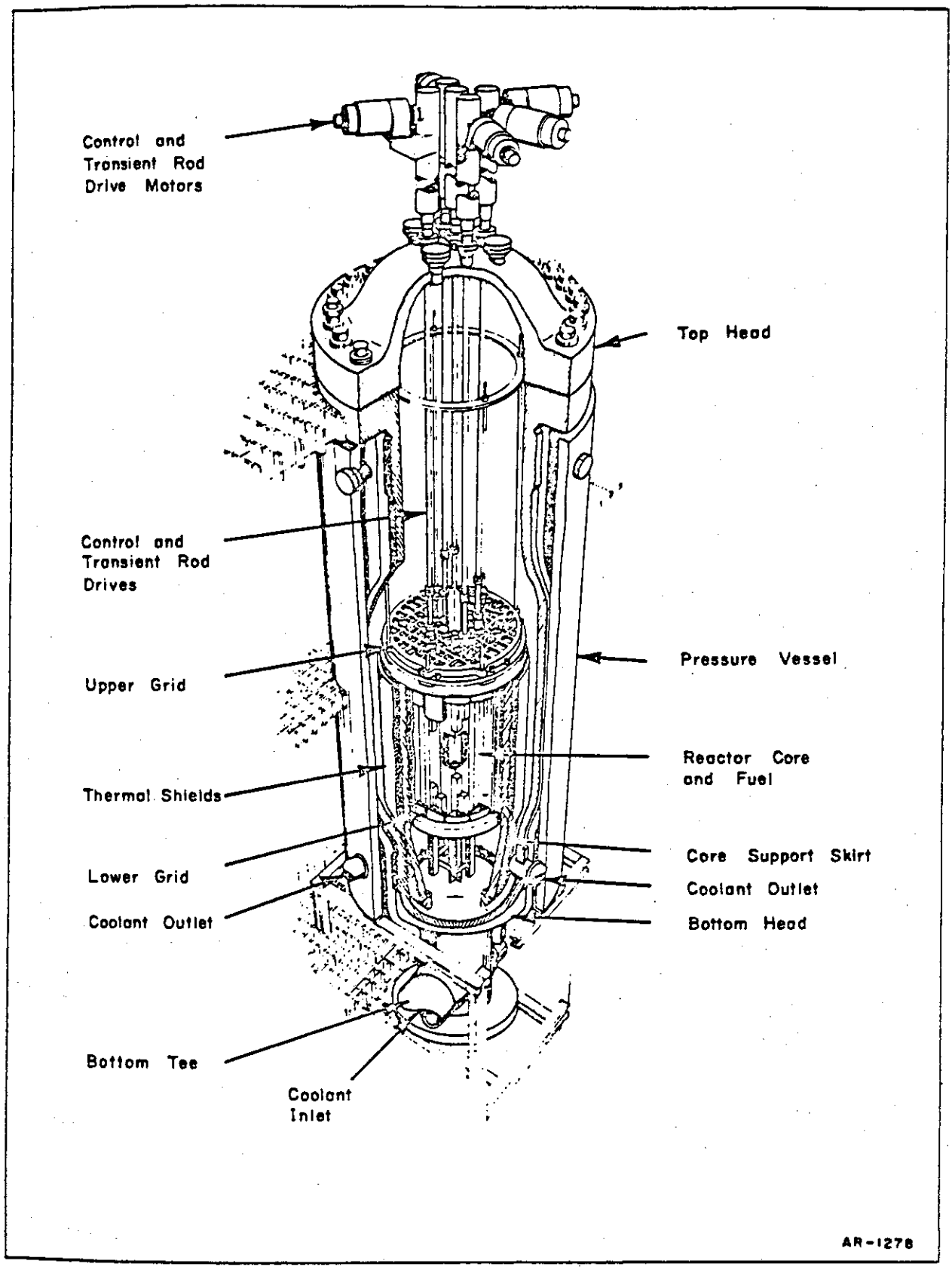

Fig. 3.2 Reactor vessel assembly

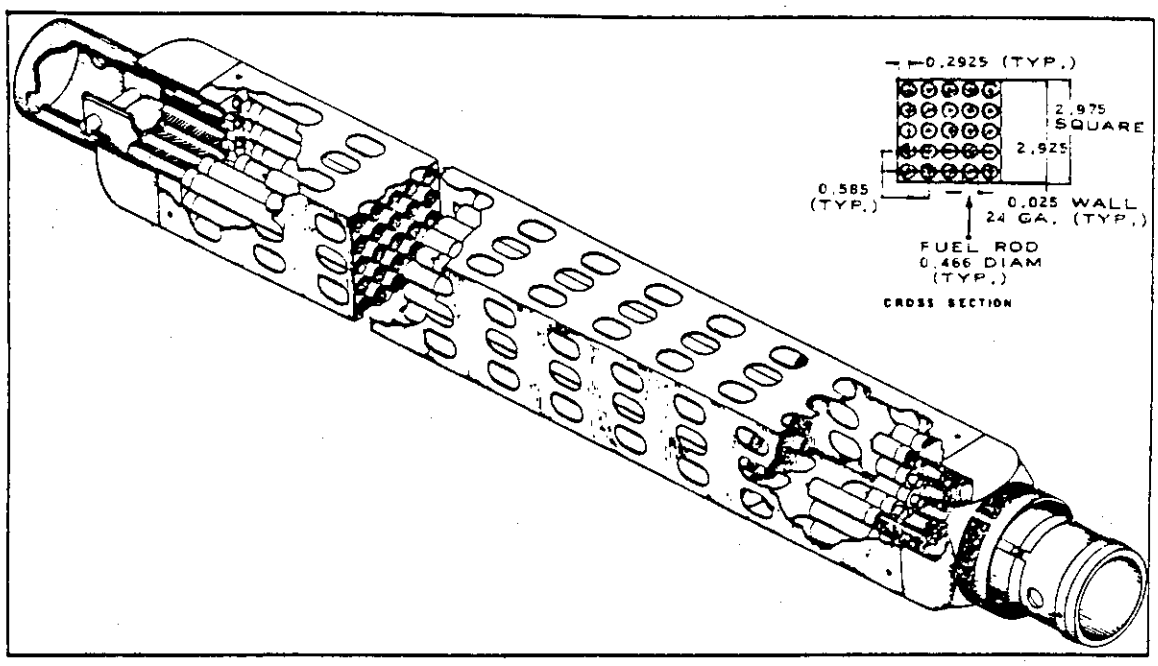

Fig. 3.4 Nominal 25 fuel rod assembly

Table 3.1 Feedback coefficient, peaking factor

Temperature (°F)	70	250	500	500 (20 MW)
Doppler coefficient (¢/°F)	−0.72	−0.56	−0.37	−0.23
Temperature coefficient (¢/°F)	−0.40	−1.97	−3.99	−4.13
Void coefficient (¢/void)	−50.0	−42.0	−35.0	−37.0
Peaking factor	5.7	5.2	3.6	3.2

4. Comparisons of the EUREKA-2 Calculations with the SPERT III E-Core Experiments

4.1 Core Model and Input Data of the EUREKA-2 Code

(1) Channel Representation

The four channel division model of the SPERT III E-Core is shown in Fig. 4.1[2]. The fraction of core fuel rods in each channel is given in the following tabulation.

Channel	Fuel Assemblies	Fuel Rods	Fraction of Core Fuel Rods
1	20	500	0.3592
2	20	500	0.3592
3	16	328	0.2356
4	4	64	0.0460

Each of these channels was subdivided axially in the core as shown in Fig. 4.2. The coolant flows upward through the channels. The hot channel is represented by the node of No. 4.

(2) Power Profile and Feedback Weighting Factor

The power profile and feedback weighting factor depend on the initial system condition. The peaking factor is shown in Table 3.1, depending on the inlet coolant temperature. The temperature dependency of the peaking factor is due to movement of the control rod bank critical position. In the figure presented in the reference 6), the calculated axial cold neutron flux profiles are presented as a function of control rod position. The control rod bank critical positions are shown in the Table II in reference 7) to be at 14.6 inches above bottom of the core for the 20°F cold start-up test and at 28.3 inches for the 500°F test. The power profiles at the 70°F and 260°F tests were assumed to be the profile for the control rods withdrawal 15.8 inches of the Fig. 7 of the reference 6), because the peaking factors are almost similar for the 70°F and 260°F tests. The power profile at the 500°F test was assumed to be the profile interpolated from the profiles for the control rods withdrawal 23.6 inches and 38.3 inches. The feedback weighting factors were obtained by squaring the power profile with radial weighting factors. Fig. 4.3 and Fig. 4.4 show the axial heat source profile of each channel and the reactivity weighting factor used in the calculation.

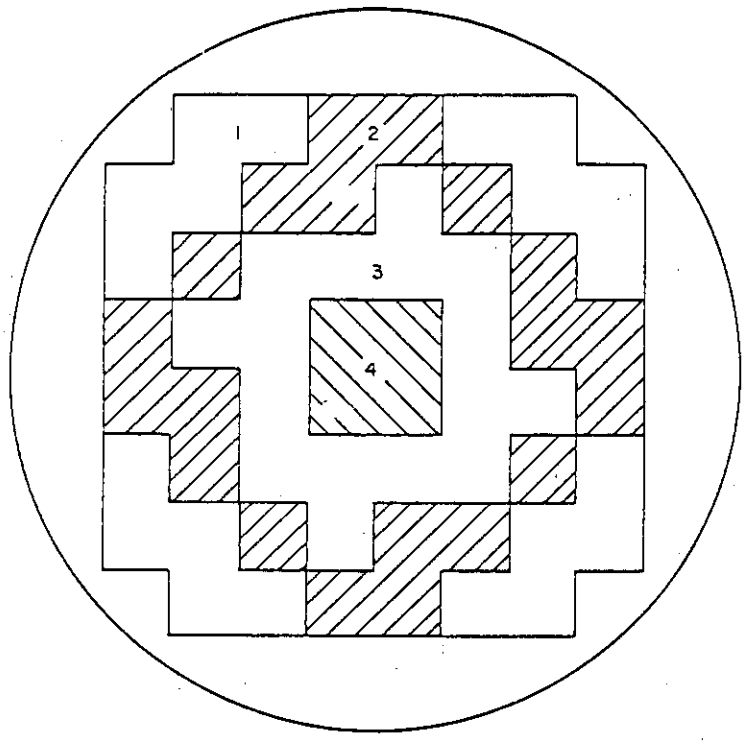

Fig. 4.1 Four-channel representation of the SPERT III E-core

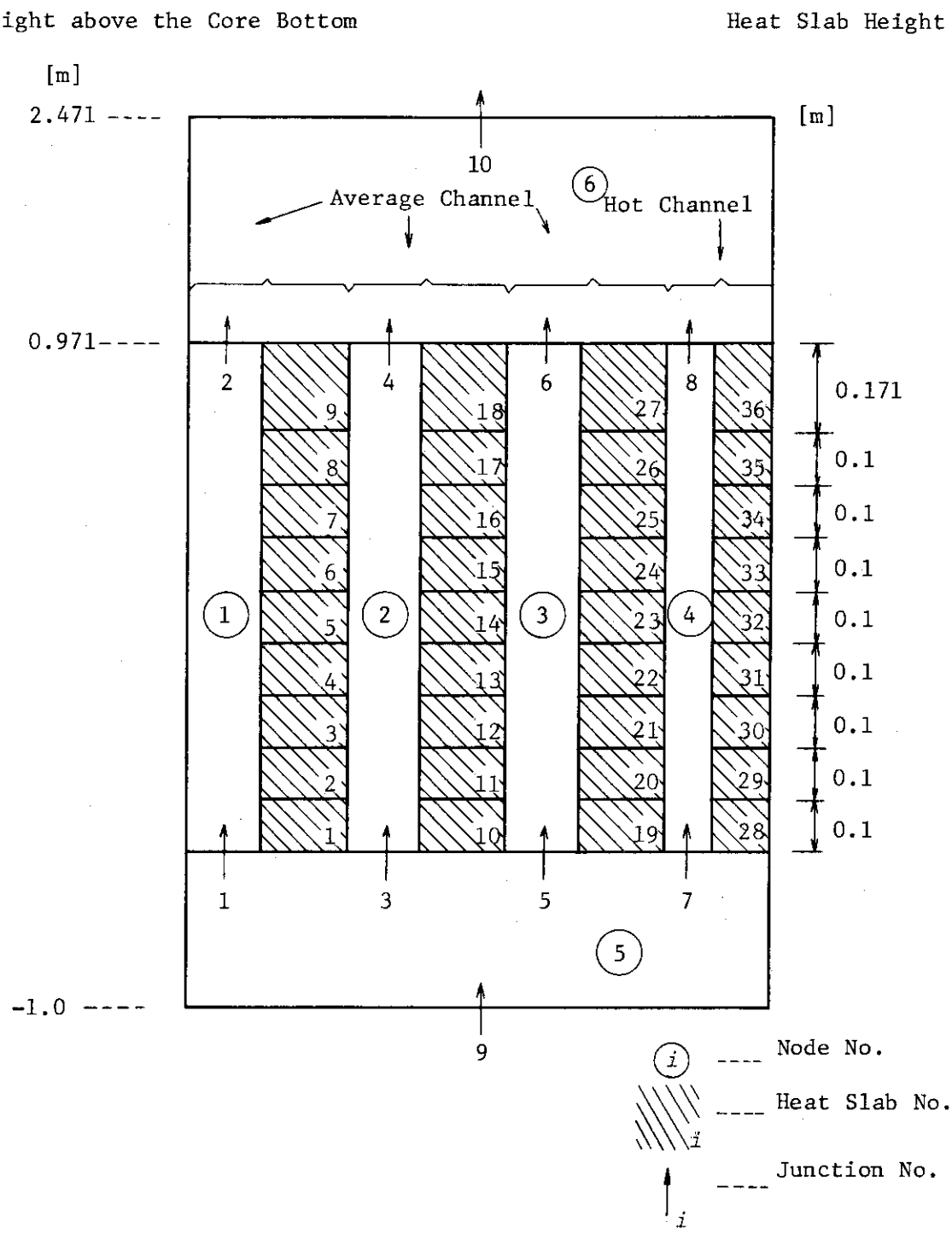

Fig. 4.2 Heat Slab and Node Division of the SPERT III E-Core.

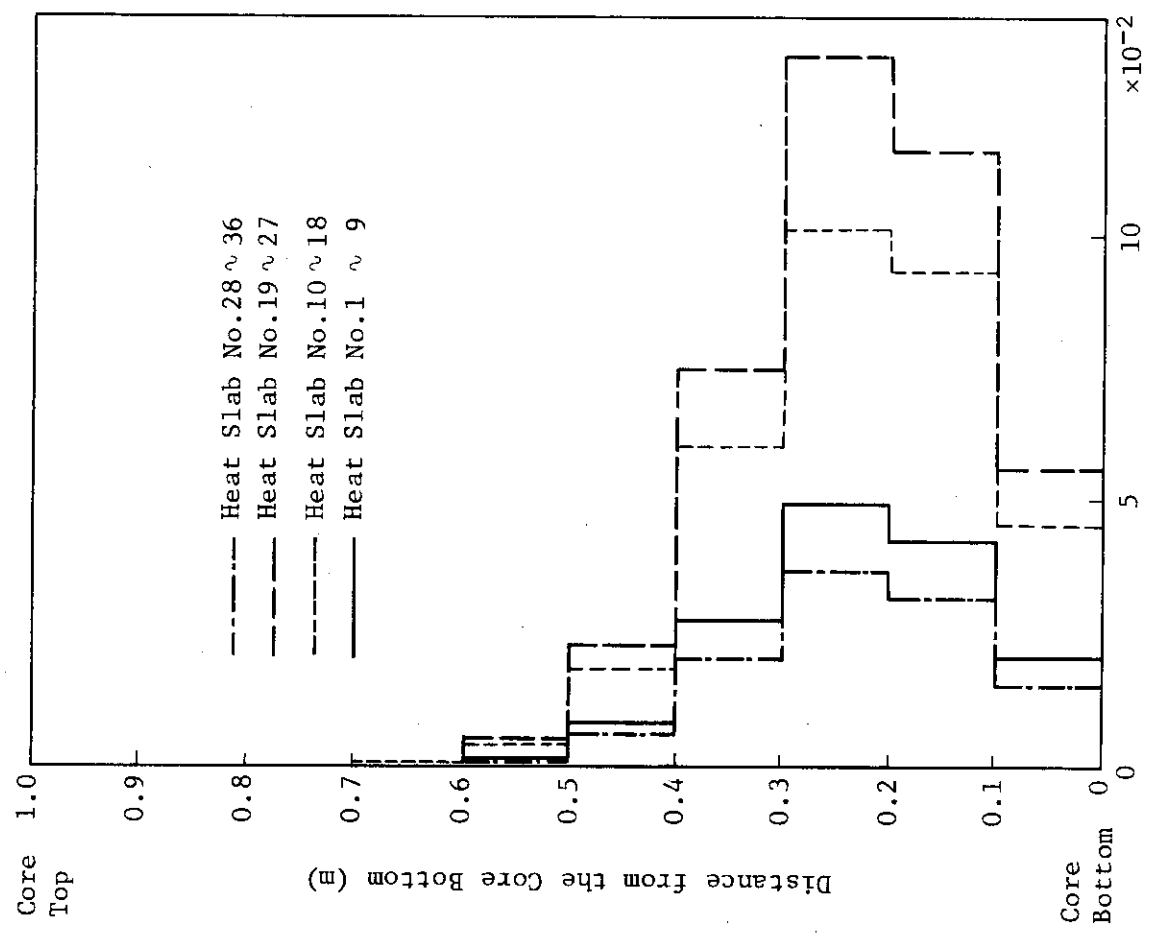

Fig. 4－3(2) Feed back Weighting Factor for the Moderator Temperature and the Void Effect used in the Analysis (70, 260 °F).

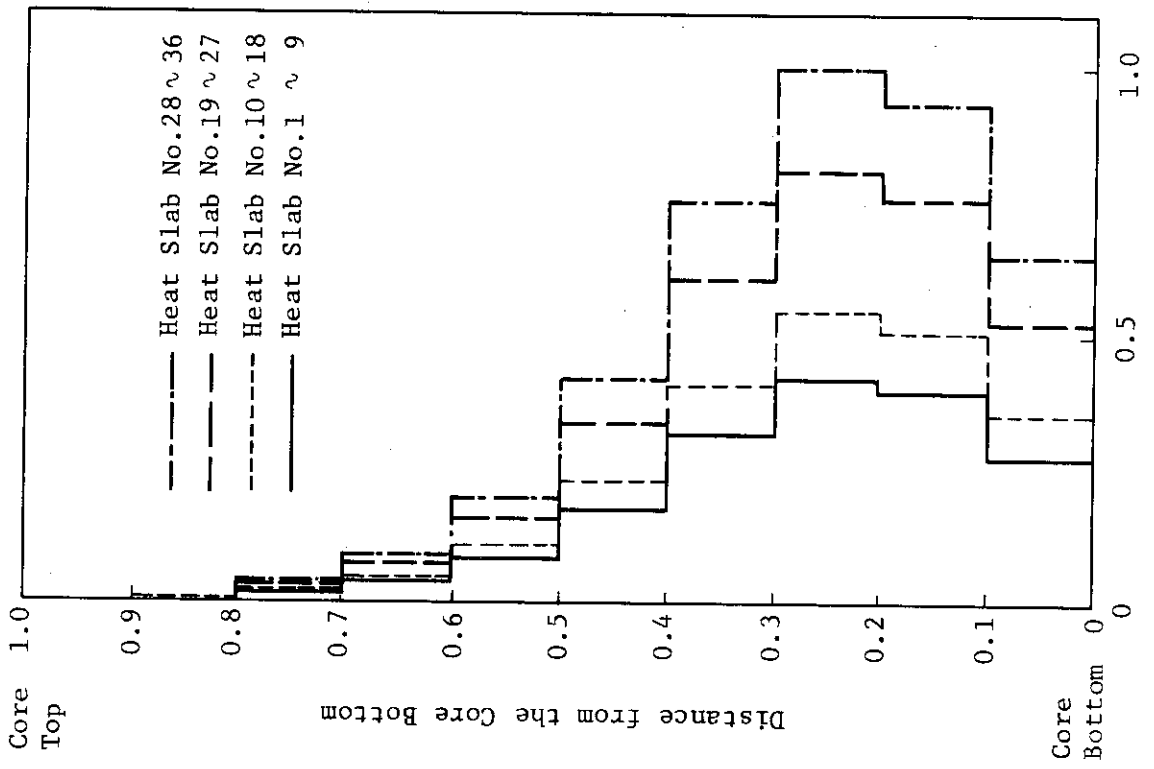

Fig. 4－3(1) Power Density Distribution used in the Analysis (70, 260 °F).

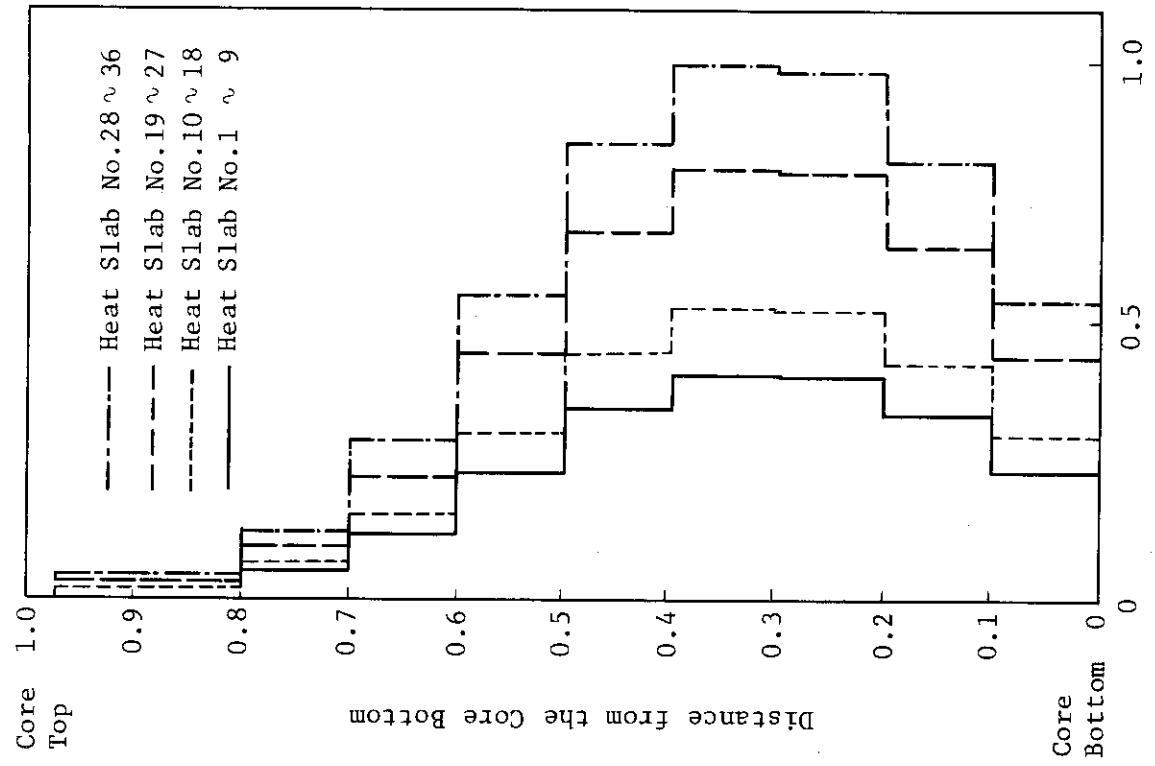

Fig. 4-4(1) Power Density Distribution used in the Analysis (500 °F).

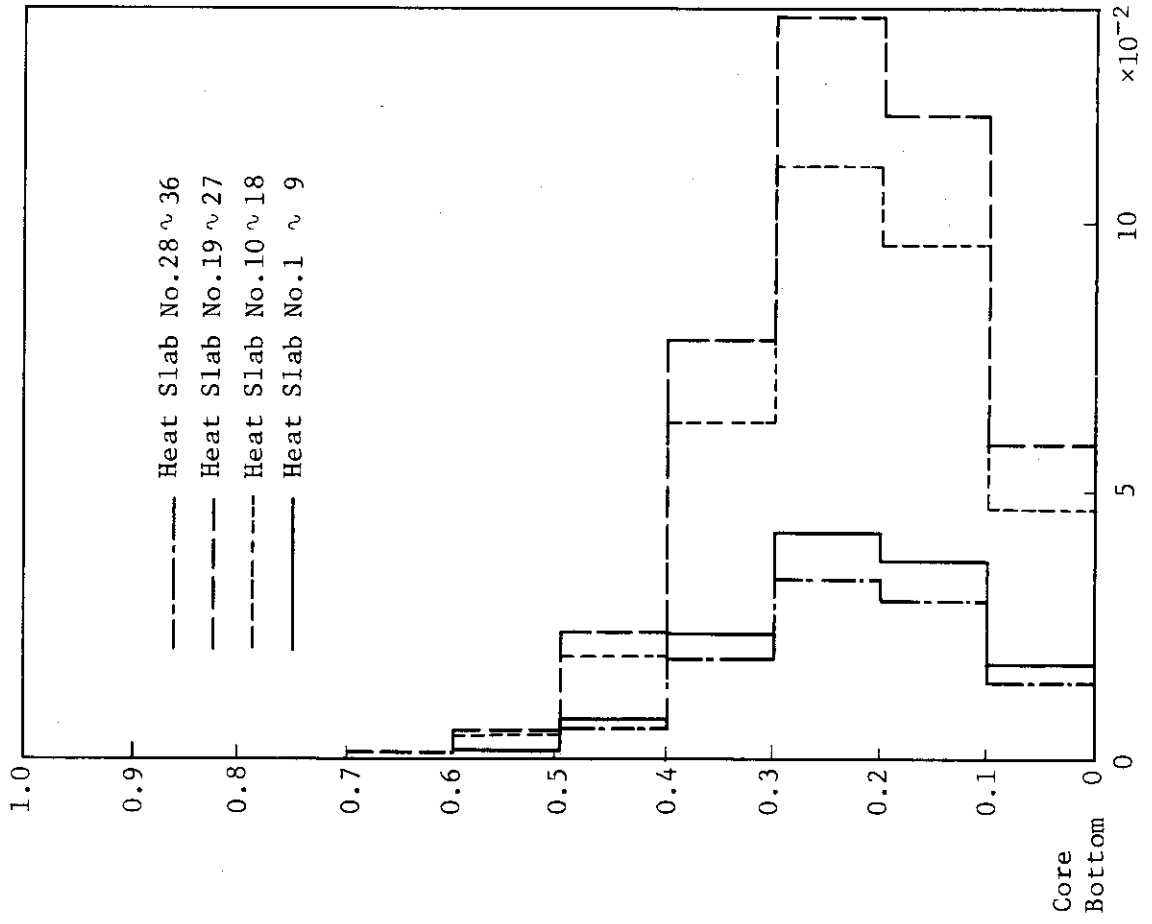

Fig. 4-3(3) Feedback Weighting Factor for the Doppler Effect used in the Analysis (70, 260 °F).

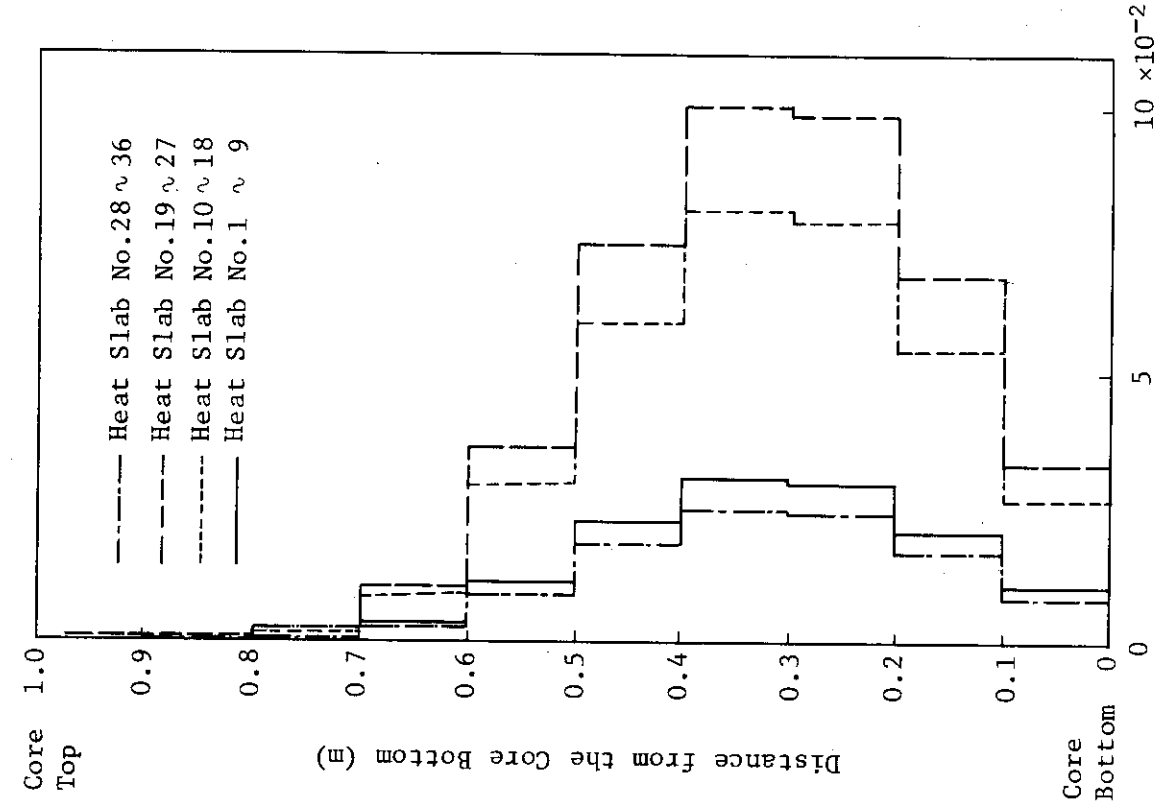

Fig. 4-4(3) Feedback Weighting Factor for the Doppler Effect used in the Analysis (500 °F).

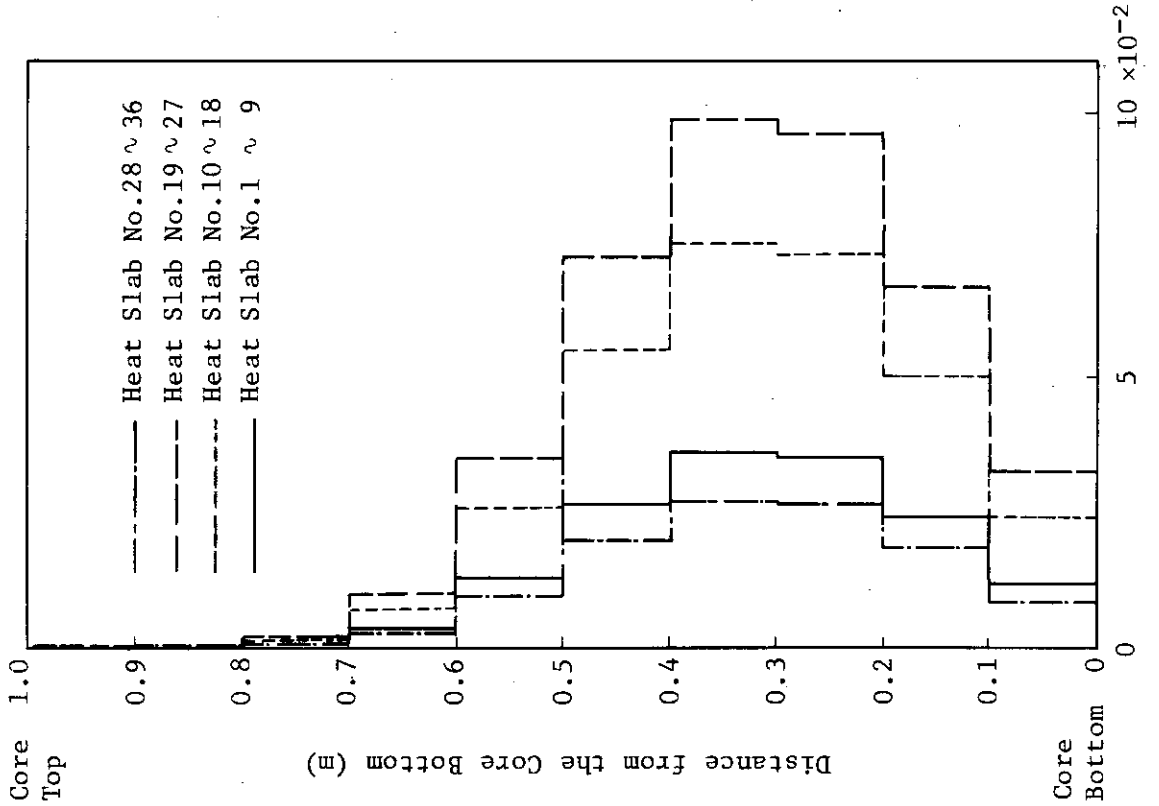

Fig. 4-4(2) Feedback Weighting Factor for the Moderator Temperature and the Void Effect used in the Analysis (500 °F).

(3) Nuclear Kinetics Parameter

Table 4.1 shows the prompt neutron generation time and the effective delayed neutron fraction for each coolant inlet temperature[8].

Table 4.1 Prompt neutron generation, effective delayed neutron fraction

Coolant inlet temperature (°F)	Effective delayed neutron fraction β_{eff}	Prompt neutron generation time ℓ (μsec)
70	0.00718	15.55
250	0.00724	15.78
500	0.00725	16.31

(4) Feedback Coefficients

The feedback coefficients except for the Doppler coefficient were used as shown in Table 3.1. The Doppler coefficient shown in Table 3.1 did not provide a good agreement with the experiment. The feedback reactivity of the Doppler effect may be represented by the equation[9]:

$$\rho = a\sqrt{T} + b$$

a and b were determined to be $1.10\times10^{-3}(\Delta k/k/\sqrt{°C})$ and $-18.18\times10^{-3}(\Delta k/k)$, respectively, with the experimental results. From this equation, the Doppler coefficient at 70, 250 and 500°F is -0.24 ¢/°F, -0.21 ¢/°F and -0.18 ¢/°F, respectively, which are much smaller than the coefficient Table 3.1.

(5) Other Parameters

The thermal conductivity of the helium gap separating the UO_2 fuel pellets from the stainless steel cladding is described as a function of the gap temperature. Anderson and Lechliter's expression for the conductivity of the gap gas was applied to the E-core fuel[10].

In specifying the prompt moderator heating effect, it was assumed that 2.6% of the energy generated in the fuel is deposited promptly in the moderator.

4.2 Computational Results and Discussions

Operating conditions for experimental investigations of the SPERT III-E tests include cold-startup, hot-startup, hot-standby and operating-power conditions[2]. The experimental data selected for investigation are reactor power, energy release, reactivity compensation and power burst shape. The comparison of the fuel cladding surface temperature for the hot standby and operating power tests was made between the experiment and the EUREKA-2 calculation.

(1) Cold-startup Reactivity Accident Tests

40 cold-startup reactivity accident tests are performed with the E-core. The tests are initiated with ambient temperature and pressure, low initial power (50W), no coolant flow and rapid reactivity insertions ranging from 0.68 to 1.21 $. A tabulation of the cold-startup reactivity accident test data is presented in Table 4.2. In the appendix, Figure A.1 through A.30 illustrate comparisons between the FUREKA-2 calculations and the experimental measures for three excursions of reactor power, energy and net system reactivity. Table 4.3 shows the summary of the analytical result for cold-startup accident tests. Fig. 4.5 and Fig. 4.6 present the experimental and EUREKA-2 calculated peak powers, the energy releases to peak power and reactivity compensations at peak power as a function of reciprocal period. In the experimental data of Table 4.2, the reactor period for a given transient is calculated from the power data assuming an initial exponential power rise. X axis of the Figures 4.5 and 4.6 shows the reciprocal period from the experiment. The figures illustrate that a good agreement between the EUREKA-2 calculation and the experiment over the entire range of reactivity insertions. The EUREKA-2 calculations are essentially within experimental uncertainty for peak power, reactivity compensation and energy release over almost the entire range of reciprocal periods, except for the energy release of test No. 22.

The largest disagreement between the experimental and EUREKA-2 curves is about 15% for peak power, about 20%, for energy release and about 15% for reactivity compensation. The EUREKA code predicts the analysis of only one cold-startup test of No. 43 (reciprocal period 100 sec^{-1})[8].

Fig. 4-7 and Fig. 4-8 shows EUREKA-2-calculated time-dependent reactivity feedback contributions for the cold-startup test 23 (111 msec

period) and 75 (33 msec), respectively. The calculations indicated that the SPERT III E-Core is essentially Doppler limited for cold-startup tests. (see Table 4.9)

Time-dependent fuel rod cladding surface temperature rises for the tests No. 18 and 42 are shown in Figures 4.9 and 4.10. The clad surface temperature rises calculated using the EUREKA-2 code agree with the unsheathed thermocoupled data to within about 10% for core locations N33, N31, N21, E22 and E21.

Table 4.2 Data summary for cold-startup accident tests

Test No.	Reactor Period (msec)	Initial Reactivity Insertion ($)	Initial Primary Coolant Temperature (°F)	Maximum Reactor Power (MW)	Energy Release to Time of Peak Power (MW-sec)	Time to Peak Power (sec)	Maximum Measured Fuel Cladding Surface Temperature Rise (°F)	Reactivity Compensation at Peak Power ($)
22	1010 ± 20	0.77 ± 0.03	74 ± 4	2.1 ± 0.3	6.9 ± 1.2	13.7 ± 0.2	92 ± 9	0.26 ± 0.03
18	351 ± 7	0.90 ± 0.04	70 ± 4	4.3 ± 0.6	6.7 ± 1.1	5.3 ± 0.1	99 ± 10	0.23 ± 0.03
13	206 ± 4	0.93 ± 0.04	63 ± 4	5.6 ± 0.8	5.1 ± 0.9	3.2 ± 0.06	127 ± 13	0.19 ± 0.02
14	195 ± 4	0.94 ± 0.04	64 ± 4	5.6 ± 0.8	5.3 ± 0.9	3.2 ± 0.06	104 ± 10	0.20 ± 0.02
39	113 ± 2	0.97 ± 0.04	65 ± 4	8.1 ± 1.2	4.7 ± 0.8	1.77 ± 0.07	143 ± 14	0.17 ± 0.02
23	111 ± 2	0.97 ± 0.04	70 ± 4	7.7 ± 1.2	4.2 ± 0.7	1.81 ± 0.05	131 ± 13	0.16 ± 0.02
45	96.8 ± 1.9	0.98 ± 0.04	78 ± 4	8.2 ± 1.2	3.6 ± 0.6	1.60 ± 0.09	150 ± 15	0.13 ± 0.01
15	95.8 ± 1.9	0.99 ± 0.04	66 ± 4	8.0 ± 1.2	3.4 ± 0.6	1.57 ± 0.02	125 ± 13	0.13 ± 0.01
50	95.7 ± 1.9	0.98 ± 0.04	82 ± 4	9.2 ± 1.4	3.3 ± 0.6	1.47 ± 0.04	150 ± 15	0.11 ± 0.01
44	95.2 ± 1.9	0.98 ± 0.04	77 ± 4	8.3 ± 1.2	3.8 ± 0.6	1.55 ± 0.03	132 ± 13	0.14 ± 0.01
46	94.0 ± 1.9	0.98 ± 0.04	69 ± 4	8.5 ± 1.3	4.0 ± 0.7	1.55 ± 0.06	149 ± 15	0.15 ± 0.02
71	94.0 ± 1.9	0.98 ± 0.04	92 ± 4	7.9 ± 1.2	3.6 ± 0.6	1.54 ± 0.06	148 ± 15	0.14 ± 0.01
17	91.0 ± 1.8	0.99 ± 0.04	68 ± 4	8.6 ± 1.3	3.3 ± 0.6	1.20 ± 0.05	117 ± 12	0.12 ± 0.01
74	89.0 ± 1.8	0.99 ± 0.04	67 ± 4	8.9 ± 1.3	3.1 ± 0.5	1.36 ± 0.04	143 ± 14	0.12 ± 0.01
87	87.0 ± 1.7	0.99 ± 0.04	66 ± 4	9.1 ± 1.4	3.8 ± 0.6	1.35 ± 0.04	187 ± 19	0.11 ± 0.01
73	83.0 ± 1.6	0.99 ± 0.04	67 ± 4	8.8 ± 1.3	3.0 ± 0.5	1.40 ± 0.04	150 ± 15	0.13 ± 0.01
51	72.3 ± 1.4	1.00 ± 0.04	82 ± 4	11 ± 2	2.4 ± 0.4	1.08 ± 0.02	130 ± 13	0.09 ± 0.01
49	68.4 ± 1.4	1.00 ± 0.04	76 ± 4	11 ± 2	2.1 ± 0.4	0.97 ± 0.04	142 ± 14	0.08 ± 0.01
16	59.3 ± 1.2	1.01 ± 0.04	67 ± 4	12 ± 2	2.0 ± 0.3	0.86 ± 0.01	118 ± 12	0.08 ± 0.01
38	55.5 ± 1.1	1.02 ± 0.04	56 ± 4	15 ± 2	2.1 ± 0.4	0.79 ± 0.02	166 ± 17	0.07 ± 0.01
19	44.0 ± 0.9	1.03 ± 0.04	69 ± 4	18 ± 3	1.9 ± 0.3	0.63 ± 0.01	115 ± 12	0.07± 0.01
20	35.0 ± 0.7	1.03 ± 0.04	72 ± 4	26 ± 4	2.0 ± 0.3	0.54 ± 0.01	123 ± 12	0.08± 0.01
75	33.0 ± 0.7	1.05 ± 0.04	68 ± 4	31 ± 5	2.1 ± 0.4	0.50 ± 0.02	152 ± 15	0.08± 0.01
21	22.3 ± 0.4	1.09 ± 0.04	72 ± 4	56 ± 8	2.8 ± 0.5	0.38 ± 0.01	118 ± 12	0.11± 0.01
40	22.0 ± 0.4	1.09 ± 0.04	67 ± 4	59 ± 9	2.8 ± 0.5	0.39 ± 0.01	158 ± 16	0.11± 0.01
48	21.1 ± 0.4	1.09 ± 0.04	74 ± 4	63 ± 9	2.8 ± 0.5	0.37 ± 0.01	141 ± 14	0.11 ± 0.01
47	19.9 ± 0.4	1.09 ± 0.04	72 ± 4	67 ± 10	3.0 ± 0.5	0.36 ± 0.01	156 ± 16	0.12 ± 0.01
41	15.9 ± 0.3	1.13 ± 0.05	70 ± 4	110 ± 17	3.8 ± 0.6	0.31 ± 0.02	146 ± 15	0.14 ± 0.01
42	12.6 ± 0.3	1.17 ± 0.05	78 ± 4	170 ± 26	4.6 ± 0.8	0.250 ± 0.006	147 ± 15	0.18 ± 0.02
43	10.0 ± 0.2	1.21 ± 0.05	78 ± 4	280 ± 42	6.0 ± 1.0	0.230 ± 0.006	148 ± 15	0.22 ± 0.02

Table 4.3 Summary of EUREKA-2 Analyses for Cold-Startup Accident Tests

Test No.	Inserted Reactivity	Peak Power	Energy*	Time**	Compensated*** Reactivity
22	0.765 $	2.3 MW	10.3 MWs	15.44 s	0.30 $
18	0.895	4.4	7.7	5.37	0.24
13	0.940	5.7	6.0	3.07	0.19
14	0.937	5.6	6.1	3.20	0.19
39	0.970	7.1	4.5	1.88	0.15
23	0.970	7.2	4.5	1.87	0.15
45	0.980	7.8	3.7	1.52	0.12
15	0.985	8.3	3.6	1.39	0.12
50	0.985	8.3	3.6	1.39	0.12
44	0.980	7.9	3.9	1.54	0.13
46	0.975	7.5	4.1	1.69	0.14
71	0.980	8.0	4.0	1.55	0.13
17	0.985	8.2	3.4	1.37	0.11
74	0.985	8.2	3.3	1.36	0.11
87	0.985	8.2	3.3	1.36	0.11
73	0.985	8.2	3.3	1.36	0.11
51	0.995	9.3	2.6	1.08	0.09
49	1.000	10.1	2.2	0.96	0.08
16	1.007	11.6	2.0	0.84	0.07
38	1.017	14.4	1.9	0.72	0.07
19	1.030	19.5	1.9	0.60	0.07
20	1.035	22.0	2.1	0.57	0.07
75	1.050	31.1	2.4	0.49	0.08
21	1.080	57.9	2.8	0.38	0.10
40	1.080	57.9	2.8	0.38	0.10
48	1.085	63.6	3.1	0.37	0.10
47	1.090	69.4	3.3	0.36	0.12
41	1.120	112.6	4.1	0.31	0.14
42	1.160	190.9	5.2	0.26	0.18
43	1.200	292.0	6.2	0.23	0.21

* : Energy Release to Time of Peak Power
** : Time to Peak Power
*** : Reactivity Compensation at Peak Power

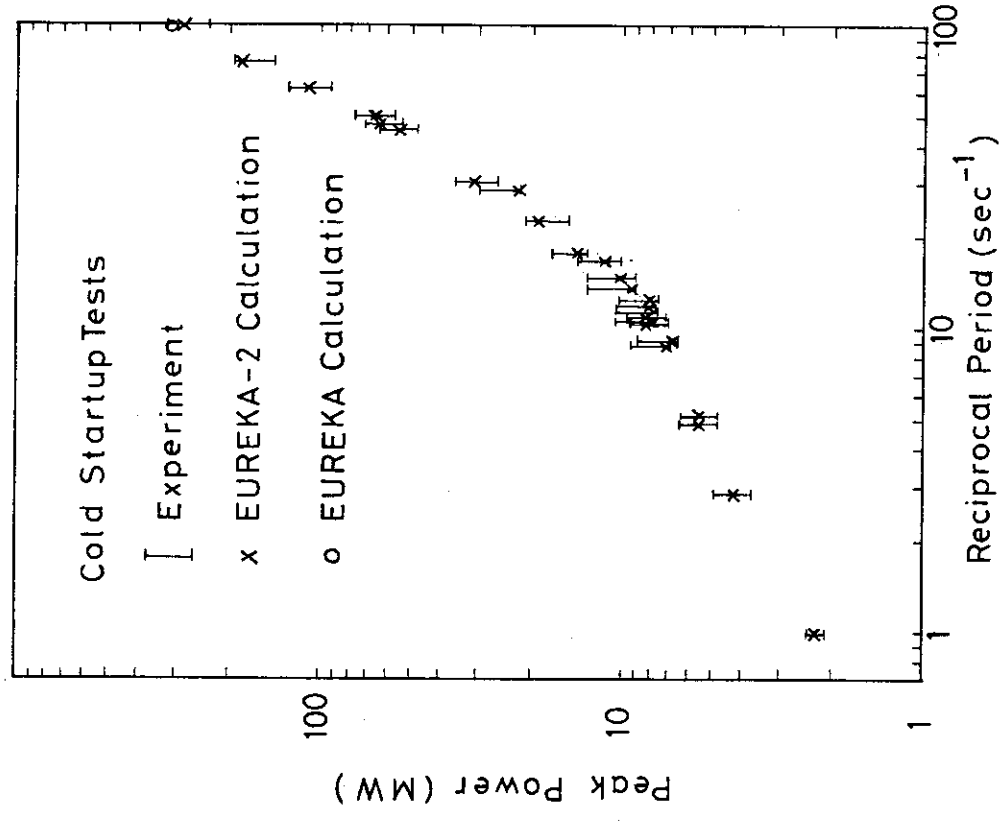

Fig. 4.5 Experimental and EUREKA-2 calculated peak power as functions of reciprocal period for the cold-startup tests

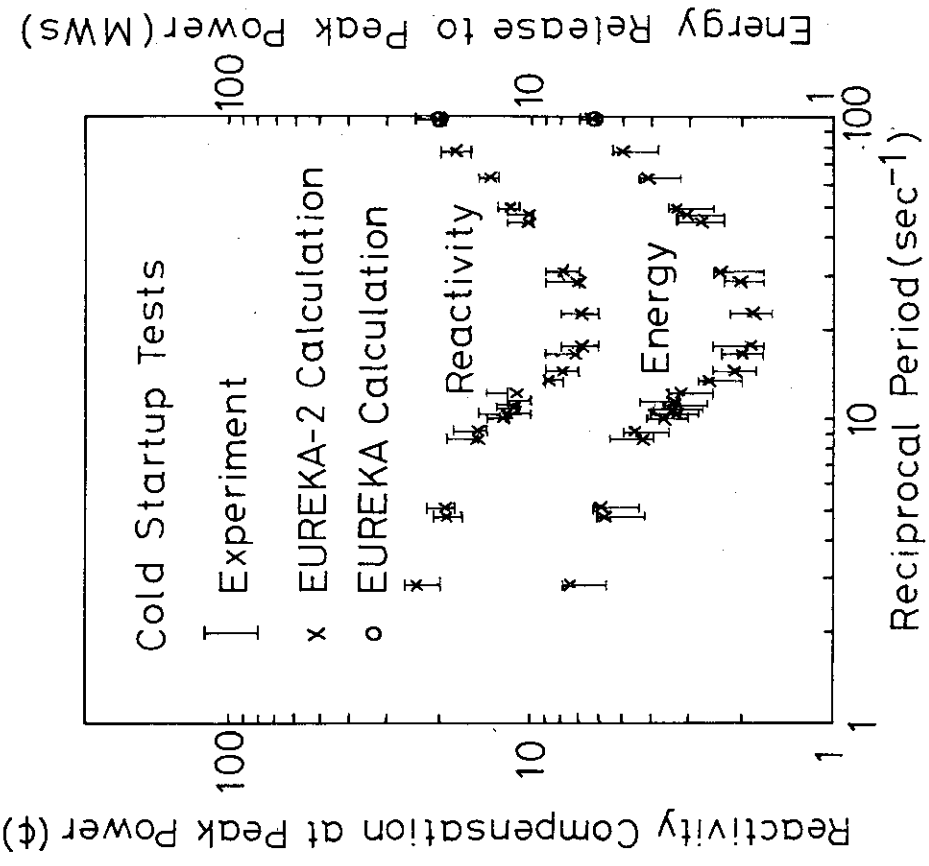

Fig. 4.6 Experimental and EUREKA-2 calculated energy release to peak power and reactivity compensation at peak power as functions of reciprocal period for the cold-startup tests

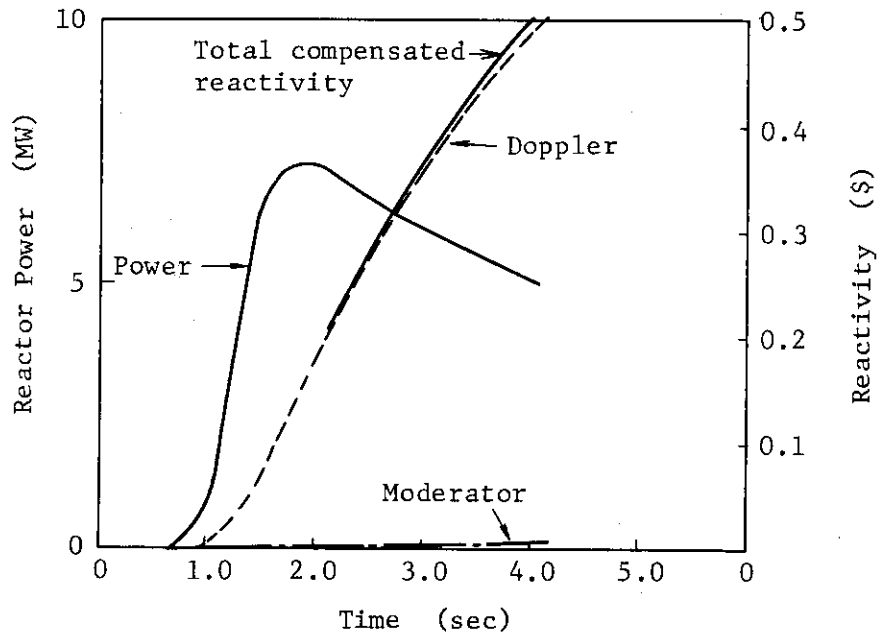

Fig. 4.7 EUREKA-2 calculated reactivity compensation for 70°F cold-startup test 23.

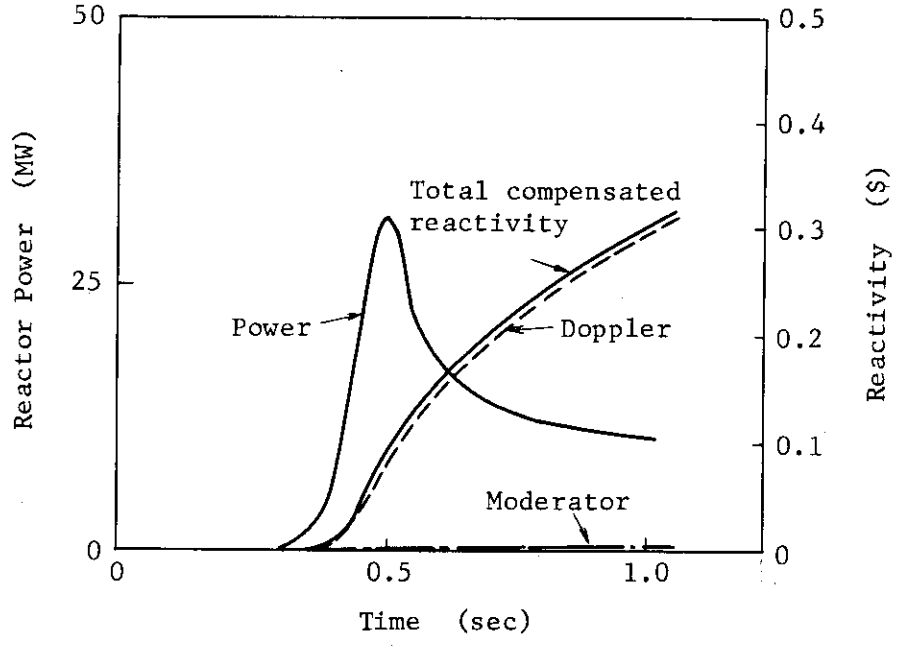

Fig. 4.8 EUREKA-2 calculated reactivity compensation for 70°F cold-startup test 75.

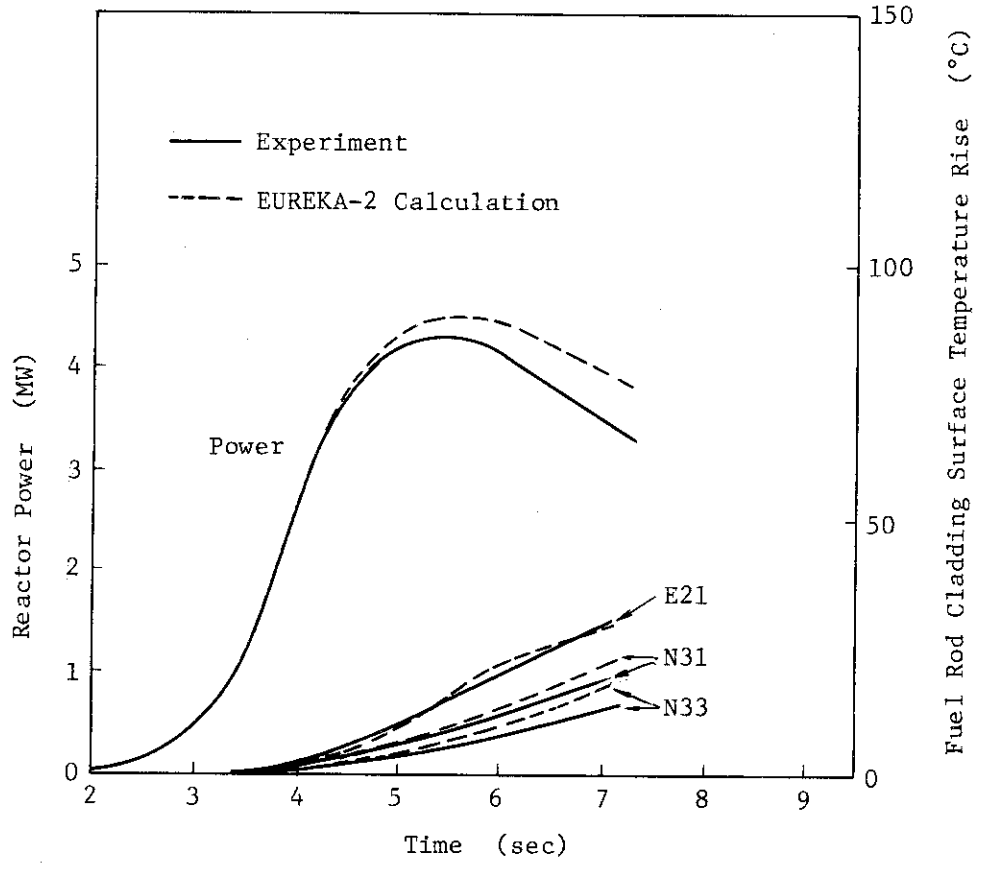

Fig. 4.9 Experimental and EUREKA-2 calculated fuel rod cladding surface temperature rises for cold-startup test 18.

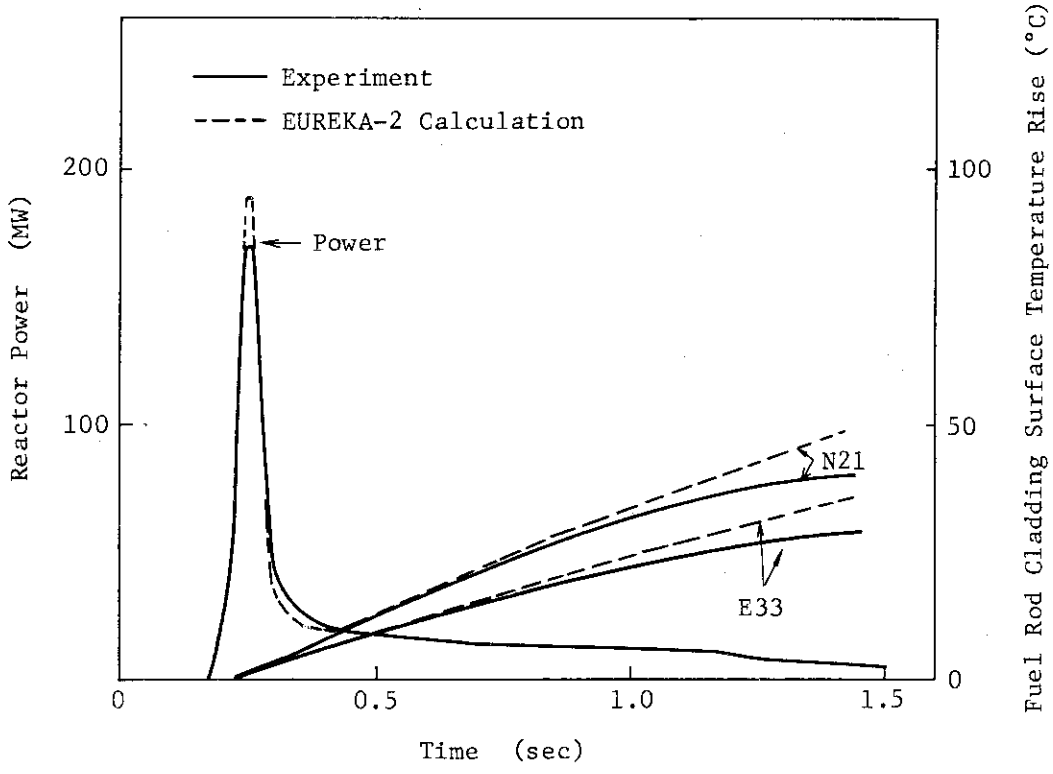

Fig. 4.10 Experimental and EUREKA-2 calculated fuel rod cladding surface temperature rises for cold-startup test 42.

(2) Hot-startup Reactivity Accident Tests

33 hot-startup tests are reported in the SPERT III-E tests. The transient tests are all performed from the initial powers (10 to 50 watts) and an initial system pressure of 1500 psig. Two complete series of hot-startup reactivity accident tests are done. The first test is initiated from the system temperature of about 260°F and the second is performed with an initial temperature of about 500°F. A summary of the hot-startup reactivity accident test data is presented in Table 4.4.

Comparisons between EUREKA-2 calculation and experimental measurements for time-dependent reactor power, energy and system reactivity are shown in the appendix in Fig. B.1 through B.13 for an initial system temperature of 260°F and in Fig. B.14 through B.31 for 500°F tests. Table 4.5 presents the summary of the analytical result for hot-startup accident tests. EUREKA-2 calculated and experimental peak power, energy release to peak power and reactivity compensation at peak power are shown as a function of reciprocal period in Fig. 4.11 and 4.12 for the 260°F and in Fig. 4.13 and 4.14 for the 500°F hot-startup tests. The EUREKA-2 calculated points fall within the experimental uncertainties in the entire range of reciprocal periods. Exception was the data of energy release of test No. 53 and 65. Over the 26 hot-startup tests except for these two tests, the largest disagreement between the experiment and the EUREKA-2 calculation is about 13% for peak power, about 18% for energy release and 20% for reactivity compensation. The EUREKA code calculates the excursions of three hot-startup tests of No. 56, 60 and 62[8]. EUREKA-2 calculated time-dependent reactivity feedback contributions for the 250°F hot-startup test 29 (19.6 msec period) and the 500°F test 62 (20.6 msec period) are shown in Fig. 4.15 and 4.16, respectively. The EUREKA-2 calculated fuel and moderator heating reactivity compensation at the time of peak power is shown in Table 4.9. For the E-core, PMH (prompt moderator heating) reactivity feedback becomes an important feedback mechanism at elevated initial system temperature as a result of the change in water density with temperature. PHM feedback contributes about 1% of the total reactivity feedback for the 70°F tests, about 5% for the 260°F test, and about 14% for the 500°F test. While these percentages are smaller than those of the PARET calculated PHM feedback, EUREKA-2 and PARET are shown to present a similar dependency of the moderator heating on initial system temperature.

Table 4.4 Data summary for hot-startup reactivity accident tests

Test No.	Reactor Period (msec)	Initial Reactivity Insertion ($)	Primary Coolant Inlet Temperature (°F)	Average Primary Coolant Flow Rate (fps)	Maximum Reactor Power (MW)	Energy Release to Time of Peak Power (MW-sec)	Time to Peak Power (sec)	Maximum Measured Fuel Cladding Surface Temperature Rise (°F)	Reactivity Compensation at Peak Power ($)
24	1140 ± 20	0.75 ± 0.03	259 ± 4	14	3.0 ± 0.5[a]	16 ± 2.7	18.0 ± 0.1	13 ± 1	0.35 ± 0.04
25	1090 ± 20	0.76 ± 0.03	259 ± 4	14	2.8 ± 0.4[a]	8.9 ± 1.5	14.9 ± 0.1	8 ± 1	0.22 ± 0.02
36	249 ± 5	0.92 ± 0.04	259 ± 4	22	6.2 ± 0.9	9.0 ± 1.5	4.5 ± 0.2	21 ± 2	0.25 ± 0.03
26	209 ± 4	0.93 ± 0.04	259 ± 4	14	6.8 ± 1.0	7.6 ± 1.3	3.6 ± 0.1	24 ± 2	0.22 ± 0.02
30	118 ± 2	0.97 ± 0.04	259 ± 4	2.4	7.8 ± 1.2	4.8 ± 0.8	1.98 ± 0.05	66 ± 7	0.15 ± 0.02
37	108 ± 2	0.98 ± 0.04	259 ± 4	19	8.9 ± 1.3	5.7 ± 1.0	1.9 ± 0.1	22 ± 2	0.18 ± 0.02
33	103 ± 2	0.98 ± 0.04	259 ± 4	22	9.4 ± 1.4	5.1 ± 0.9	1.7 ± 0.1	28 ± 3	0.16 ± 0.02
27	102 ± 2	0.98 ± 0.04	259 ± 4	14	9.1 ± 1.4	4.3 ± 0.7	1.6 ± 0.05	26 ± 3	0.14 ± 0.02
35	87.0 ± 1.7	0.99 ± 0.04	259 ± 4	22	9.8 ± 1.5	4.1 ± 0.7	1.4 ± 0.1	28 ± 3	0.14 ± 0.02
34	69.9 ± 1.4	1.00 ± 0.04	259 ± 4	22	11 ± 2	3.2 ± 0.5	1.17 ± 0.03	25 ± 3	0.11 ± 0.01
28	41.6 ± 0.8	1.03 ± 0.04	259 ± 4	14	22 ± 3	2.0 ± 0.3	0.64 ± 0.01	31 ± 3	0.08 ± 0.01
31	39.6 ± 0.8	1.04 ± 0.04	259 ± 4	2.4	23 ± 3	2.0 ± 0.3	0.60 ± 0.02	88 ± 9	0.08 ± 0.01
32	21.8 ± 0.4	1.09 ± 0.04	259 ± 4	2.4	66 ± 10	3.3 ± 0.5	0.39 ± 0.01	103 ± 10	0.11 ± 0.01
29	19.6 ± 0.4	1.10 ± 0.04	259 ± 4	14	78 ± 12	3.2 ± 0.5	0.36 ± 0.01	44 ± 4	0.12 ± 0.01
70	10.3 ± 0.2	1.21 ± 0.05	251 ± 4	14	280 ± 42	6.3 ± 1.1	0.20 ± 0.01	58 ± 6	0.22 ± 0.02
52	2260 ± 50	0.64 ± 0.03	500 ± 4	14	0.14 ± 0.01[a]	0.45 ± 0.06	20 ± 0.1	~0	0.06 ± 0.01
53	1060 ± 20	0.77 ± 0.03	500 ± 4	14	4.0 ± 0.4[a]	14 ± 2	15 ± 0.1	10 ± 1	0.27 ± 0.03
63	592 ± 10	0.84 ± 0.03	501 ± 4	14	5.6 ± 0.6	15 ± 2	9.2 ± 0.2	21 ± 2	0.29 ± 0.03
64	575 ± 10	0.82 ± 0.03	501 ± 4	4.8	4.8 ± 0.5	12 ± 2	8.8 ± 0.2	41 ± 4	0.29 ± 0.03
65	440 ± 9	0.87 ± 0.03	500 ± 4	24	6.6 ± 0.7	13 ± 2	7.0 ± 0.2	13 ± 1	0.26 ± 0.03
54	223 ± 4	0.93 ± 0.04	498 ± 4	14	8.7 ± 0.9	11 ± 1	3.8 ± 0.1	17 ± 2	0.24 ± 0.03
55	70.2 ± 1.4	1.00 ± 0.04	500 ± 4	14	16 ± 2	3.3 ± 0.4	1.00 ± 0.03	19 ± 2	0.08 ± 0.01
56	37.9 ± 0.8	1.04 ± 0.04	501 ± 4	14	35 ± 4	3.1 ± 0.4	0.62 ± 0.007	26 ± 3	0.08 ± 0.01
57	21.7 ± 0.4	1.09 ± 0.04	500 ± 4	14	89 ± 9	4.4 ± 0.6	0.400 ± 0.005	31 ± 3	0.12 ± 0.01
62	20.6 ± 0.4	1.10 ± 0.04	500 ± 4	14	97 ± 10	4.5 ± 0.6	0.370 ± 0.005	30 ± 3	0.12 ± 0.01
61	17.8 ± 0.4	1.12 ± 0.04	500 ± 4	14	120 ± 12	4.9 ± 0.6	0.335 ± 0.005	32 ± 3	0.14 ± 0.02
68	16.0 ± 0.3	1.13 ± 0.05	500 ± 4	14	160 ± 16	5.5 ± 0.7	0.300 ± 0.005	33 ± 3	0.15 ± 0.02
67	15.5 ± 0.3	1.14 ± 0.05	501 ± 4	4.8	170 ± 17	5.6 ± 0.7	0.300 ± 0.005	60 ± 6	0.16 ± 0.02
66	14.3 ± 0.3	1.15 ± 0.05	501 ± 4	24	190 ± 19	5.8 ± 0.8	0.290 ± 0.005	24 ± 2	0.17 ± 0.02
58	14.1 ± 0.3	1.15 ± 0.05	500 ± 4	14	200 ± 20	6.2 ± 0.8	0.285 ± 0.005	36 ± 4	0.17 ± 0.02
59	13.0 ± 0.3	1.17 ± 0.05	500 ± 4	14	230 ± 23	6.5 ± 0.8	0.280 ± 0.005	37 ± 4	0.18 ± 0.02
60	9.70 ± 0.19	1.23 ± 0.05	500 ± 4	14	410 ± 41	8.5 ± 1.1	0.221 ± 0.005	44 ± 4	0.24 ± 0.03

[a] Test was terminated by scram while power was still rising; peak power taken at time of scram.

Table 4.5 Summary of EUREKA-2 Analyses for Hot-Startup Accident Tests

Test No.	Inserted Reactivity	Peak Power	Energy*	Time**	Compensated*** Reactivity
36	0.915 $	5.7 MW	8.4 MWs	4.35 sec	0.22 $
26	0.930	6.2	7.3	3.54	0.20
30	0.965	7.6	5.0	2.02	0.15
37	0.965	7.9	5.5	2.07	0.16
33	0.980	8.7	4.9	1.72	0.14
27	0.980	9.0	4.4	1.55	0.13
35	0.985	9.5	4.1	1.40	0.12
34	0.993	10.4	3.3	1.17	0.10
28	1.030	21.9	2.3	0.61	0.07
31	1.035	24.4	2.2	0.57	0.07
32	1.085	70.5	3.3	0.37	0.10
29	1.092	80.4	3.5	0.36	0.11
70	1.205	317.0	7.4	0.23	0.23
53	0.775	4.3	19.4	15.03	0.31
63	0.845	5.7	16.3	9.11	0.28
64	0.840	4.6	12.9	9.42	0.27
65	0.872	6.8	16.4	7.33	0.28
54	0.928	8.8	11.2	3.84	0.21
55	1.001	16.8	3.7	1.01	0.08
56	1.035	34.3	3.2	0.60	0.07
57	1.080	88.1	4.4	0.40	0.10
62	1.086	98.3	4.7	0.39	0.11
68	1.118	164.0	5.8	0.32	0.13
67	1.121	169.4	5.8	0.32	0.13
66	1.129	193.5	6.5	0.31	0.14
58	1.135	206.9	6.3	0.30	0.14
59	1.145	236.0	7.2	0.29	0.16
60	1.201	435.5	9.7	0.24	0.21

* : Energy Release to Time of Peak Power
** : Time to Peak Power
*** : Reactivity Compensation at Peak Power

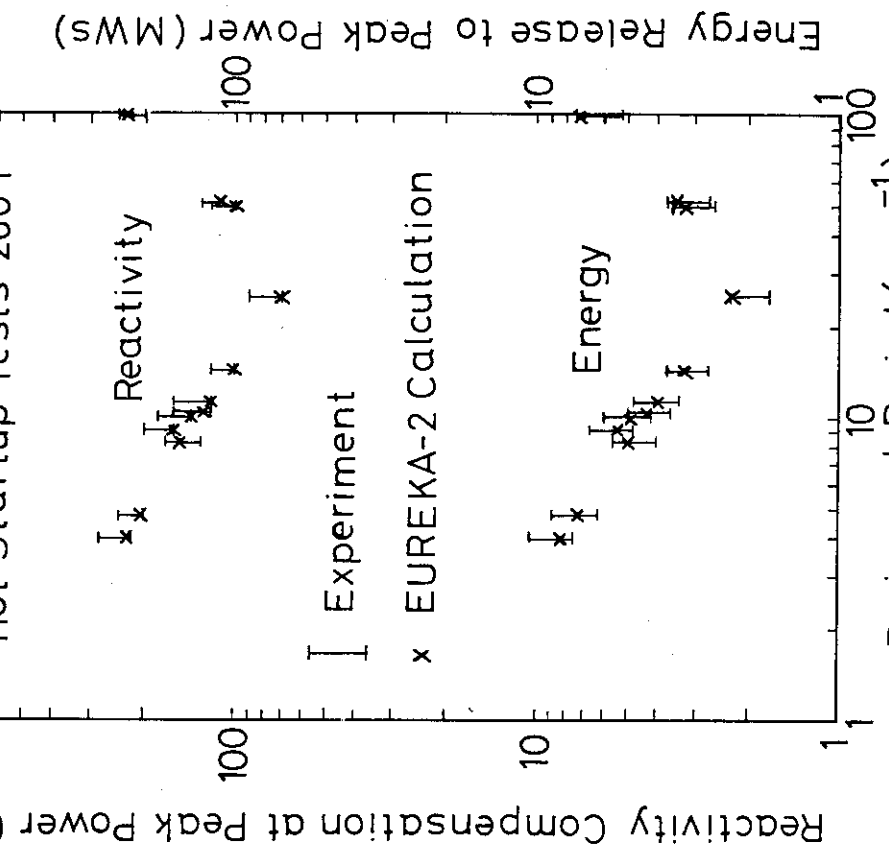

Fig. 4.12 Experimental and EUREKA-2 calculated energy release to peak power and reactivity compensation at peak power as functions of reciprocal period for the 260°F hot-standby tests

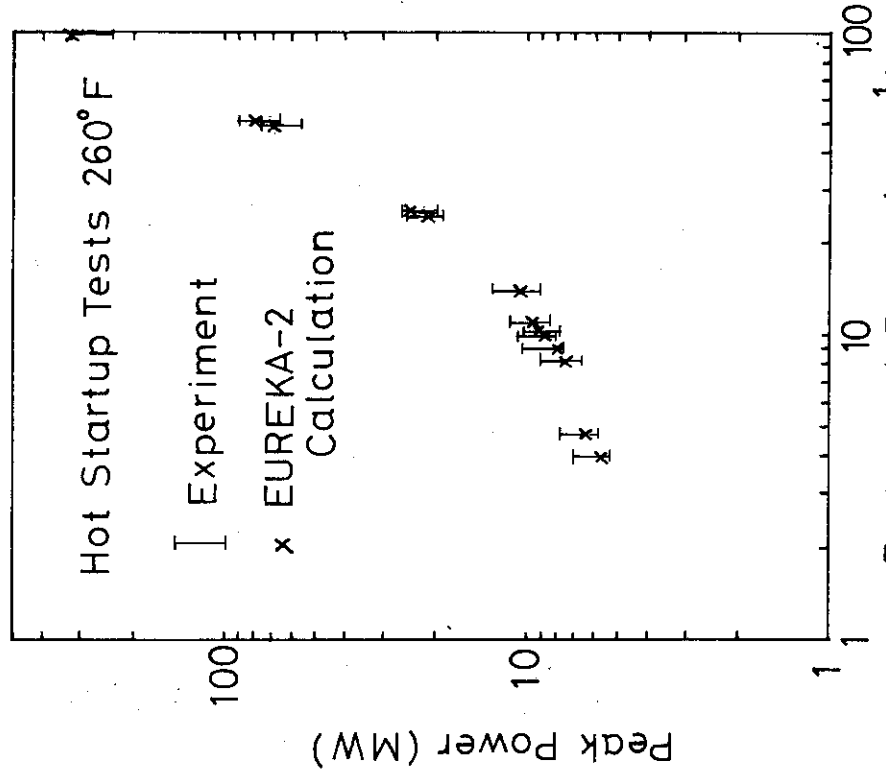

Fig. 4.11 Experimental and EUREKA-2 calculated peak power as functions of reciprocal period for the 260°F hot-startup tests

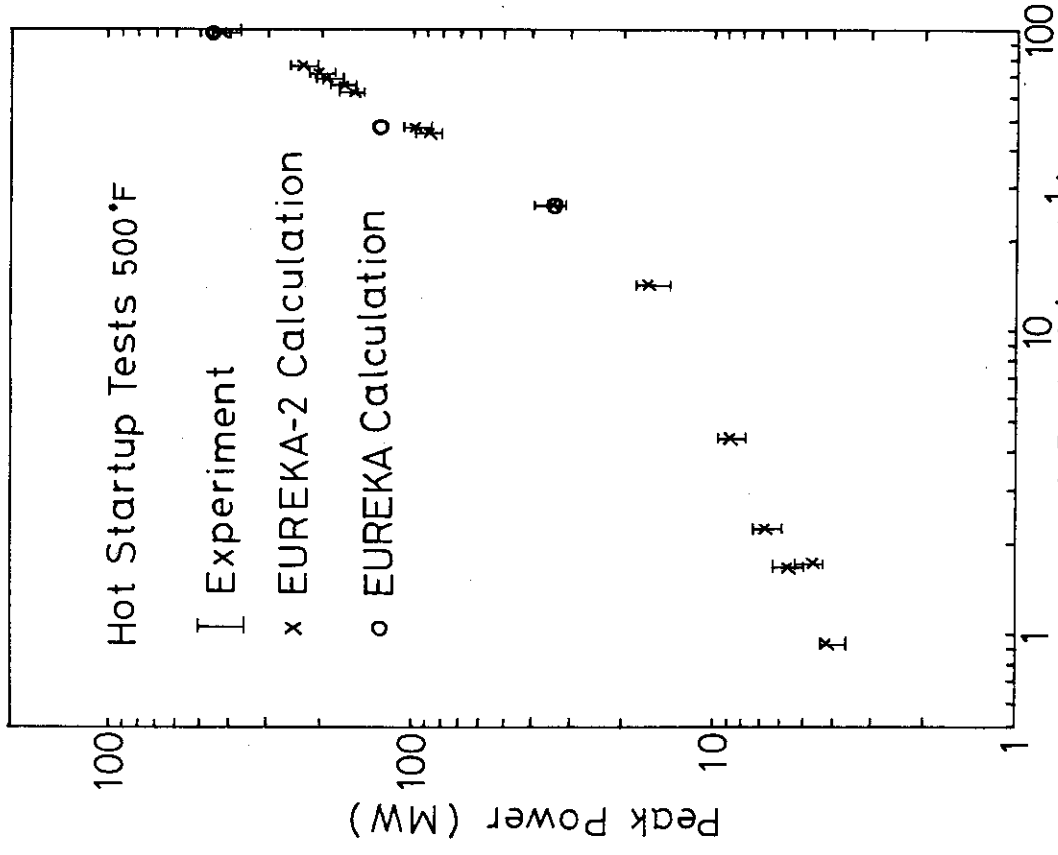

Fig. 4.13 Experimental and EUREKA-2 calculated peak power as functions of reciprocal period for the 500°F hot-startup tests

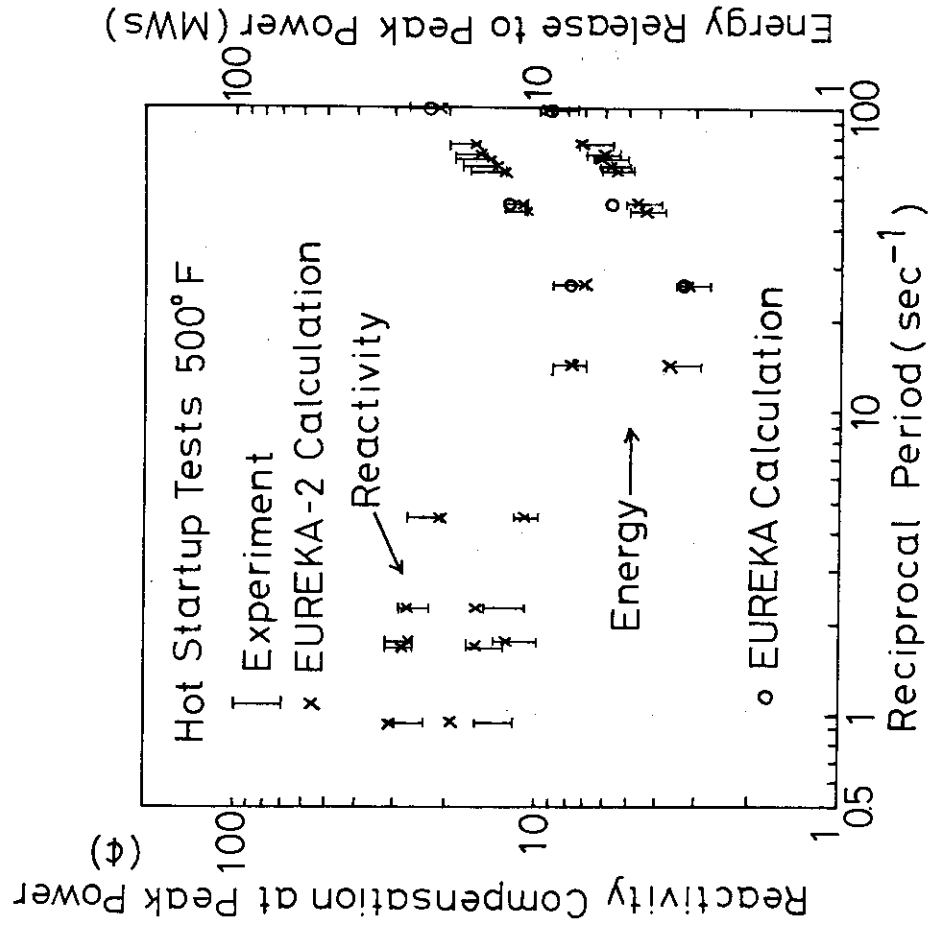

Fig. 4.14 Experimental and EUREKA-2 calculated energy release to peak power and reactivity compensation at peak power as functions of reciprocal period for the 500°F hot-standby tests

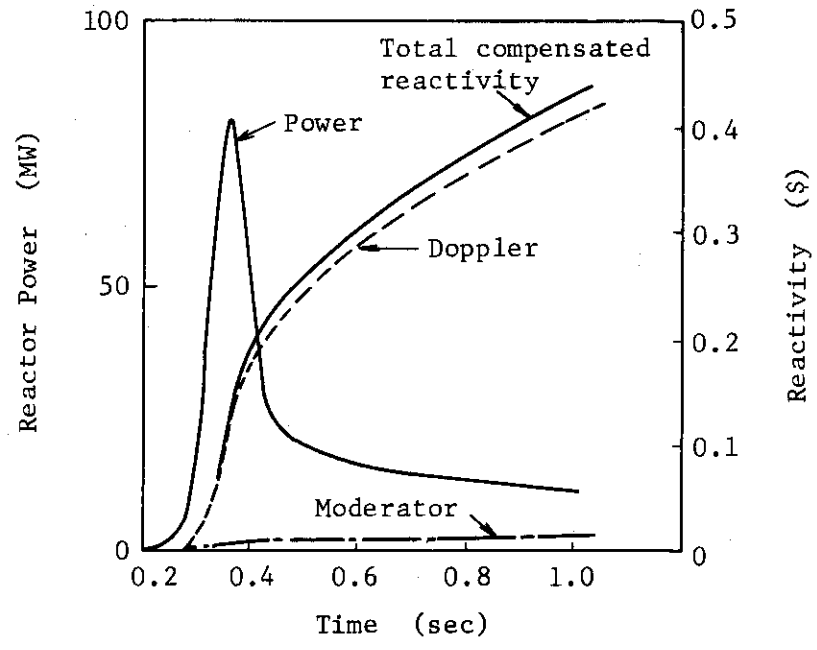

Fig. 4.15 EUREKA-2 calculated reactivity compensation for 260 °F, hot-startup test 29.

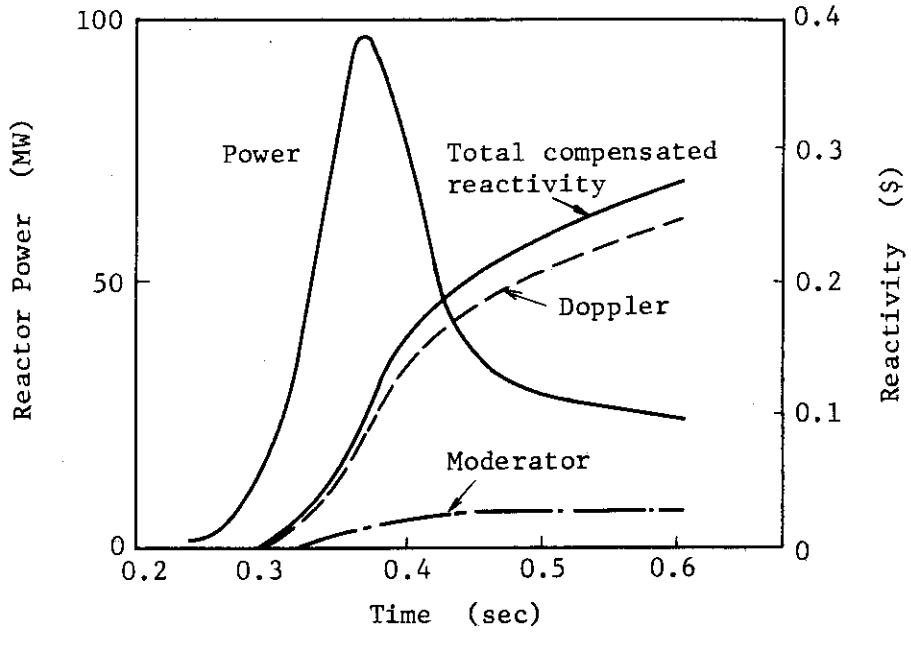

Fig. 4.16 EUREKA-2 calculated reactivity compensation for 500 °F hot-startup test 62.

(3) High-initial-power Reactivity Accident Tests

The high-initial-power tests provide experimental data for reactivity accidents initiated from hot-standby and operating power conditions. The operating conditions chosen for the tests are 500°F inlet coolant temperature, 1500 psig system pressure and 1200 gpm coolant flow. The first series of the tests are performed from a steady state reactor power of about 1 MW. This corresponds to a peak density of about 30 kW/litre of UO $_2$(specific power of 0.8 kW/kg of UO_2), which is representative of hot-standby conditions in commercial PWR's. The second series of the tests are done from an initial reactor power of about 20 MW. This initial power yields a peak power density of about 550 kW/litre of UO_2 (specific power of 16 kW/kg of UO_2) and represents operating-power conditions in commercial PWR's. A summary of the experimental results is presented in Table 4.6. The calculated peak power and net energy release to peak power are shown in Fig. 4.17 and 4.18, respectively. Time-dependent reactor power, net energy release and net system reactivity are shown in the Figure C.1 through C.8 of the appendix. The EUREKA-2 calculations are well within the uncertainties of the experimental data. Table 4.7 shows the summary of the analytical result for hot-standby and operating-power reactivity accident tests. The largest disagreement between the experiment and the EUREKA-2 calculation is about 8% for peak power, about 15% for energy release and about 22% for reactivity compensation for the entire hot-standby tests. The EUREKA code shows the analytical results of a hot-standby test (No. 81) and an operating-power tests (No. 86)[8]. The core hot-spot cladding surface temperature is measured by the thermo couple located 16 inches above the bottom of the fuel rod. Table 4.8 shows the calculated surface temperature along with the experimental data. The calculation provides a good agreement with the experiment, although the calculated maximum surface temperature of the operating power test is rather higher than the experimental data. EUREKA-2 calculated time-dependent reactivity feedback contributions for the 500°F hot-standby test 81 and the 20 MW operating power test 86 are shown in Fig. 4.19 and Fig. 4.20.

Table 4.6 Data summary for hot-standby and operating-power reactivity accident tests

Test No.	Initial Reactivity Insertion ($)	Primary Coolant Inlet Temperature (°F)	Average Primary Coolant Flow Rate (fps)	Initial Reactor Power (MW)	Maximum Reactor Power (MW)	Net Energy Release[a] to time of Peak Power (MW-sec)	Time to Peak Power (sec)	Maximum Measured Fuel Cladding Surface Temperature (°F)	Reactivity Compensation[b] at Peak Power ($)
79	0.86 ± 0.03	513 ± 4	14	1.1 ± 0.1	13 ± 1	6.7 ± 0.9	0.68 ± 0.08	510 ± 10	0.09
80	1.08 ± 0.04	506 ± 4	14	1.3 ± 0.1	120 ± 10	4.5 ± 0.6	0.150 ± 0.003	530 ± 10	0.11
81	1.17 ± 0.04	504 ± 4	14	0.9 ± 0.1	330 ± 30	7.8 ± 1	0.135 ± 0.003	540 ± 10	0.18
83	1.25 ± 0.04	504 ± 4	14	1.1 ± 0.1	620 ± 60	11 ± 1	0.117 ± 0.002	540 ± 10	0.26
82	1.29 ± 0.04	505 ± 4	14	1.2 ± 0.1	880 ± 90	15 ± 2	0.118 ± 0.002	550 ± 10	0.30
84	0.46 ± 0.02	505 ± 4	14	19 ± 1	39 ± 4	4.7 ± 0.6	0.18 ± 0.02	590 ± 10	0.03
85	0.87 ± 0.04	503 ± 4	14	19 ± 1	130 ± 10	14 ± 2	0.155 ± 0.005	590 ± 10	0.04
86	1.17 ± 0.05	502 ± 4	14	19 ± 1	610 ± 60	17 ± 2	0.110 ± 0.005	600 ± 10	0.22

[a] Incremental energy released during burst above that resulting from steady state operation.

[b] Because of uncertainties in initial reactivity insertions and peak power times these values are only approximate.

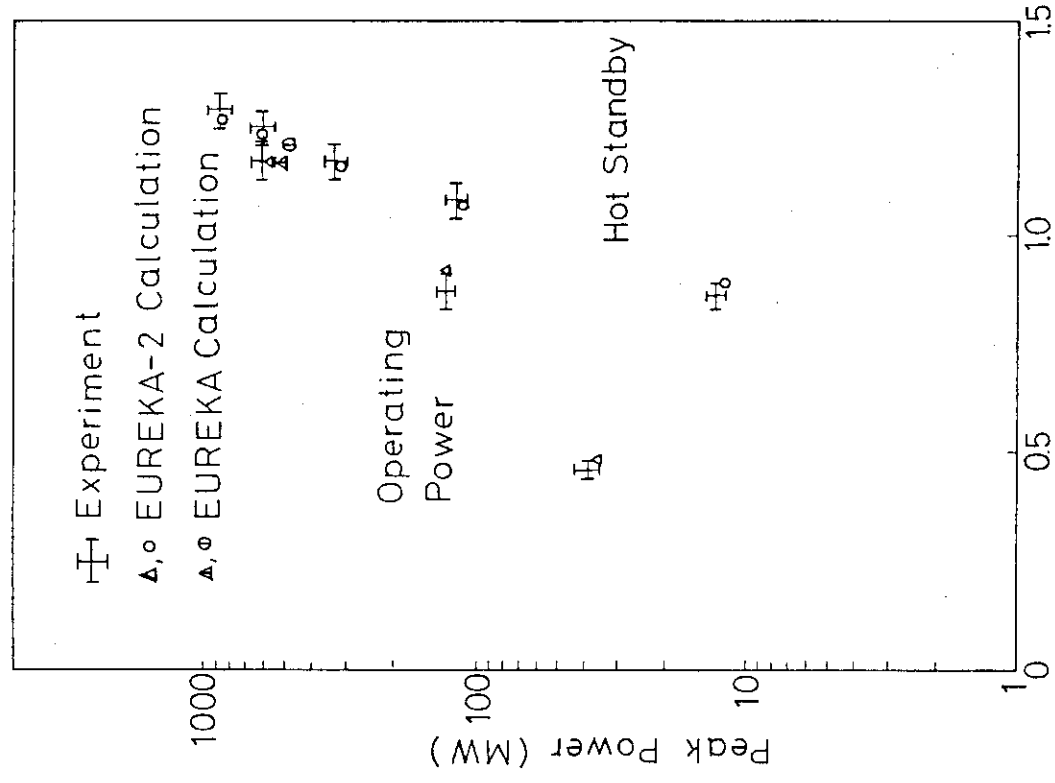

Fig. 4.17 Experimental and EUREKA-2 calculated peak reactor powers as functions of reactivity for the hot-standby and operating-power tests

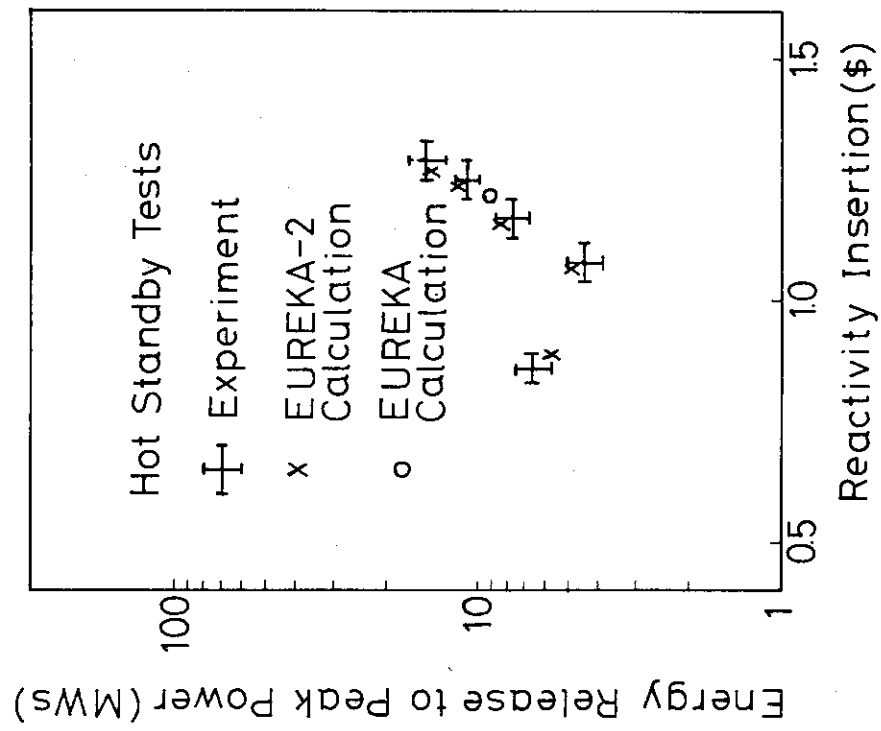

Fig. 4.18 EUREKA-2 calculated and experimental net energy release to peak power as functions of reactivity insertion for hot-standby tests

Table 4.7 Summary of EUREKA-2 analyses for hot-standby and operating-power reactivity accident tests

Test No.	Inserted Reactivity	Peak Power	Energy*	Time**	Compensated Reactivity***
79	0.89 $	12.0 MW	5.7 MWs	0.58 s	0.11 $
80	1.07	114.7	5.0	0.151	0.10
81	1.16	323.8	8.6	0.137	0.18
82	1.27	874.9	14.8	0.117	0.30
83	1.228	626.9	12.2	0.123	0.25
84	0.48	35.1	2.7	0.098	0.01
85	0.92	131.5	6.0	0.104	0.07
86	1.17	589.4	10.4	0.100	0.21

* : Energy Release to Time of Peak Power
** : Time to Peak Power
*** : Reactivity Compensation at Peak Power

Table 4.8 Maximum fuel cladding surface temperature - hot standby and operating power tests

Test No.	Experiment	EUREKA-2 Calculation
79	266 ± 6 °C	280 °C
80	277 ± 6	281
81	282 ± 6	281
82	288 ± 6	286
83	282 ± 6	284
84	310 ± 6	319
85	310 ± 6	326
86	316 ± 6	333

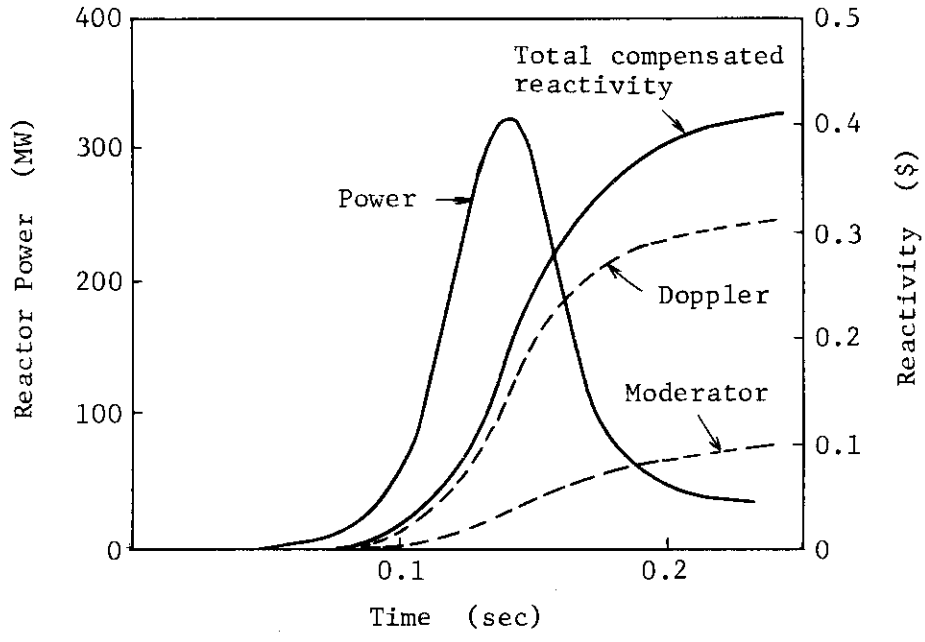

Fig. 4.19 EUREKA-2 calculated reactivity compensation for 500 °F hot-standby test 81.

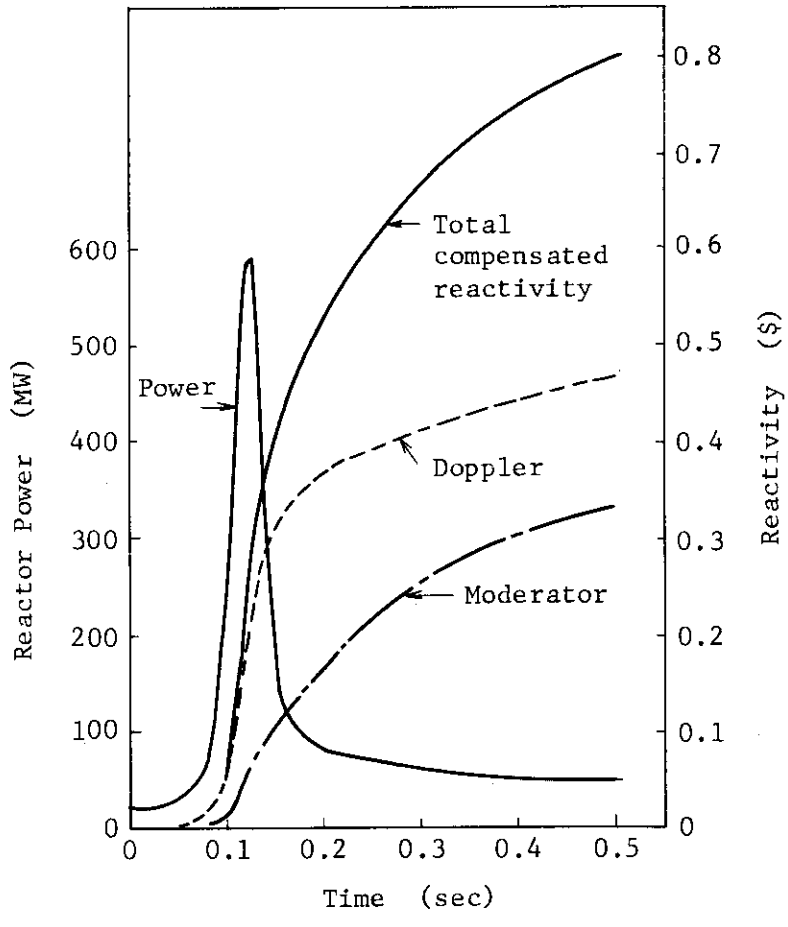

Fig. 4.20 EUREKA-2 calculated reactivity compensation for 20 MW operating power test 86.

Table 4.9 EUREKA-2 Calculated Fuel and Moderator Heating Reactivity Compensation at the Time of Peak Power

Test No.	Initial Reactor Power (MW)	Primary Coolant Inlet Temperature (°F)	Initial Reactivity Insertion ($)	Fuel Heating Compensation (% of total)	Moderator Heating Compensation (% of total)
23	5×10^{-5}	70	0.97	99	1
75	5×10^{-5}	68	1.05	99	1
29	5×10^{-5}	260	1.092	95	5
62	5×10^{-5}	500	1.086	86	14
81	0.9	500	1.16	80	20
86	19.0	500	1.17	78	22

5. Concluding Remarks

The EUREKA-2 code was evaluated by using the experimental data of the SPERT III E-Core reactivity accident tests. The code yielded excellent predictions comparing with the experiment in the range of 10 to 25% for all accident conditions tested. The Doppler coefficient was shown to be much smaller than the value used in the PARET calculation. We could not discuss the UO_2-fuel temperature because the fuel temperature is not available in the SPERT III E-Core experiment. However, the good agreement between the EUREKA-2 calculated reactor power and net energy release and the experimental results, would make the Doppler coefficient obtained by the EUREKA-2 calculation reasonable.

The EUREKA-2 code will be evaluated using the experimental data of the SPERT III C-Core (plate type fuel) where the power excursions are essentially limited by the voiding in the moderator.

Acknowledgements

We are grateful to Dr. M. Ishikawa for continuous encouragement and support.

5. Concluding Remarks

The EUREKA-2 code was evaluated by using the experimental data of the SPERT III E-Core reactivity accident tests. The code yielded excellent predictions comparing with the experiment in the range of 10 to 25% for all accident conditions tested. The Doppler coefficient was shown to be much smaller than the value used in the PARET calculation. We could not discuss the UO_2-fuel temperature because the fuel temperature is not available in the SPERT III E-Core experiment. However, the good agreement between the EUREKA-2 calculated reactor power and net energy release and the experimental results, would make the Doppler coefficient obtained by the EUREKA-2 calculation reasonable.

The EUREKA-2 code will be evaluated using the experimental data of the SPERT III C-Core (plate type fuel) where the power excursions are essentially limited by the voiding in the moderator.

Acknowledgements

We are grateful to Dr. M. Ishikawa for continuous encouragement and support.

References

1) N. Ohnishi, T. Harami, H. Hirose and M. Uemura, "EUREKA-2: A Computer Code for the Reactivity Accident Analysis in a Water Cooled Reactor", JAERI-M 84-074 (1984)

2) R.K. McCardell, D.I. Herborn and J.E. Houghtaling, "Reactivity Accident Test Results and Analyses for the SPERT III E-Core -- A Small, Oxide-Fueled, Pressurized-Water Reactor", IDO-17281 (1969)

3) M. Ishikawa, Y. Kuge, N. Ohnishi, E. Takeuchi and Y. Kanbayashi, "EUREKA: A Computer Code for Uranium-Oxide Fueled, Water Cooled Reactor Kinetic Analysis", JAERI-1235 (1974)

4) C.F. Obenchain, "PARET: A Program for the Analysis of Reactor Transients", IDO-17282 (1969)

5) R.J. Wagner, "IREKIN: Program for the Numerical Solution of the Reactor Kinetic Equations", IDO-16928 (1963)

6) J.E. Houghtaling, J.A. Norberg and J.C. Haire, "Addendum to the SPERT III Hazards Summary Report --- Low-Enrichment Oxide Core", IDO-17003 (1965).

7) R.M. Potenza, J.C. Haire and W.E. Nyer, "Quarterly Technical Report SPERT Project, January, February, March", IDO-17206 (1966)

8) M. Ishikawa, Y. Kuge, Y. Kambayashi, E. Takeuchi, N. Ohnishi, and H. Hatta, "Fast Transient Analysis for Light Water Power Reactor by EUREKA, Coupled Nuclear Thermal-Hydrodynamic Kinetic Code", JAERI-1201 (1971).

9) M. Ishikawa, "Analysis of Prompt Moderator Heating Reactivity Feedback Effect", JAERI 1214 (1971)

10) W.K. Anderson and G.L. Lechliter, "Some Input Properties for Computer Description of Fuel Properties-Part I Thermal Properties", ANS Trans. Act. Vol. 9, No. 2, p.375-376 (1966)

Appendix Plots of the calculated and the experimental reactor power, energy release and total compensated reactivity

A summary of transient data of the EUREKA-2 calculated and the experimental reactor power, energy release and total compensated reactivity is presented in graphical form in this appendix. The cold-startup reactivity accident tests are shown in the figure of A.1 through A.30, the hot-startup reactivity accident tests are presented in the figure of B.1 through B.31 and the high-initial tests are shown in the figure of C.1 through C.8. Each figure has the following symbols.

ρ_i^E = total reactivity inserted experimentally
ρ_i^C = total reactivity inserted in the calculation
T_i = inlet coolant temperature
Flows = average coolant flow rate through the core
P_i = initial system temperature
τ = asymptotic reactor period.

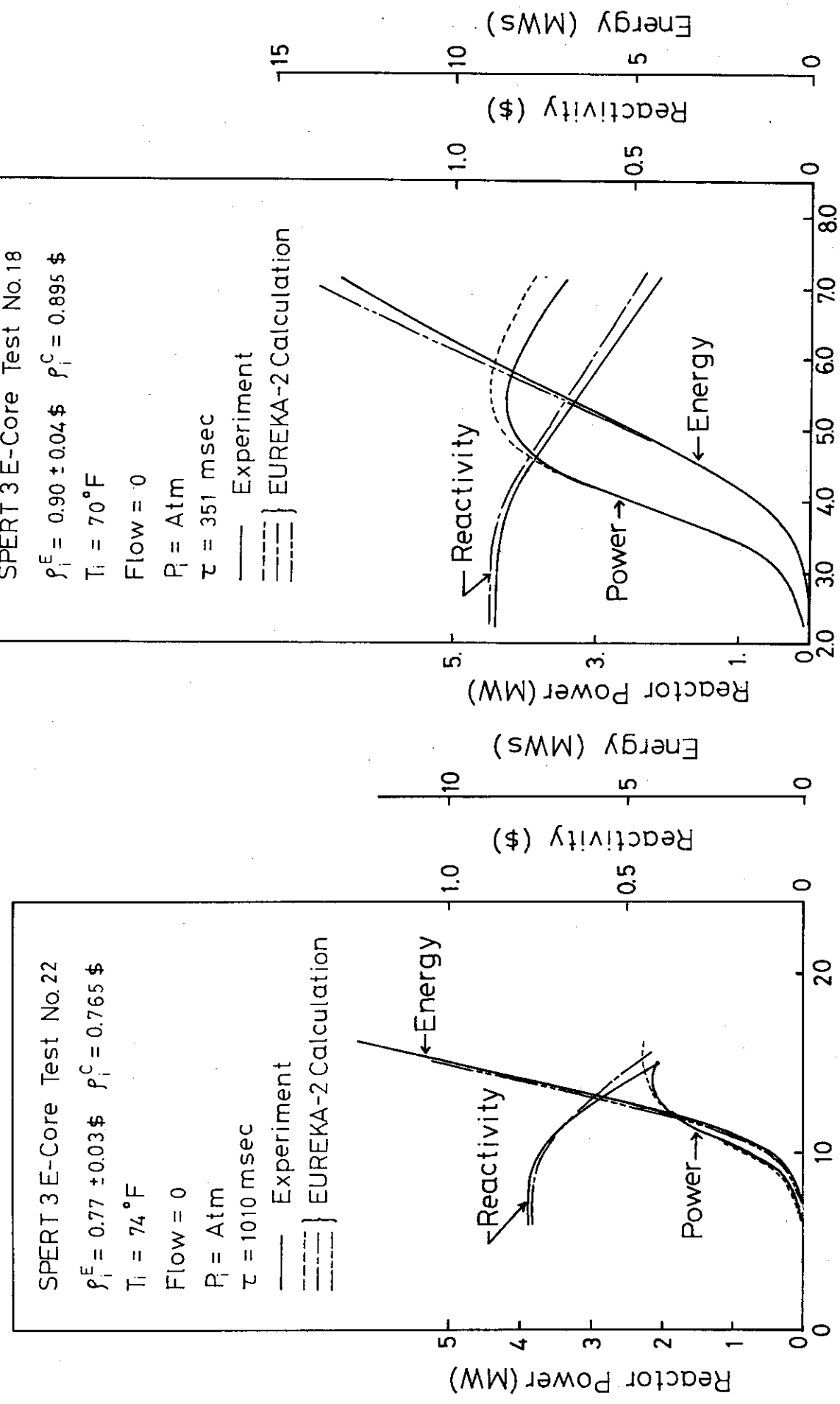

Fig. A.1 SPERT3E-core test No. 22

Fig. A.2 SPERT 3E-Core Test No. 18

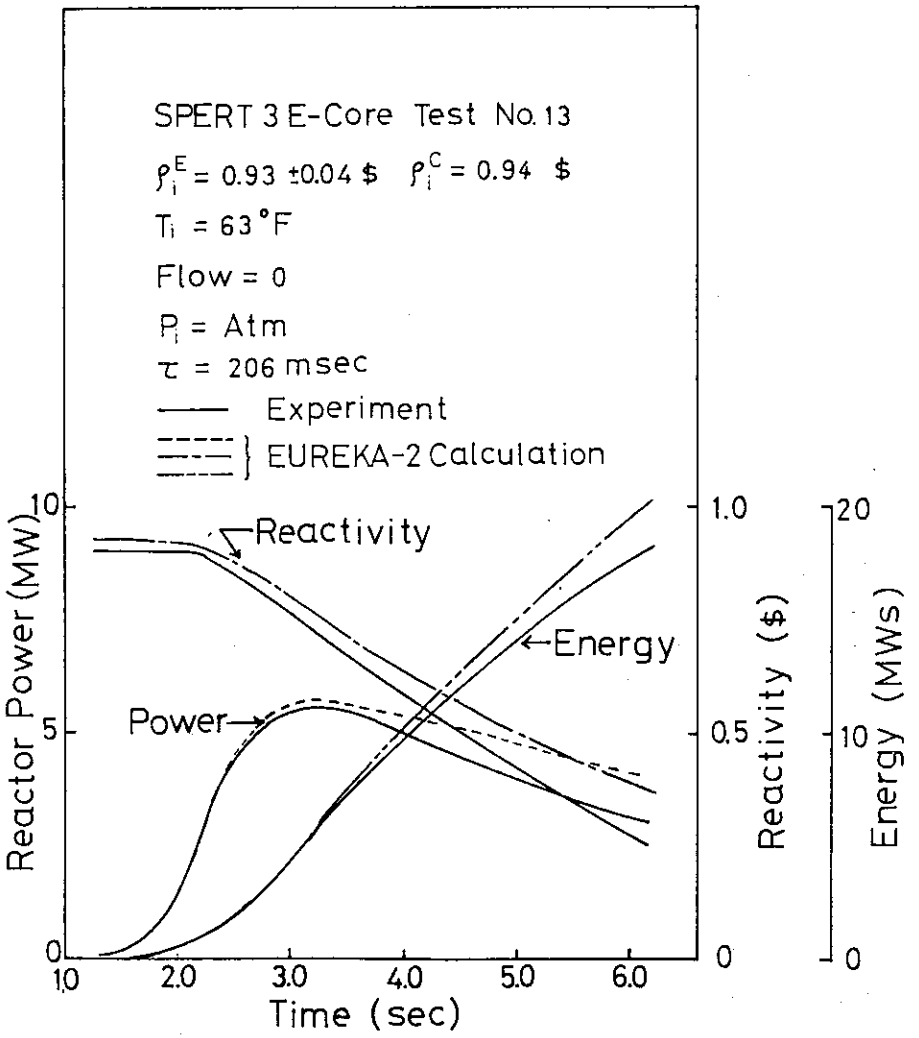

Fig. A.3 SPERT 3E-Core Test No. 13

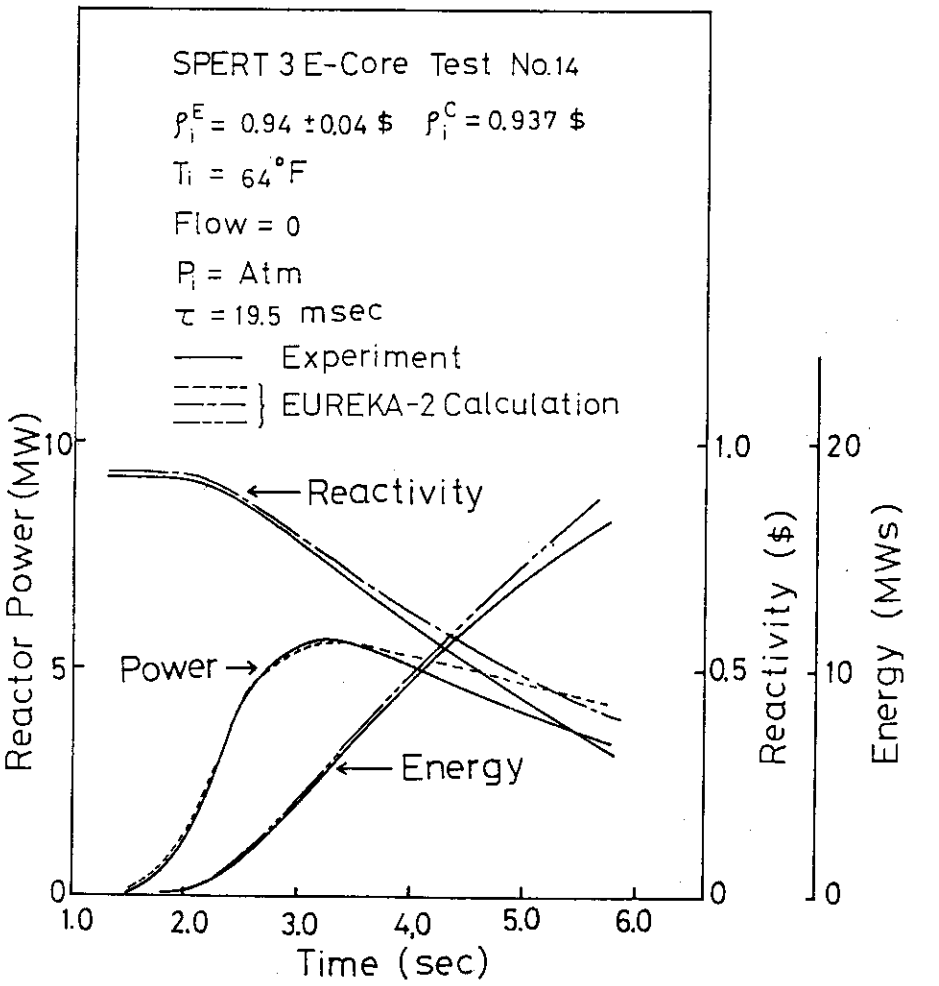

Fig. A.4 SPERT 3E-Core Test No. 14

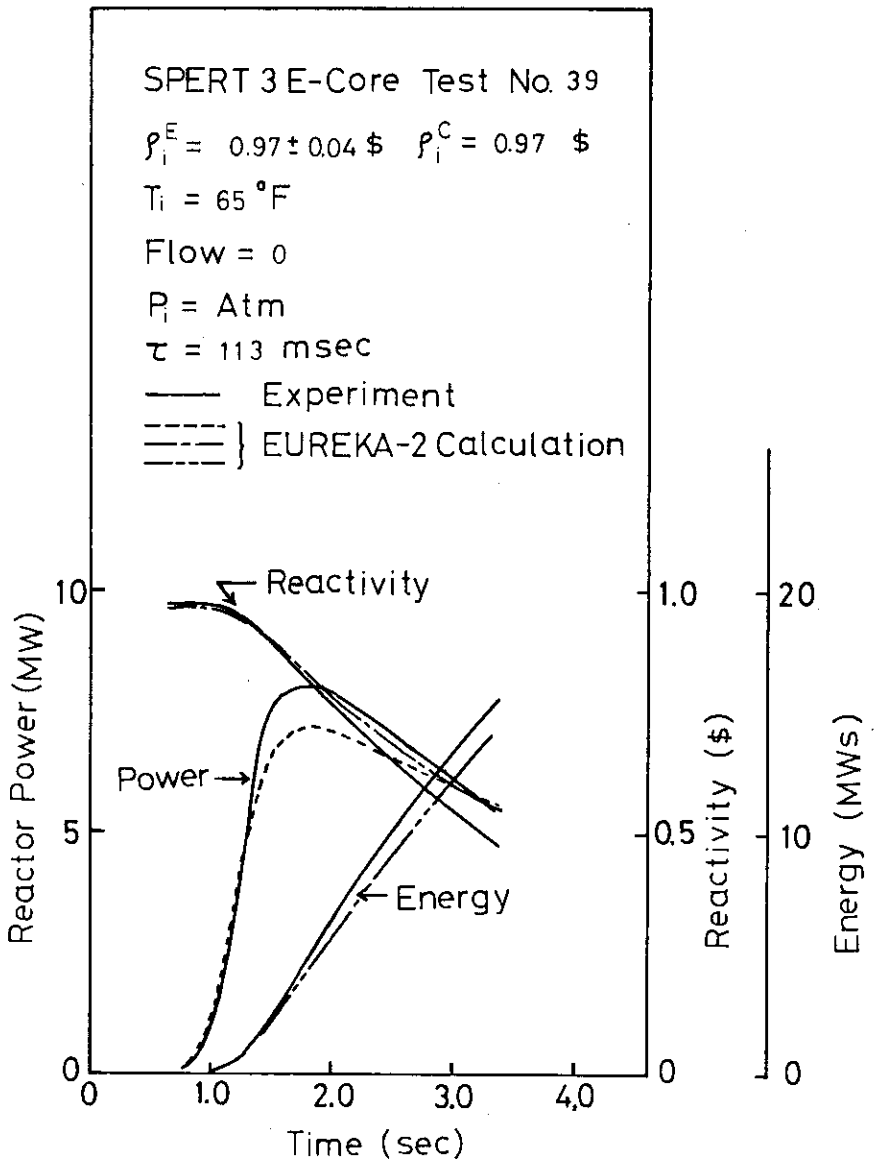

Fig. A.5 SPERT 3E-Core Test No. 39

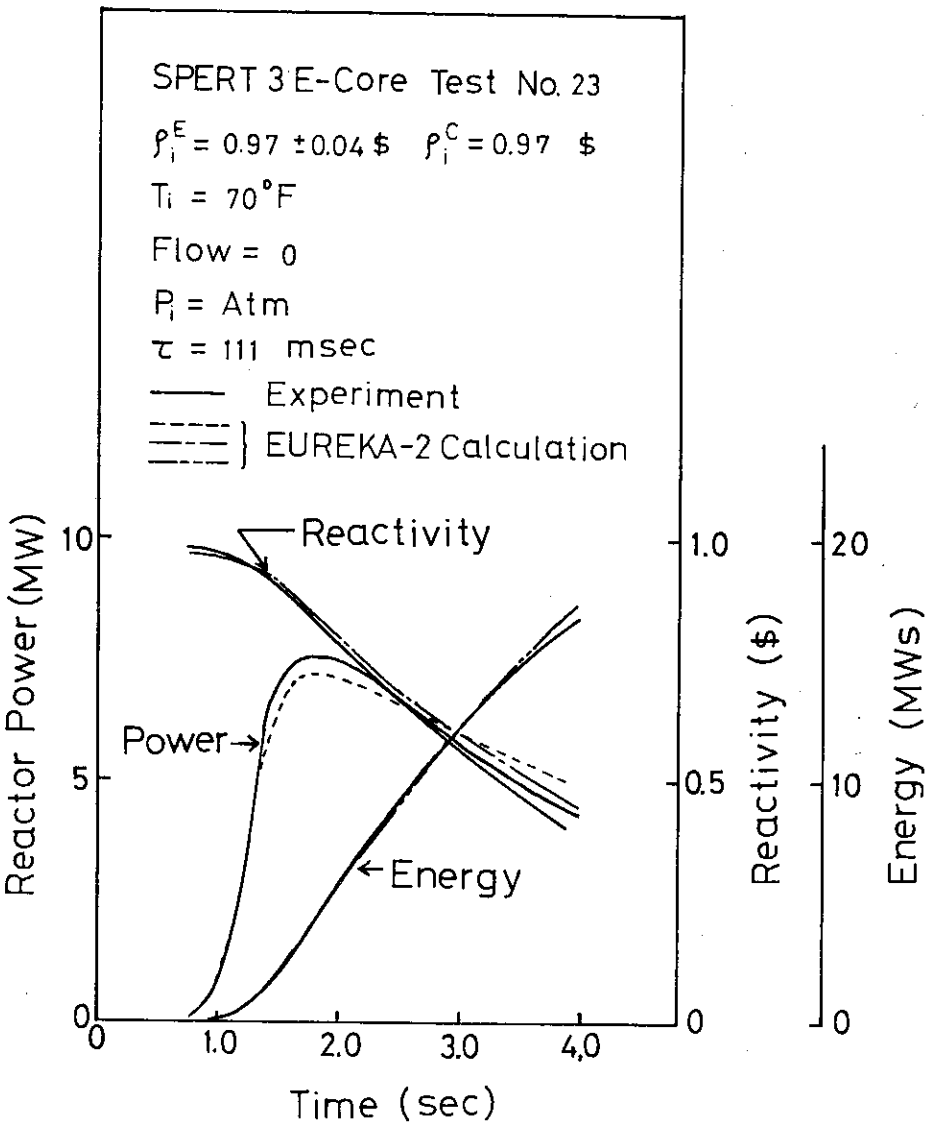

Fig. A.6 SPERT 3E-Core Test No. 23

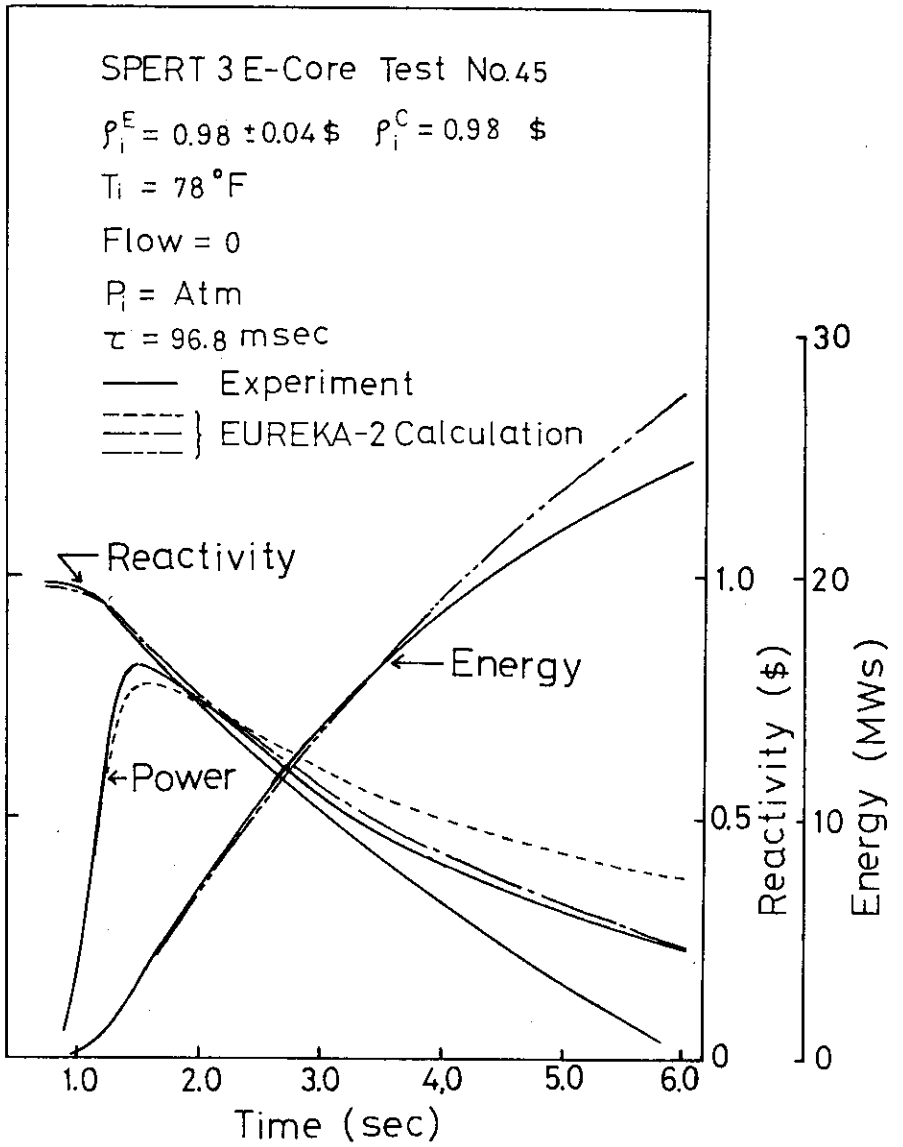

Fig. A.7 SPERT 3E-Core Test No. 45

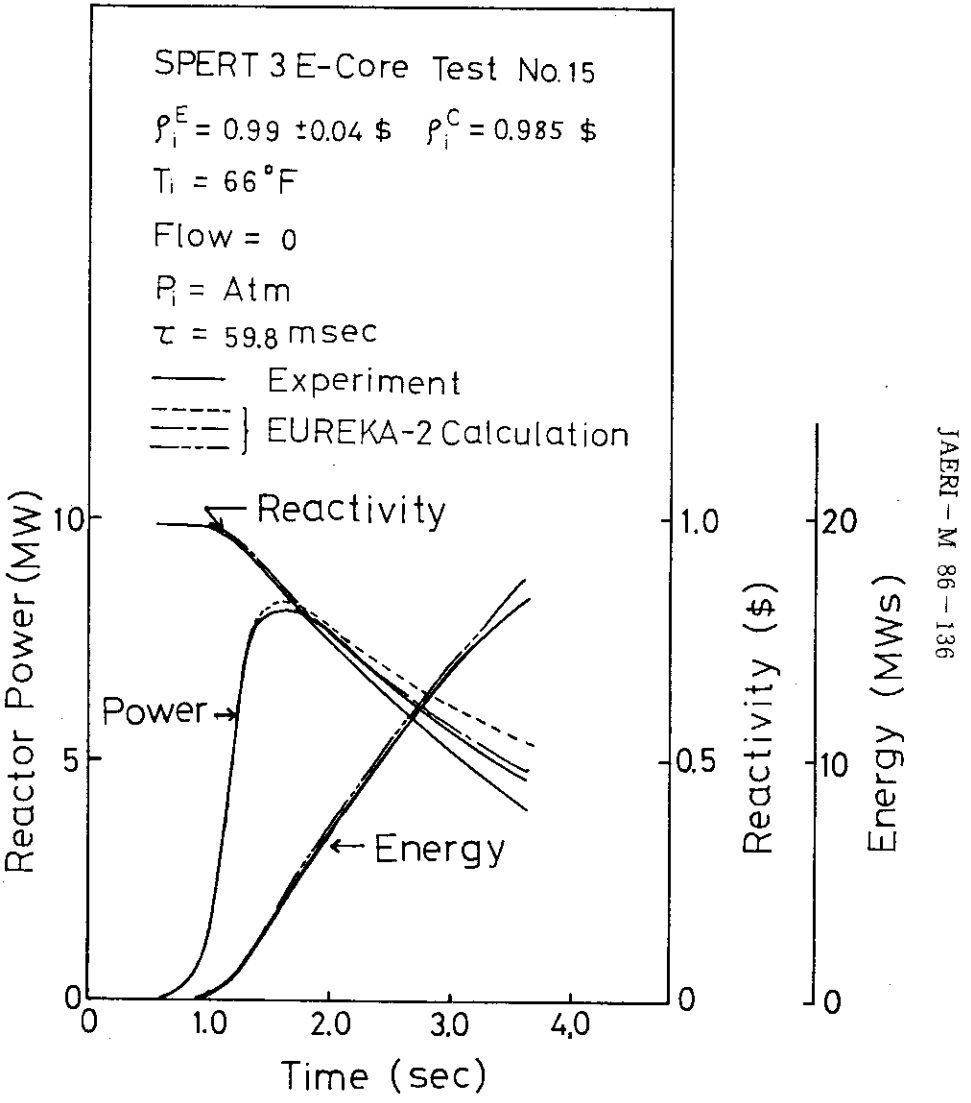

Fig. A.8 SPERT 3E-Core Test No. 15

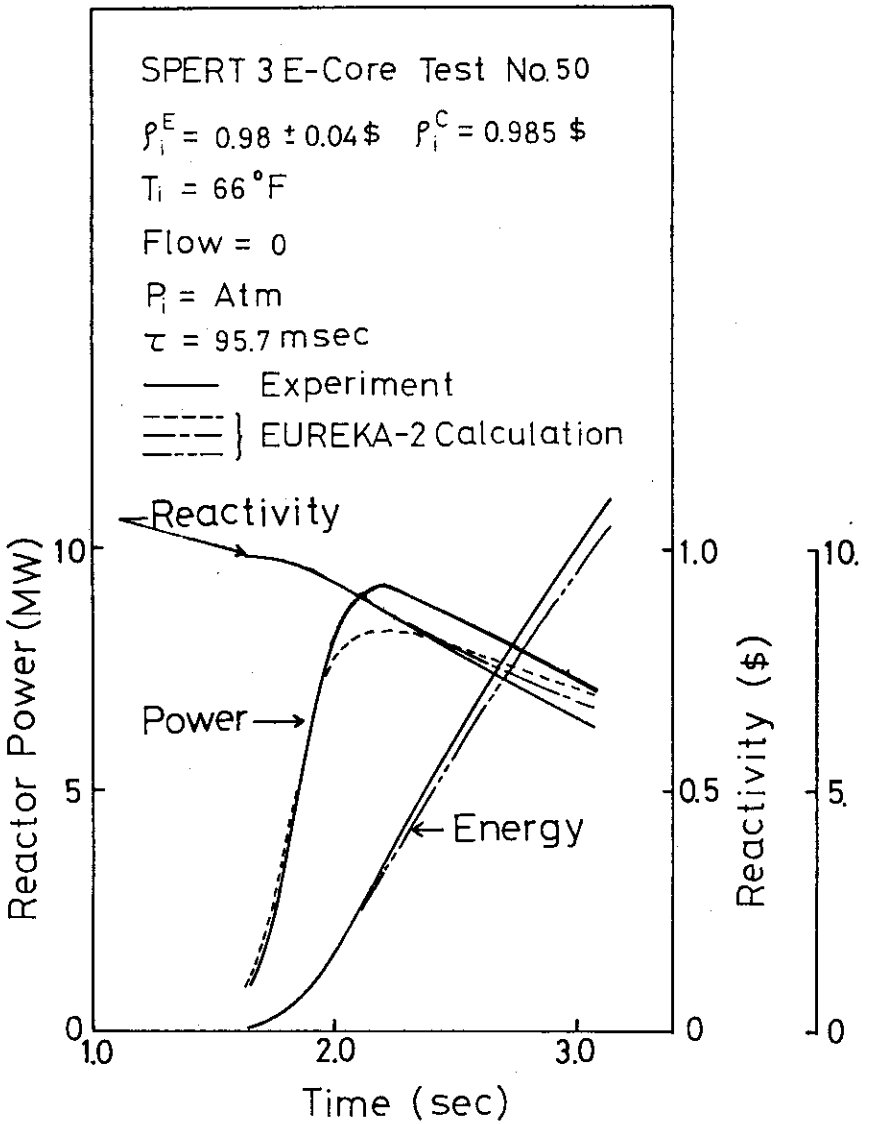

Fig. A.9 SPERT 3E-Core Test No. 50

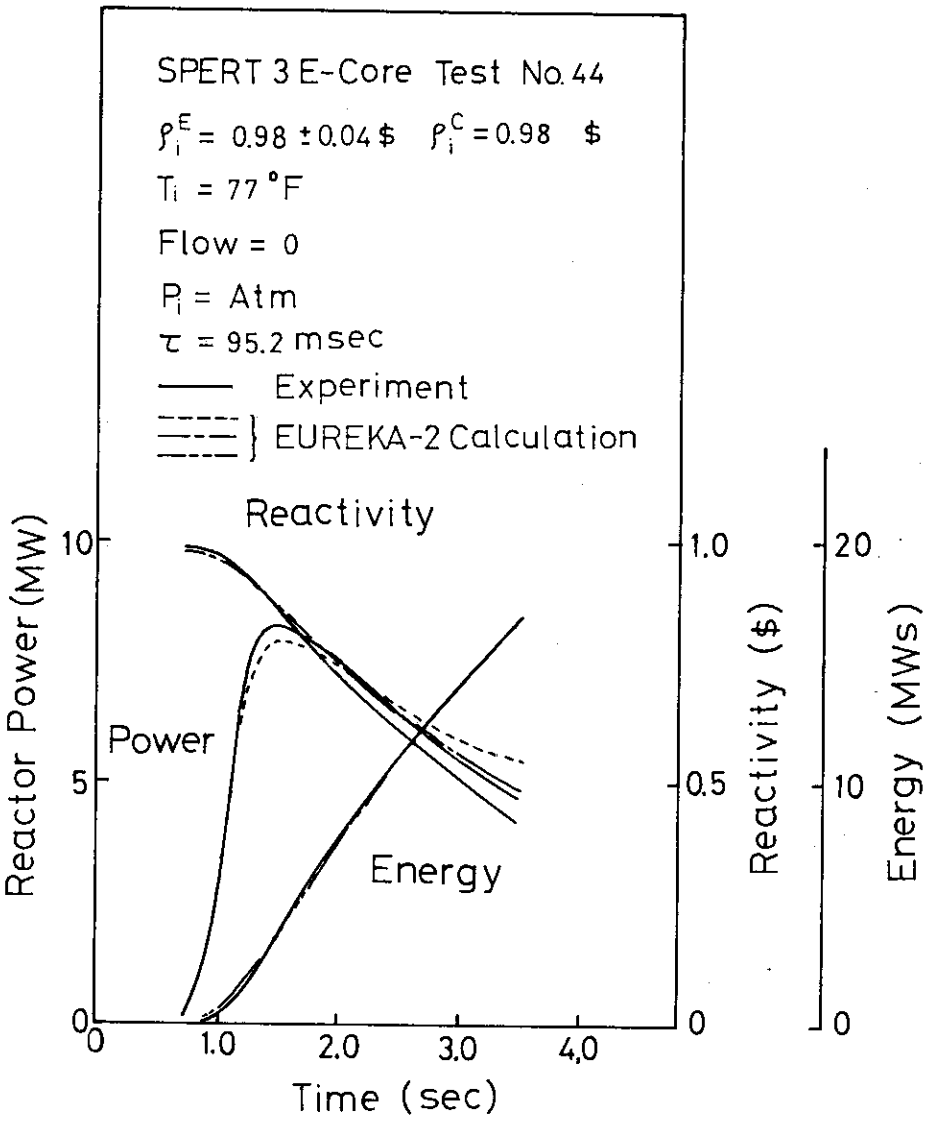

Fig. A.10 SPERT 3E-Core Test No. 44

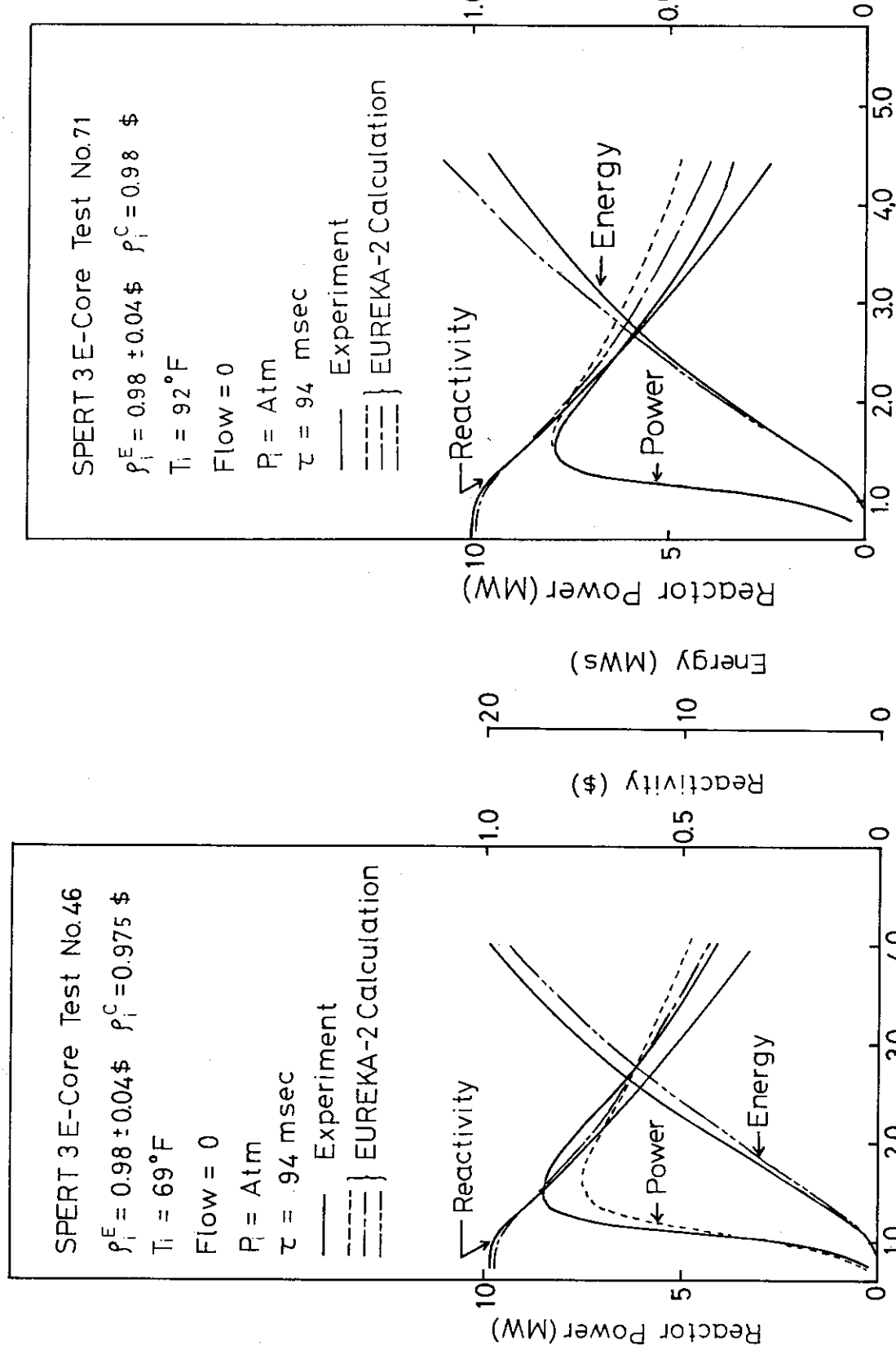

Fig. A.11 SPERT 3E-Core Test No. 46

Fig. A.12 SPERT 3E-Core Test No. 71

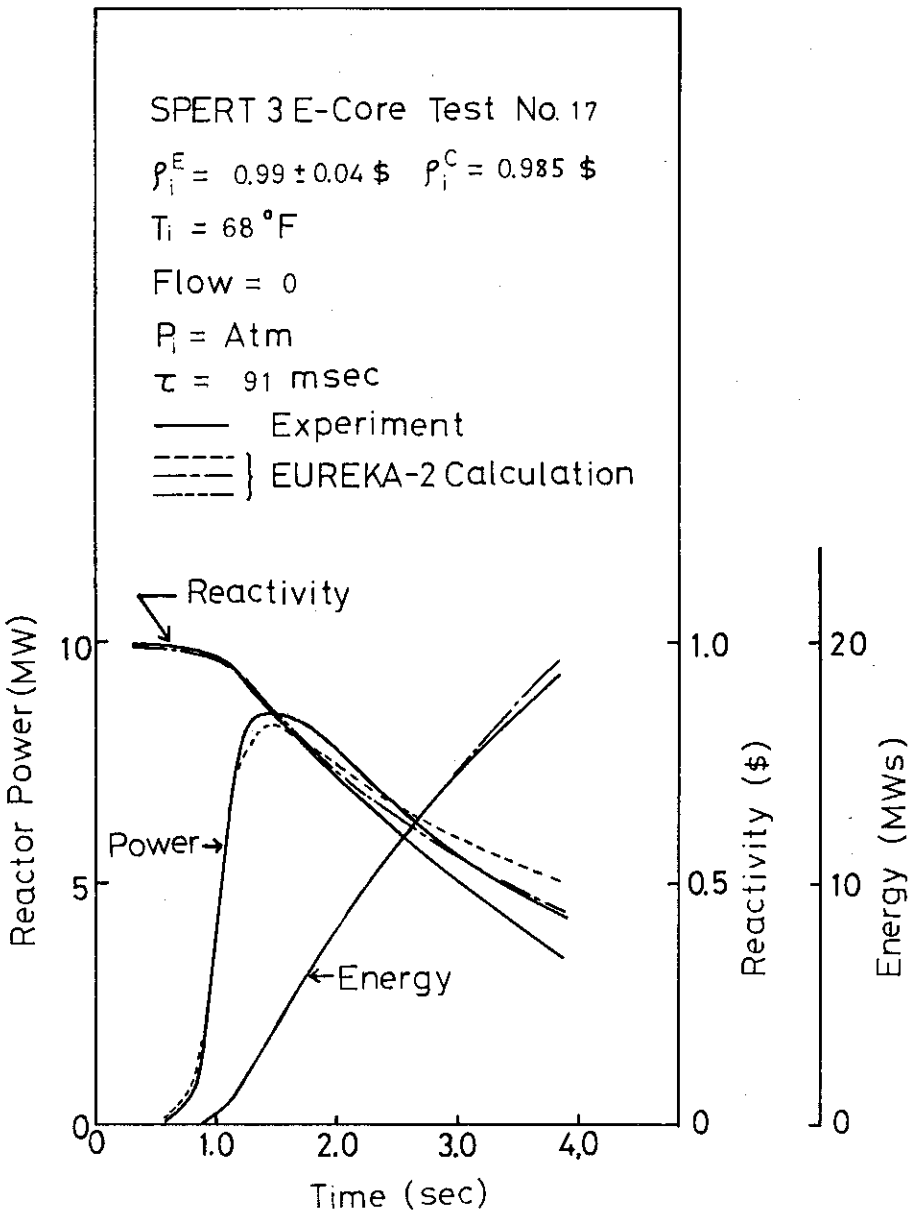

Fig. A.13 SPERT 3E-Core Test No. 17

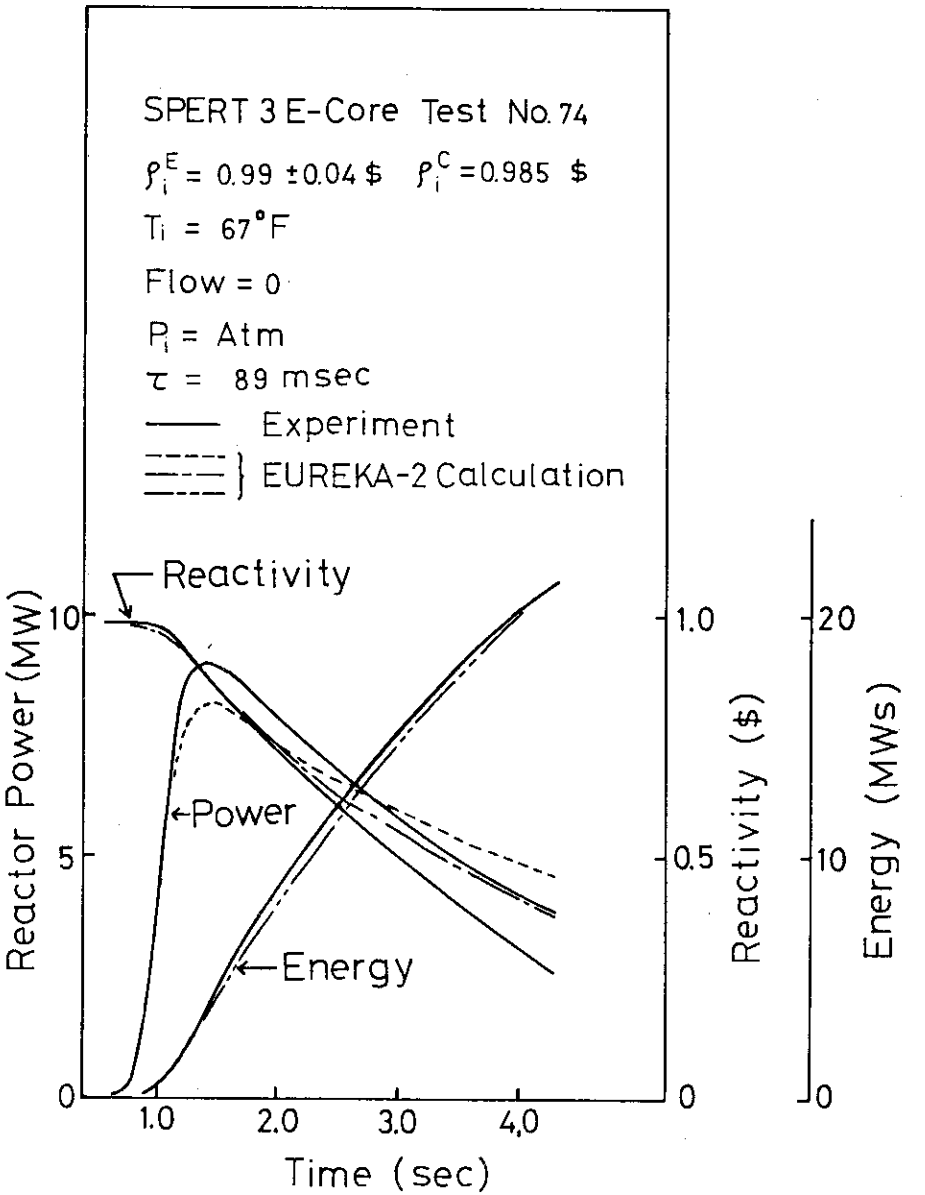

Fig. A.14 SPERT 3E-Core Test No. 74

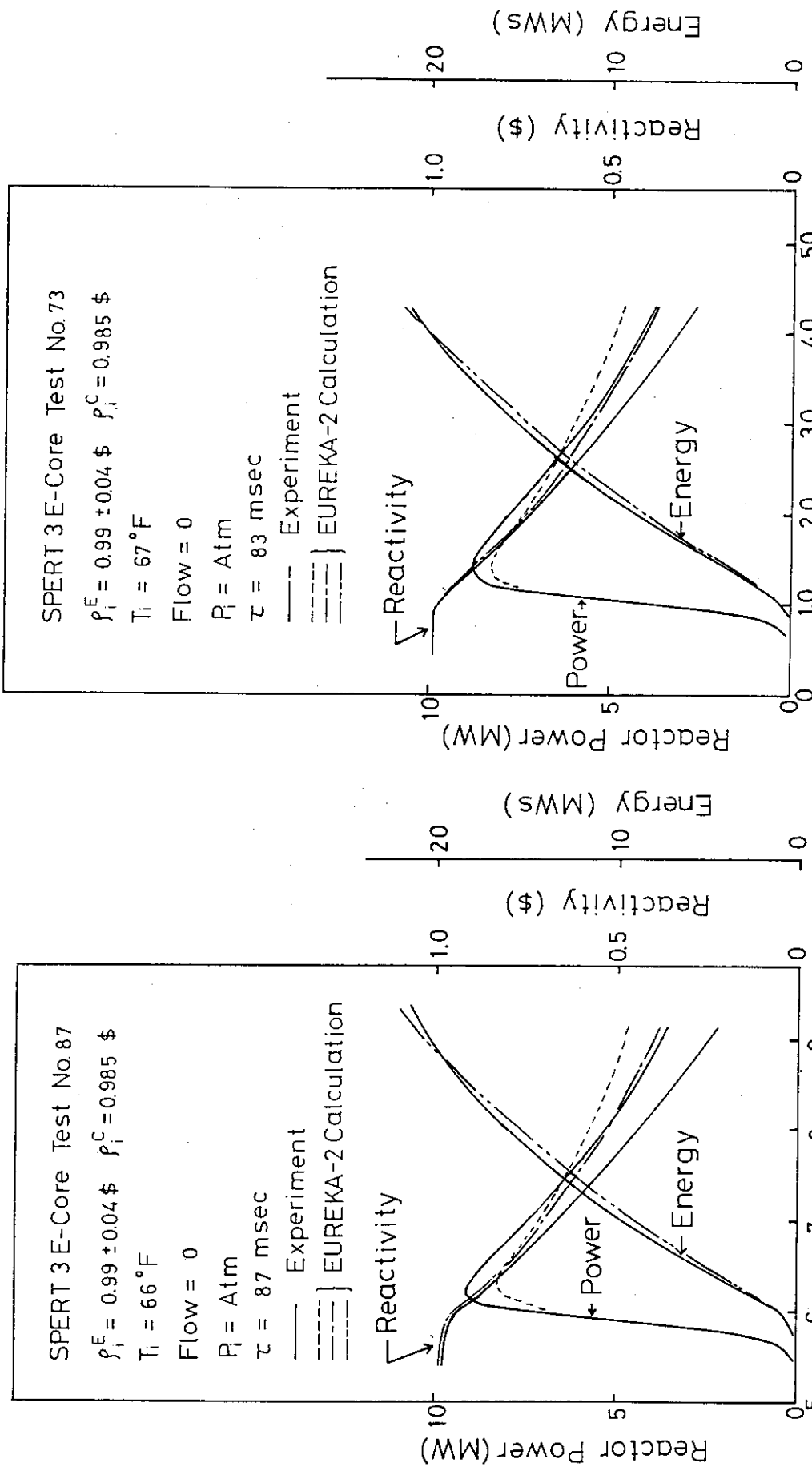

Fig. A.15 SPERT 3E-Core Test No. 87

Fig. A.16 SPERT 3E-Core Test No. 73

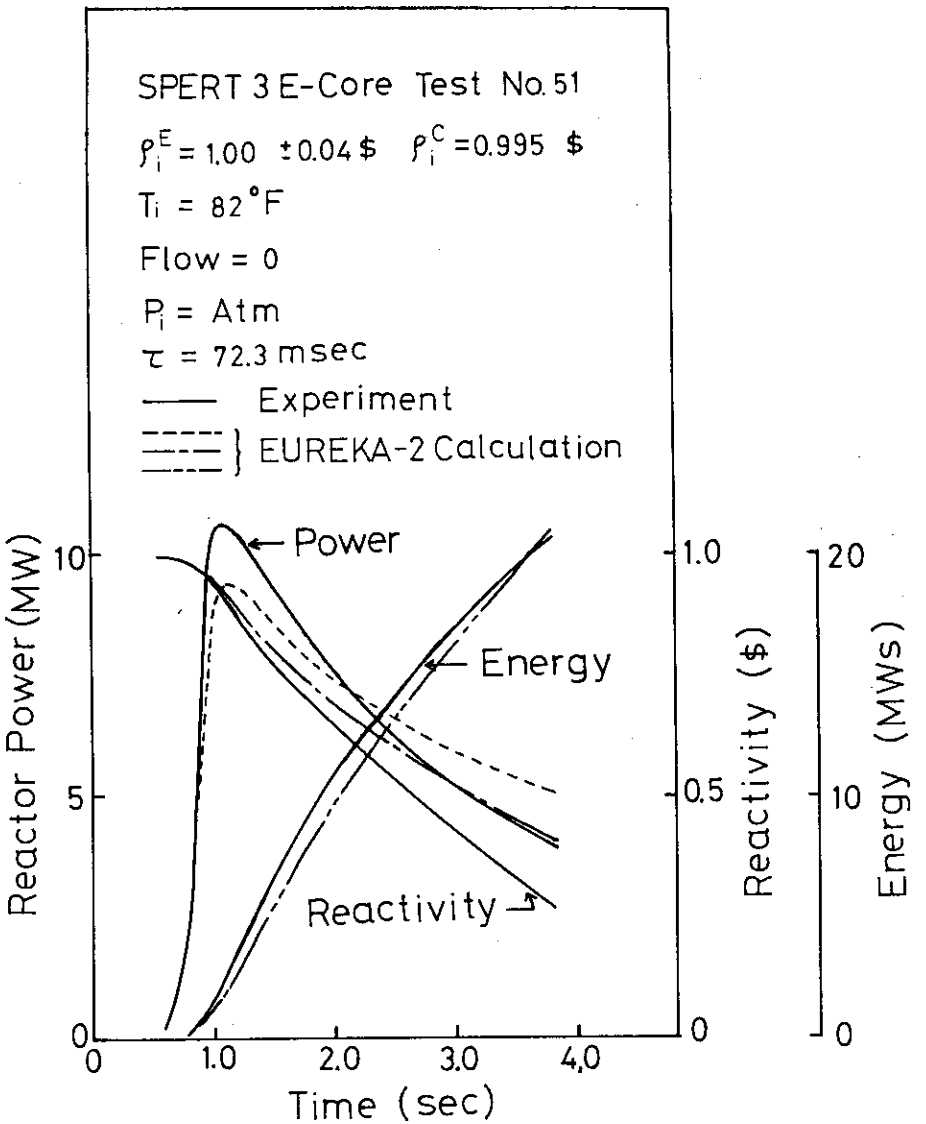

Fig. A.17 SPERT 3E-Core Test No. 51

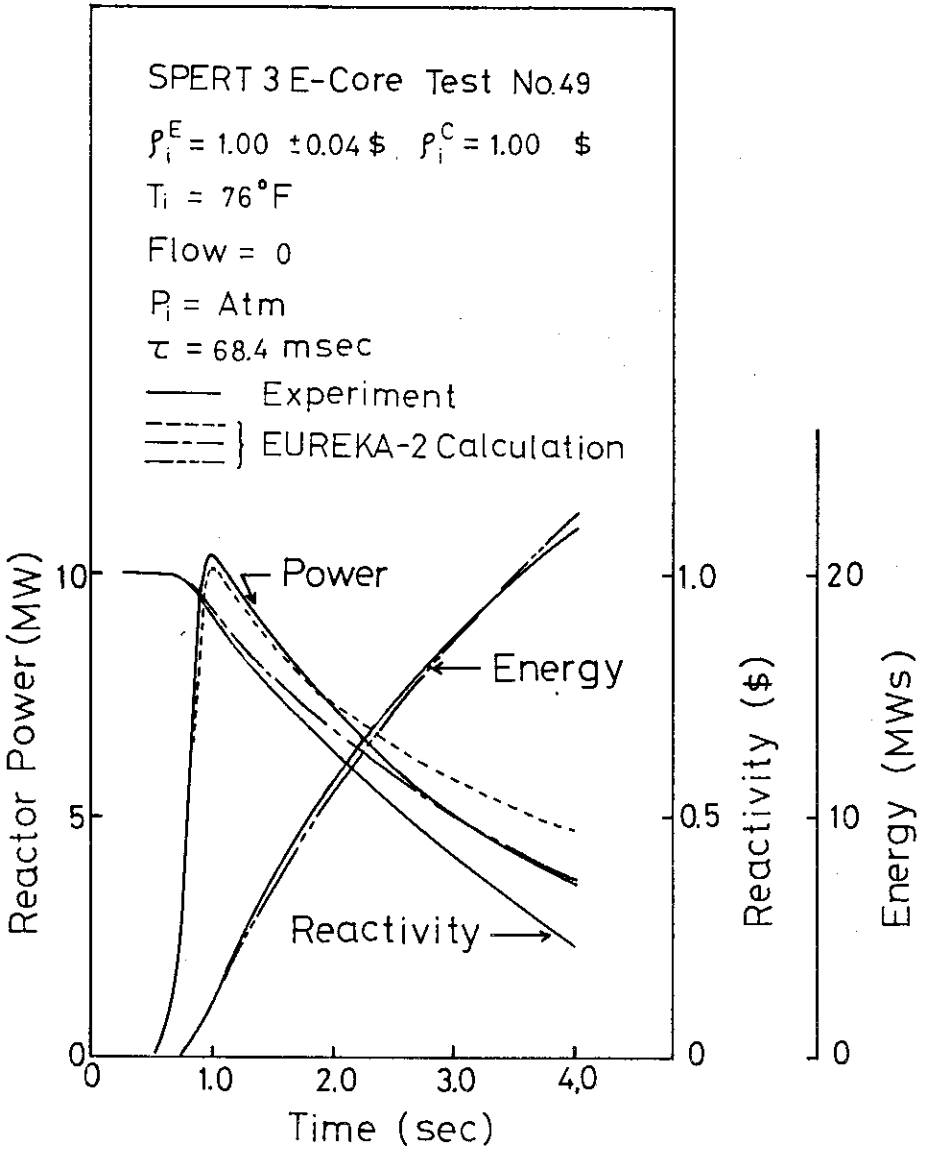

Fig. A.18 SPERT 3E-Core Test No. 49

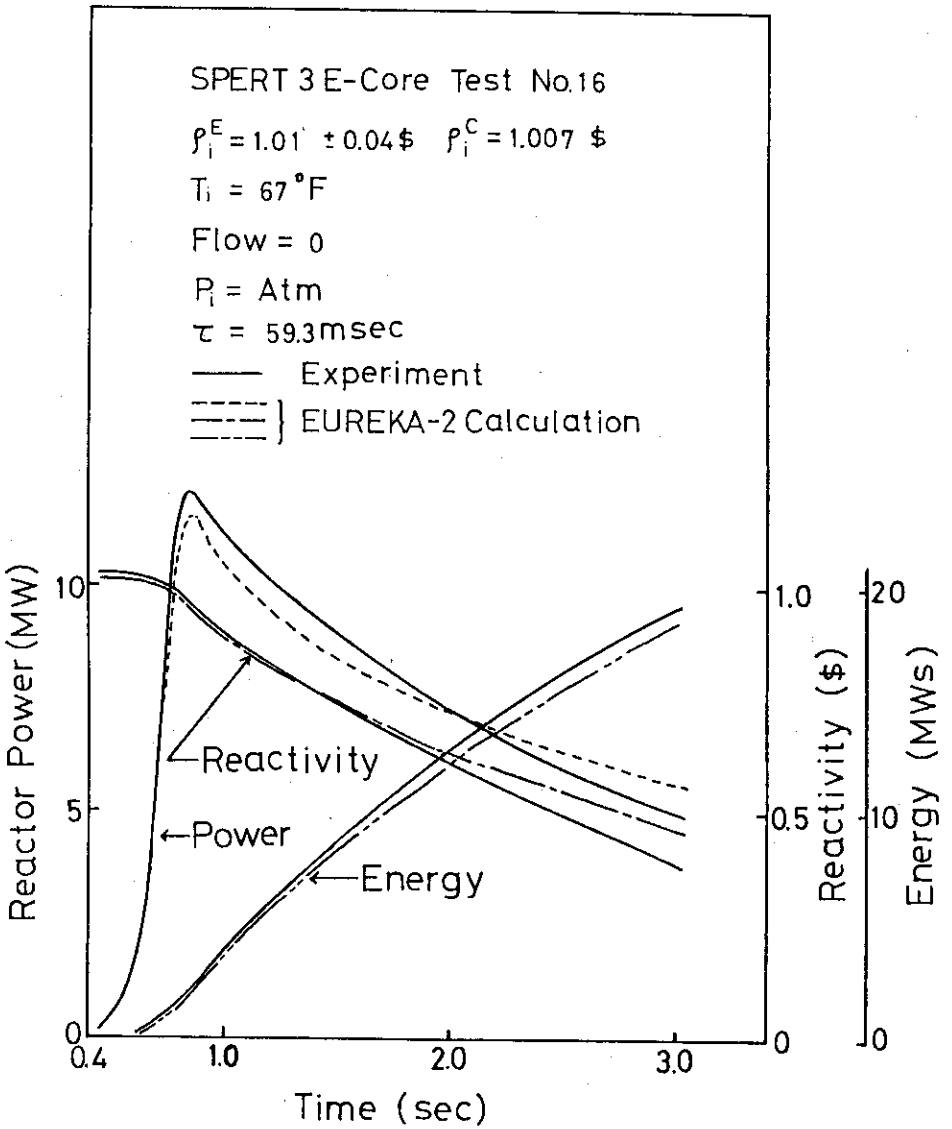

Fig. A.19 SPERT 3E-Core Test No. 16

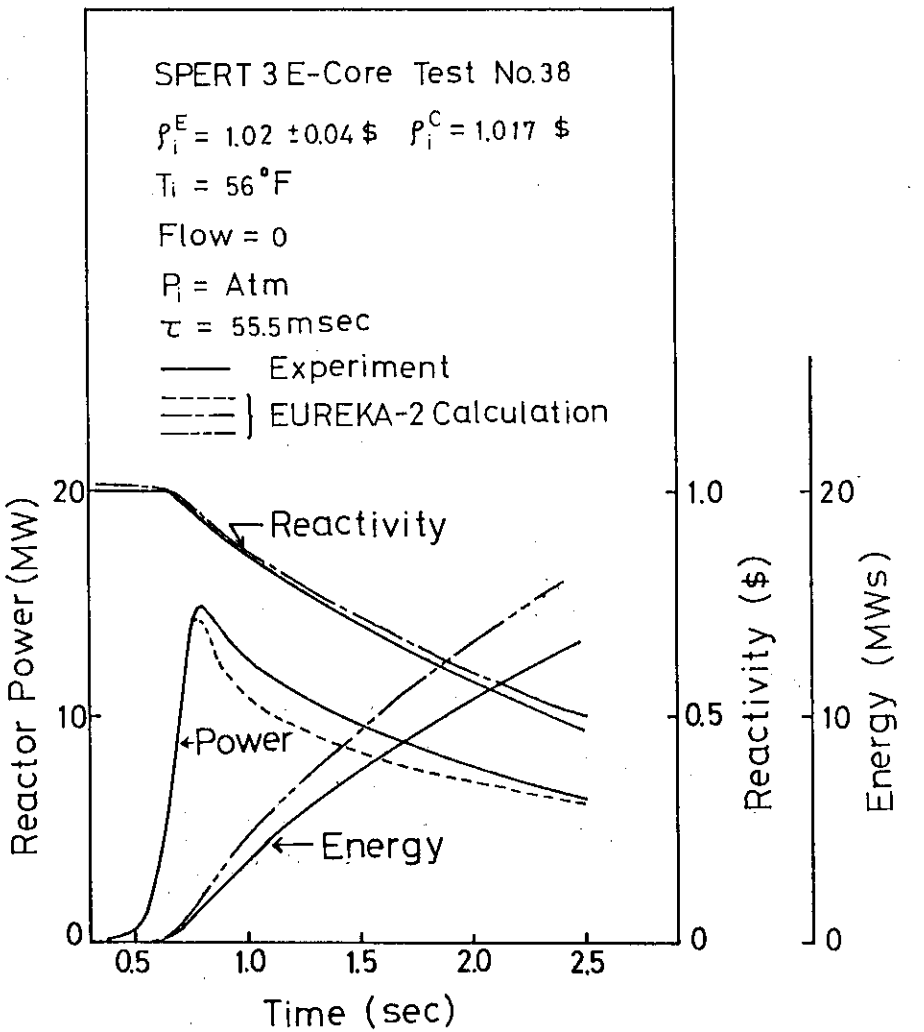

Fig. A.20 SPERT 3E-Core Test No. 38

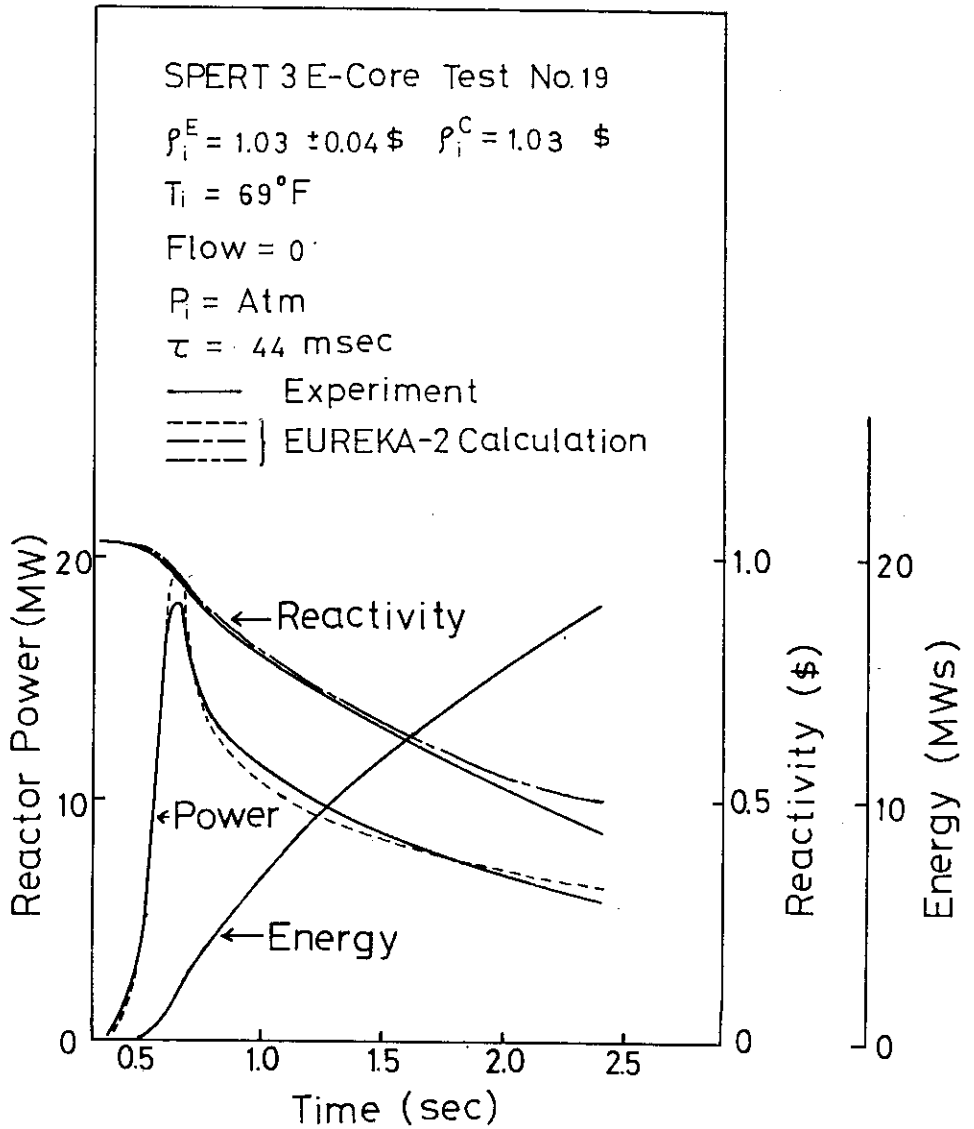

Fig. A.21 SPERT 3E-Core Test No. 19

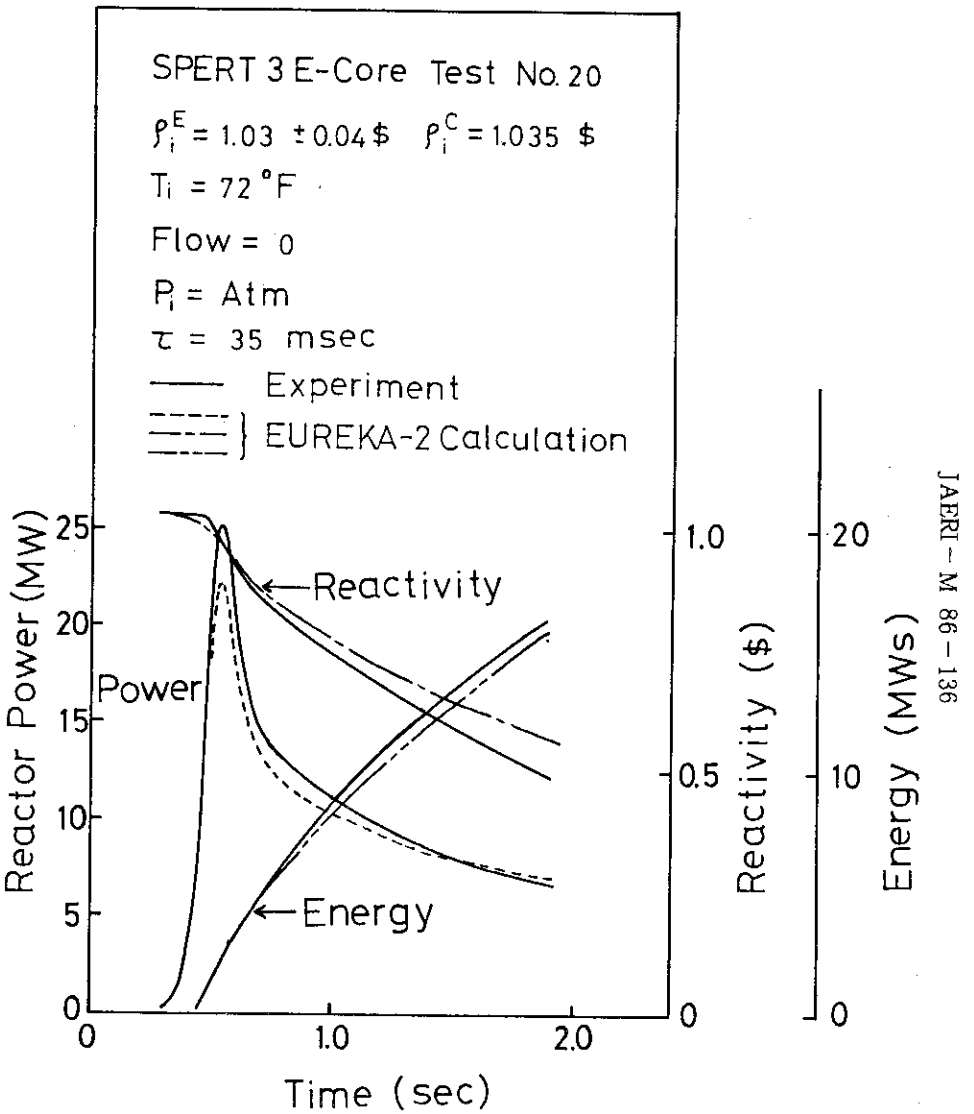

Fig. A.22 SPERT 3E-Core Test No. 20

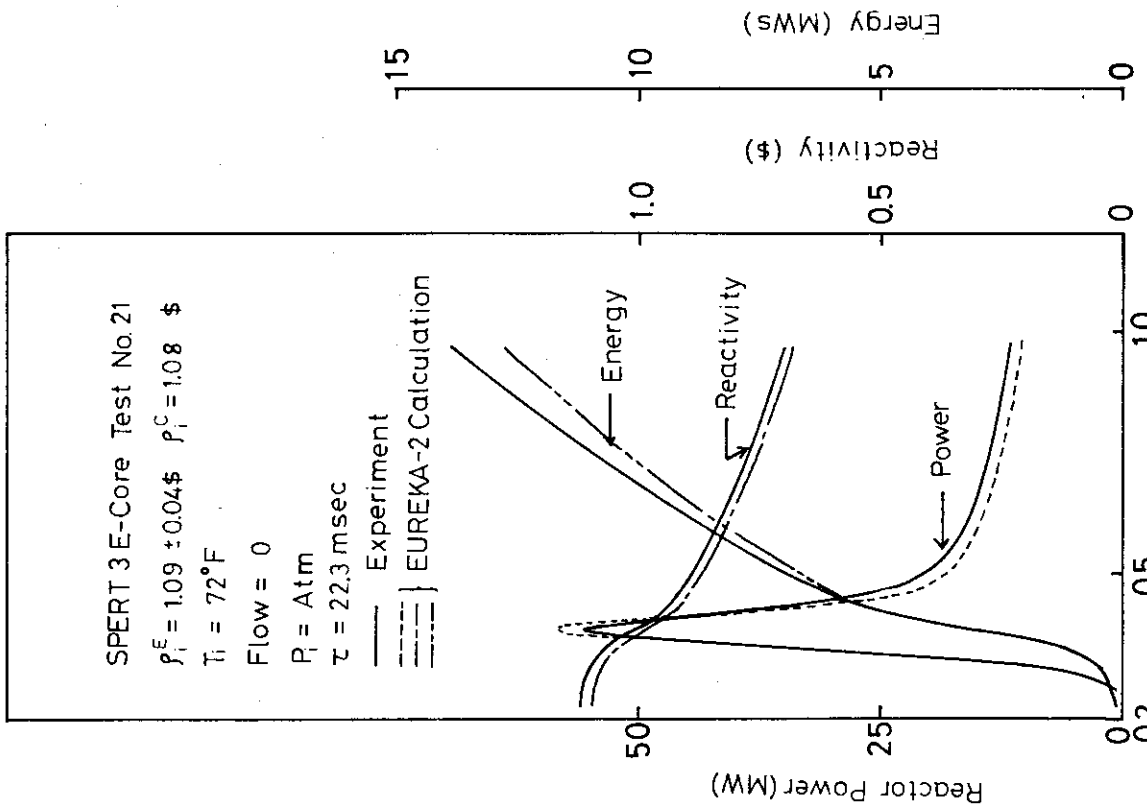

Fig. A.24 SPERT 3E-Core Test No. 21

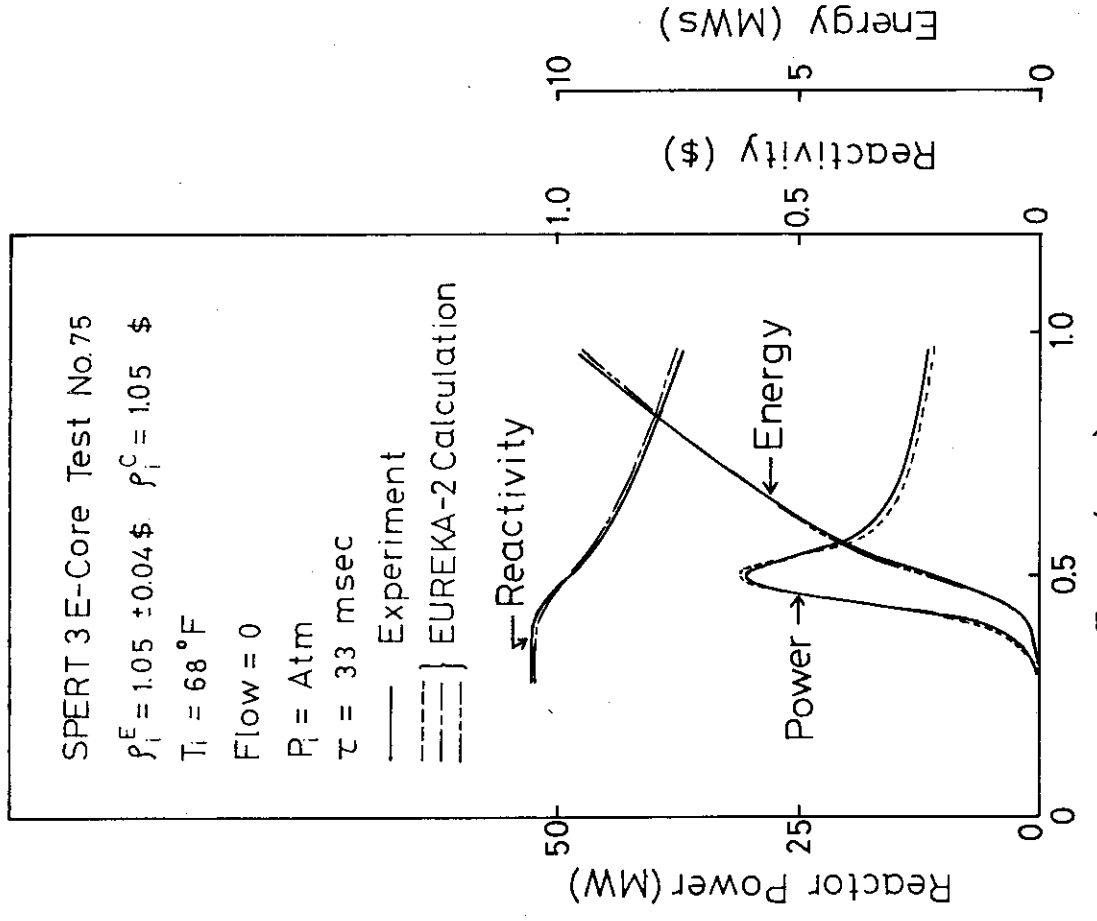

Fig. A.23 SPERT 3E-Core Test No. 75

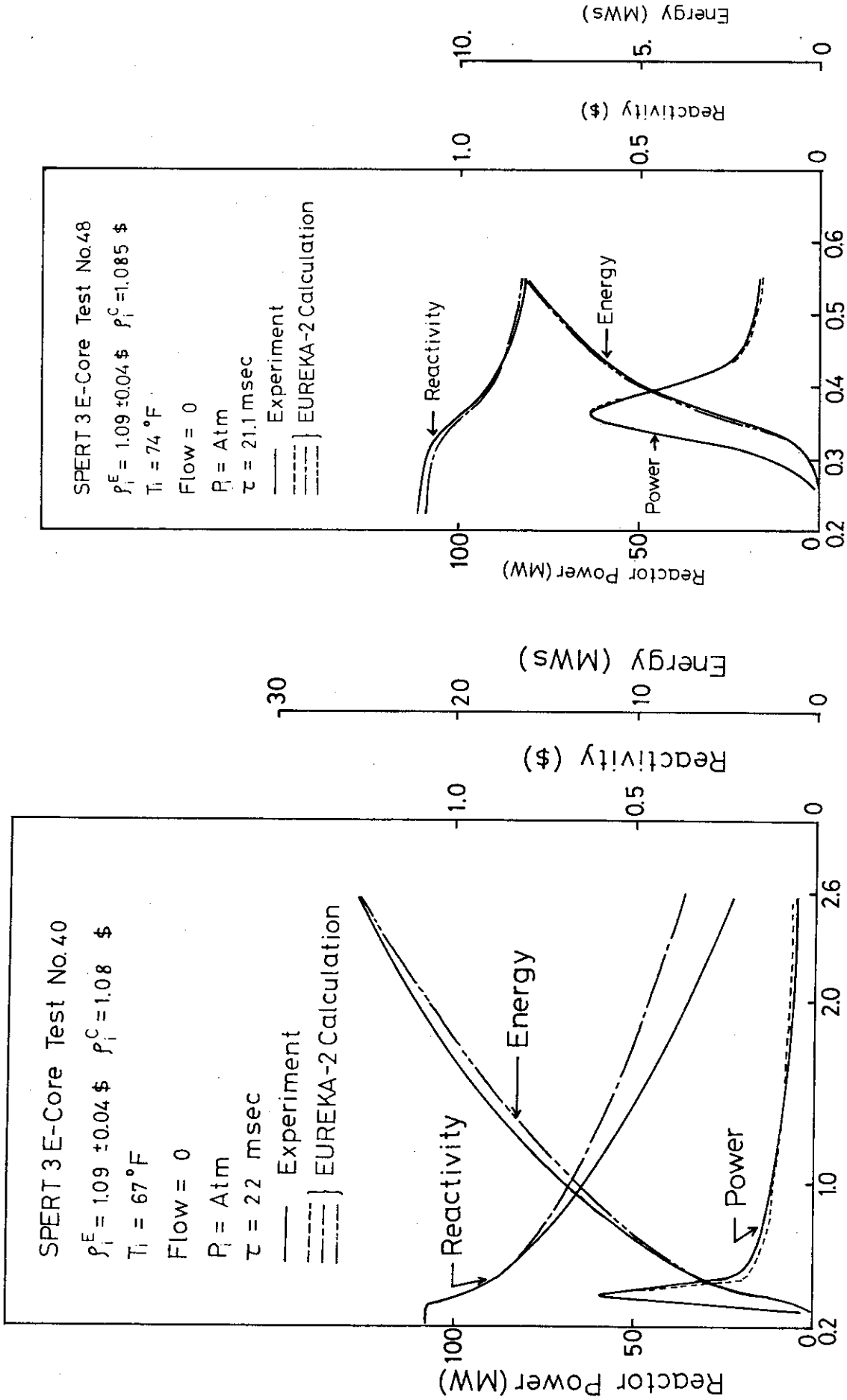

Fig. A.25 SPERT 3E-Core Test No. 40

Fig. A.26 SPERT 3E-Core Test No. 48

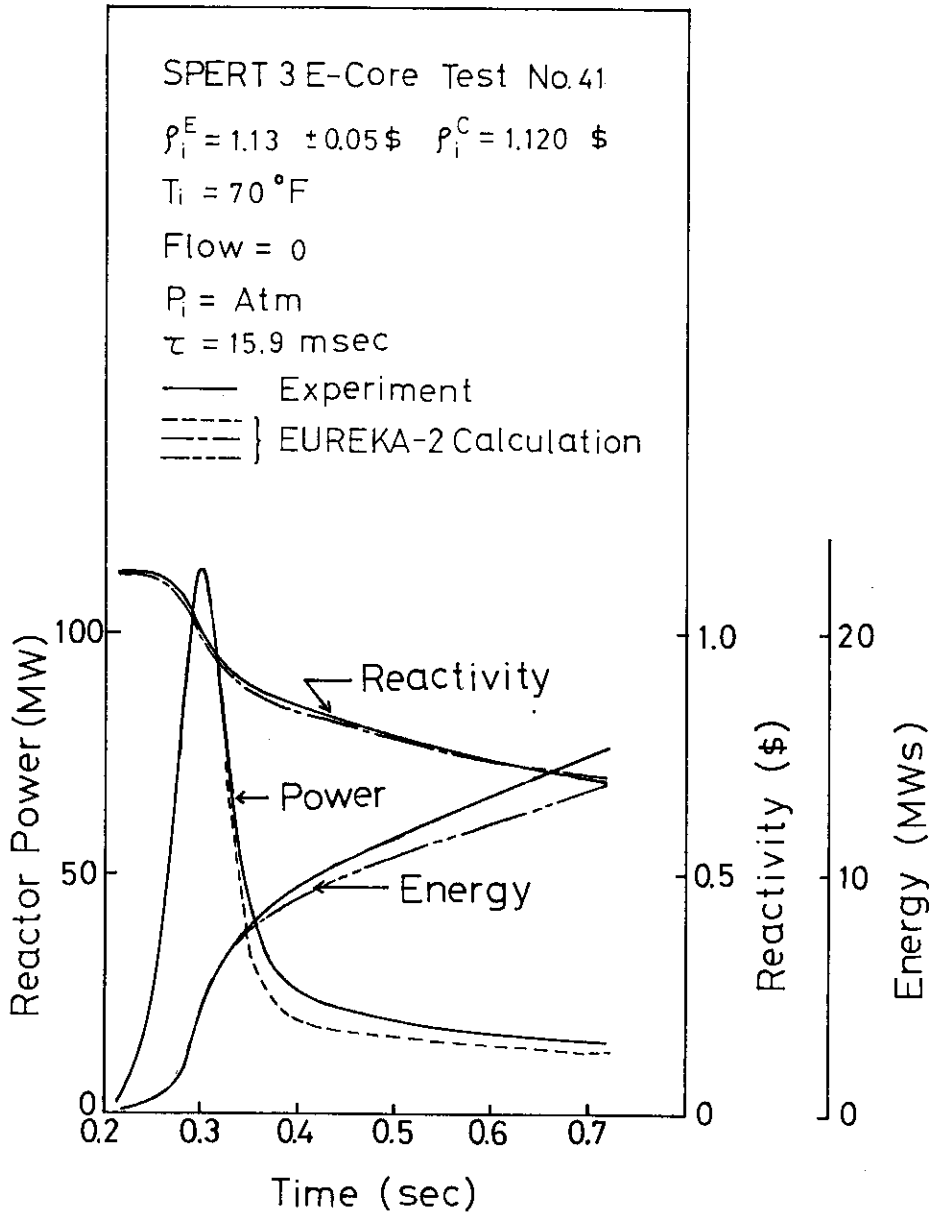

Fig. A.27 SPERT 3E-Core Test No. 47

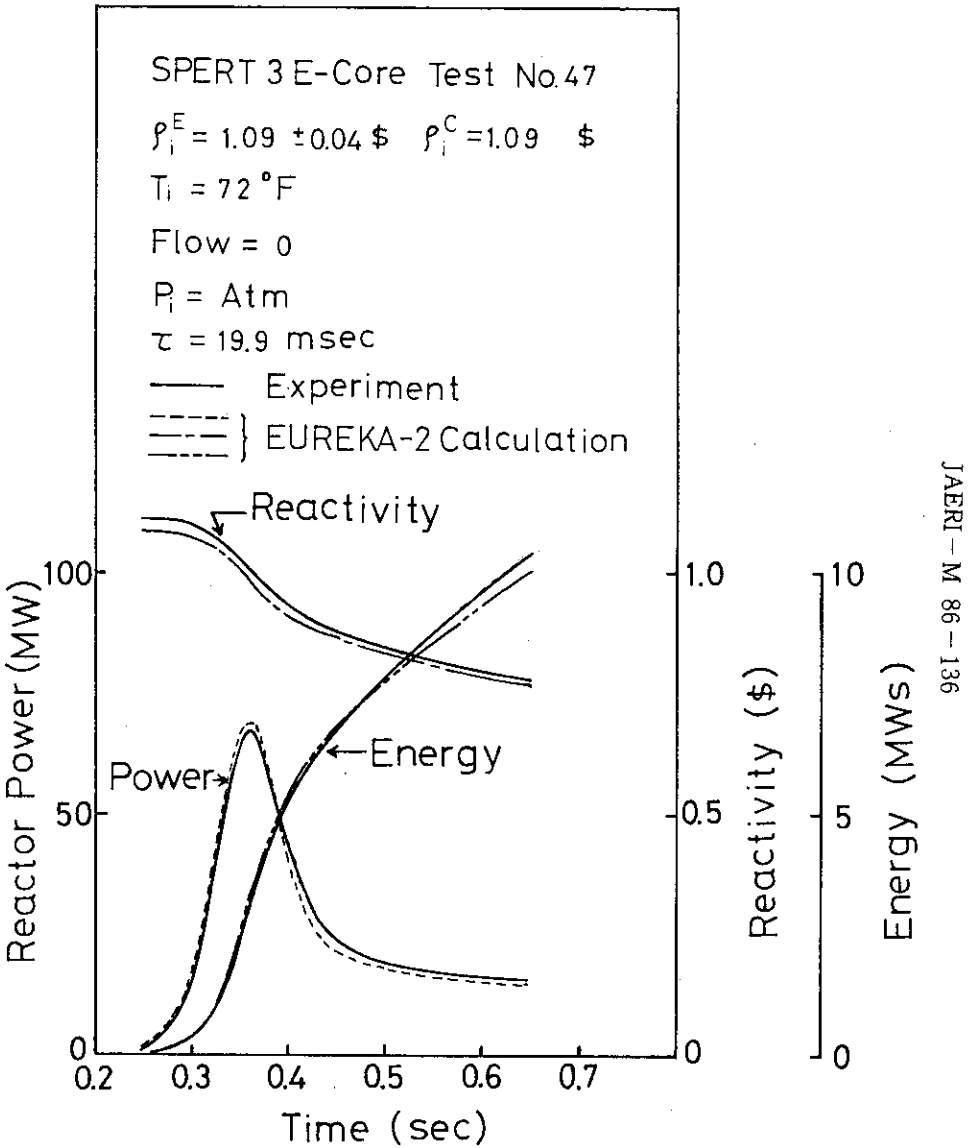

Fig. A.28 SPERT 3E-Core Test No. 41

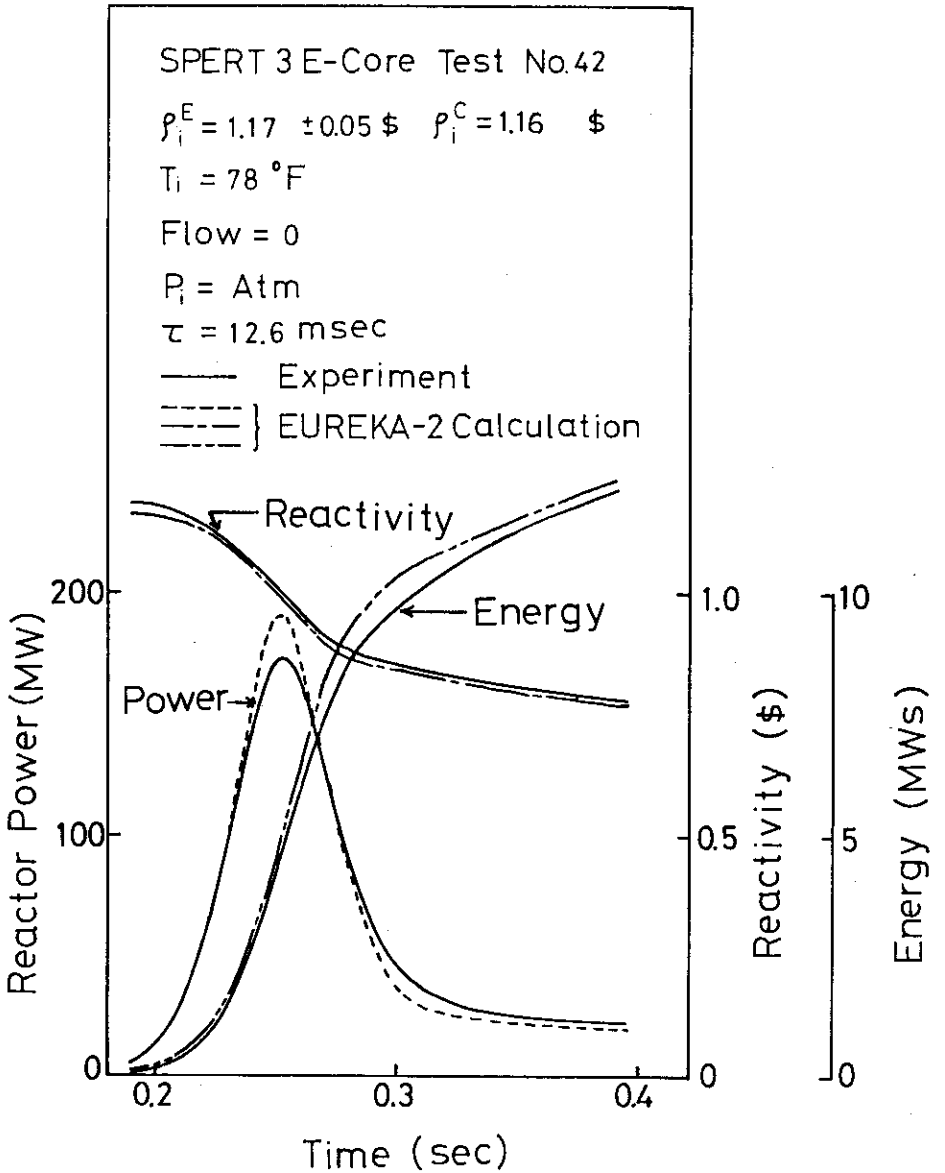

Fig. A.29 SPERT 3E-Core Test No. 42

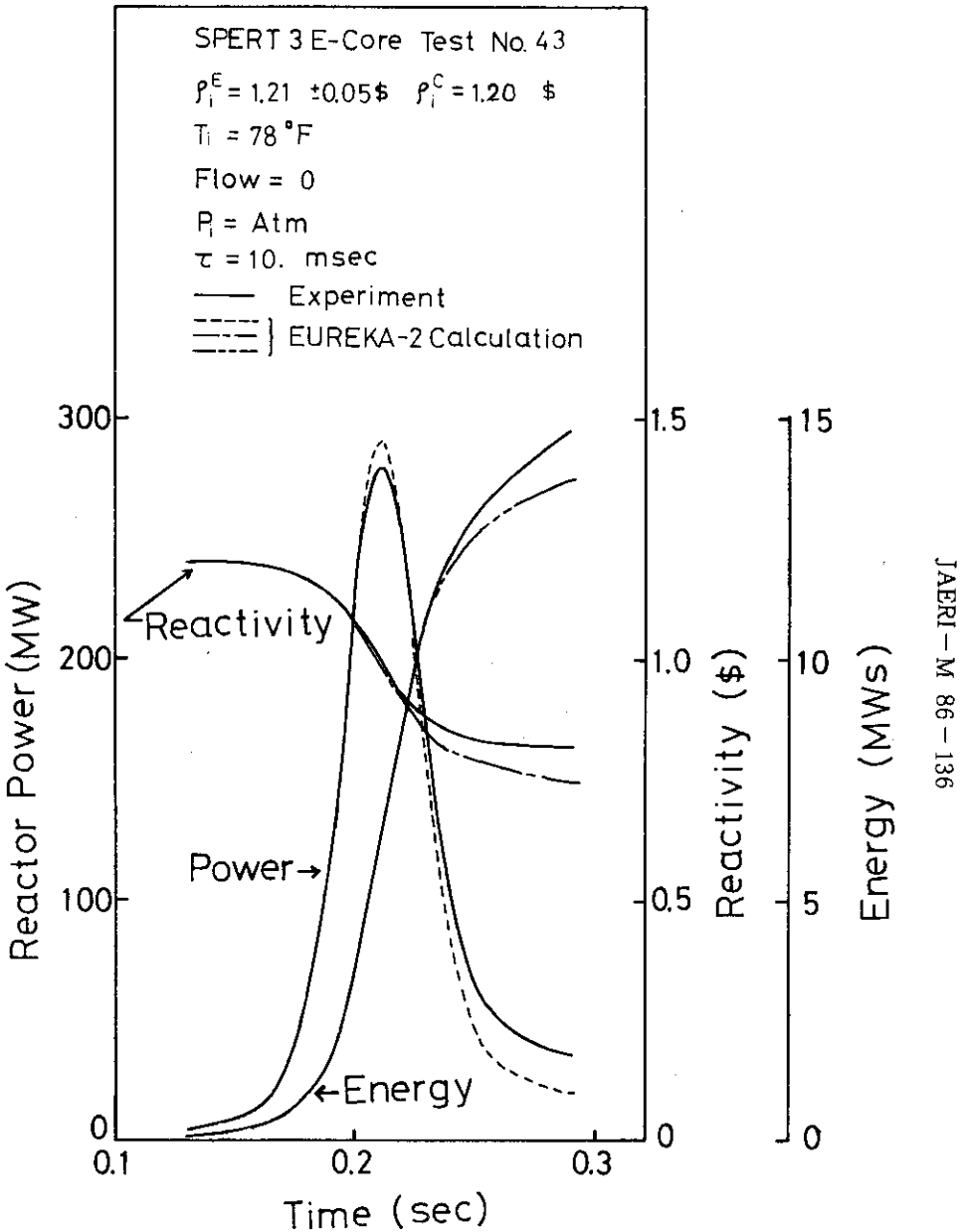

Fig. A.30 SPERT 3E-Core Test No. 43

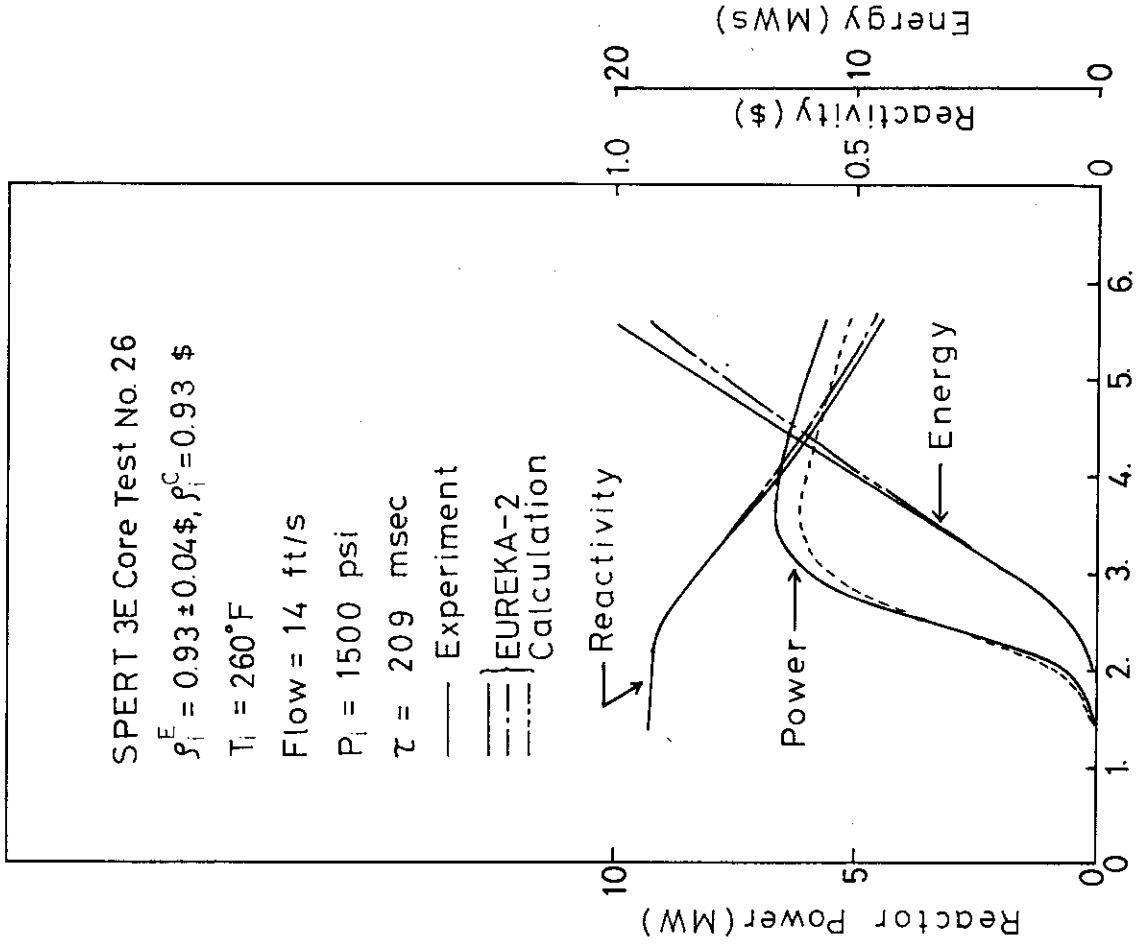

Fig. B.2 SPERT 3E-Core Test No. 26

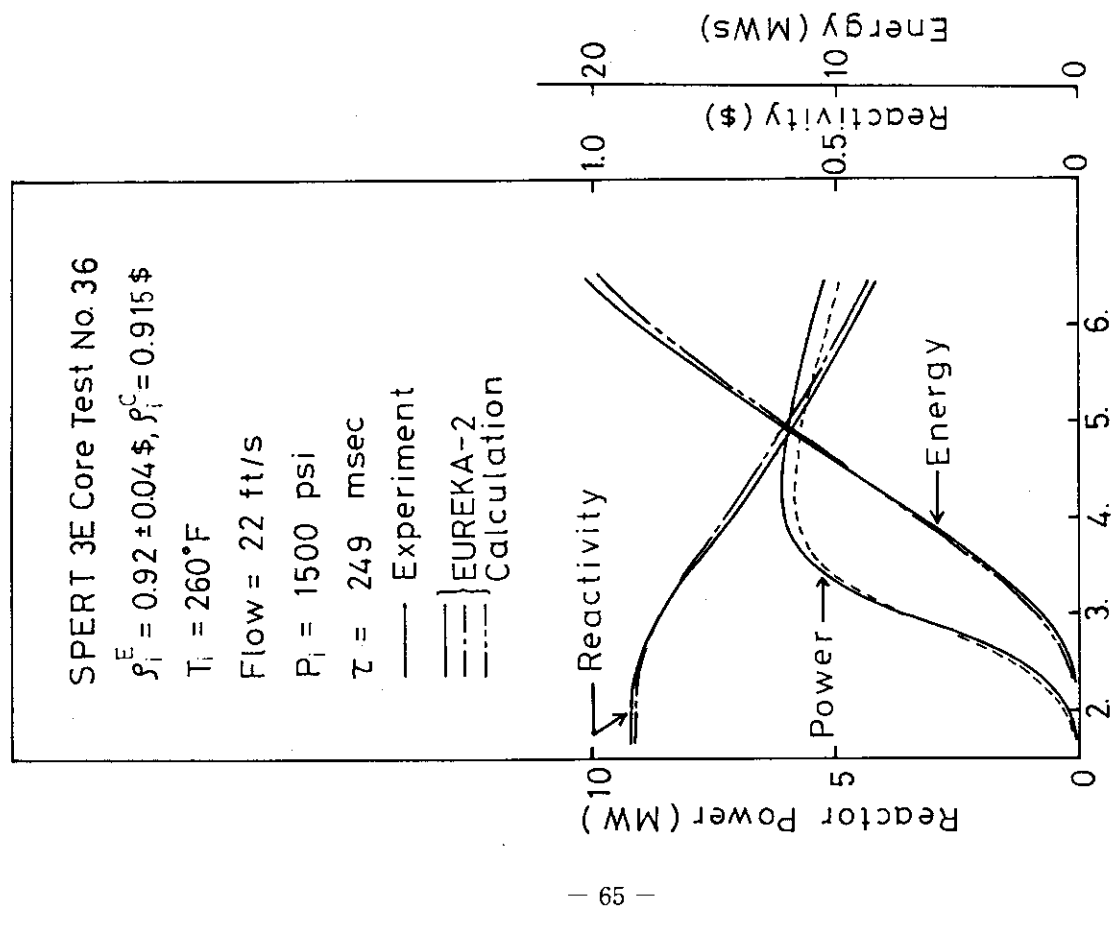

Fig. B.1 SPERT 3E-Core Test No. 36

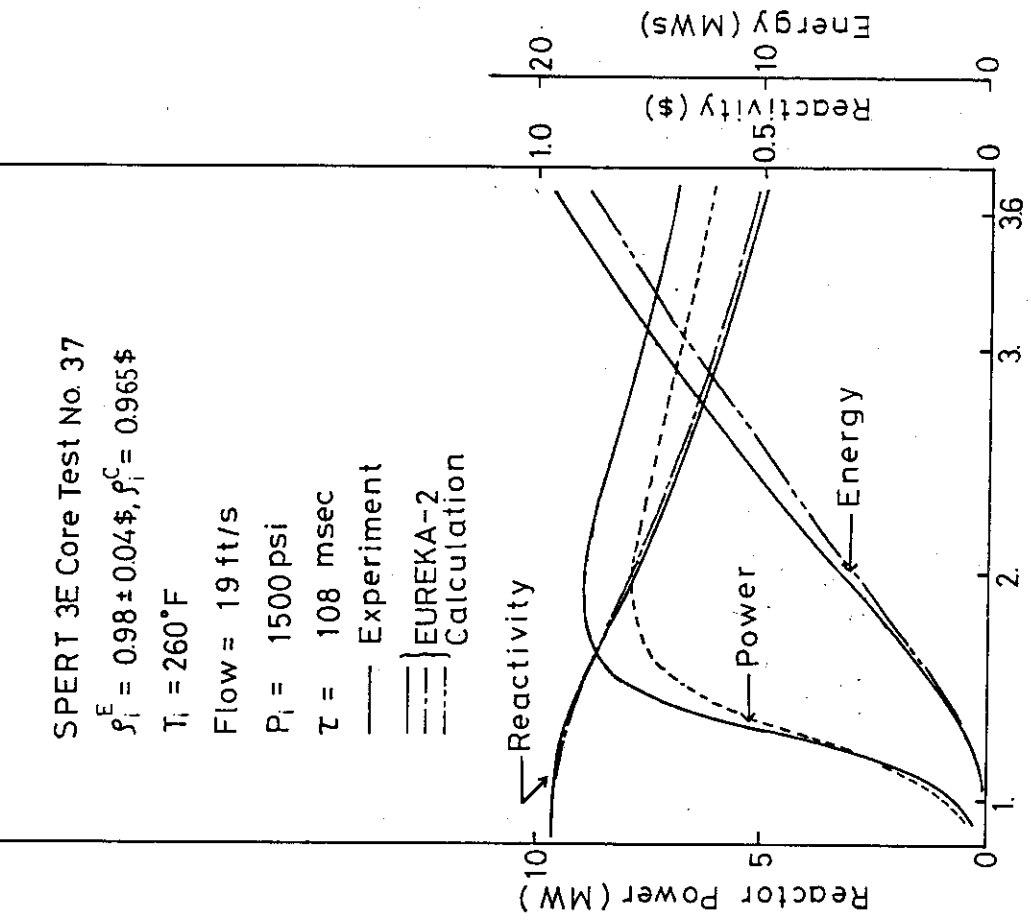

Fig. B.4 SPERT 3E-Core Test No. 37

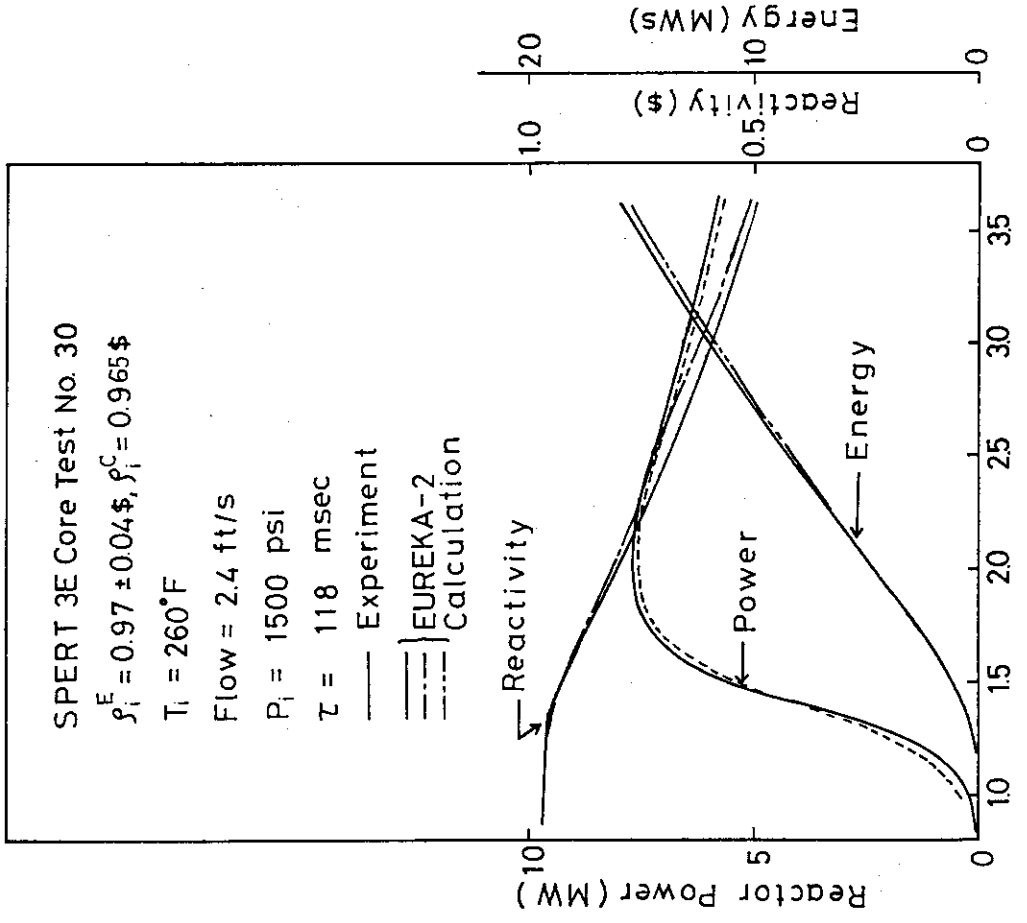

Fig. B.3 SPERT 3E-Core Test No. 30

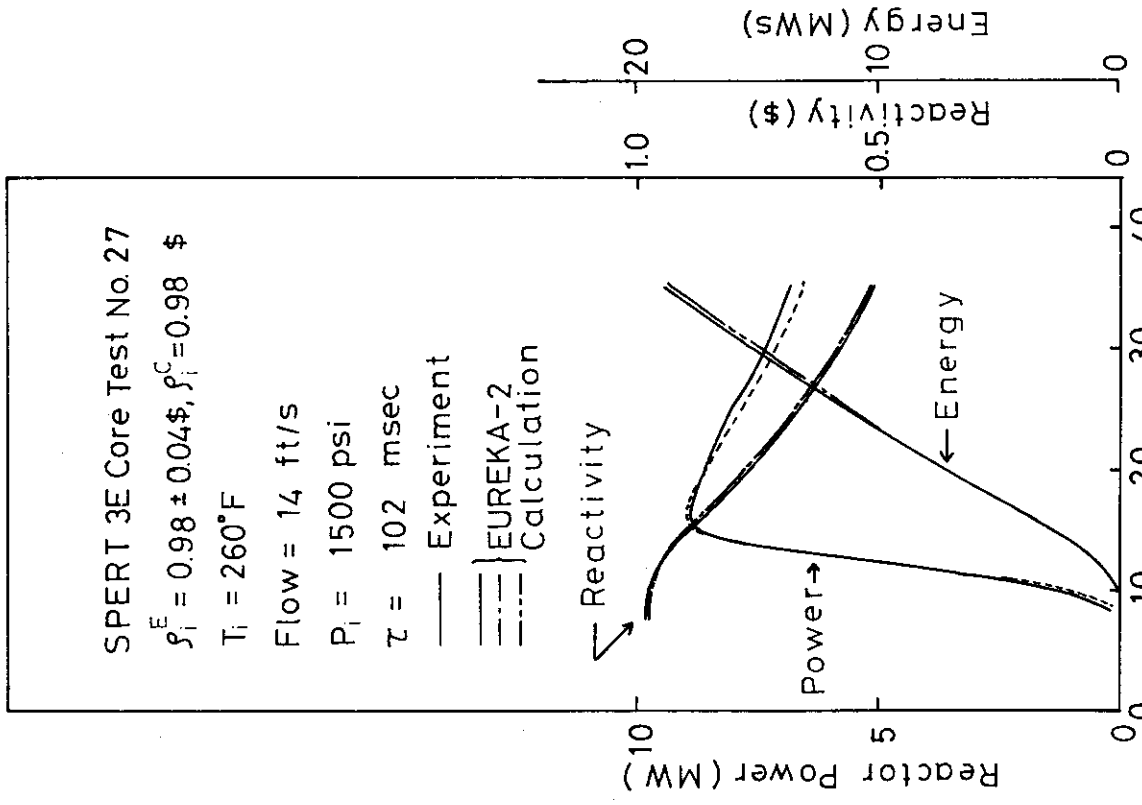

Fig. B.6 SPERT 3E-Core Test No. 27

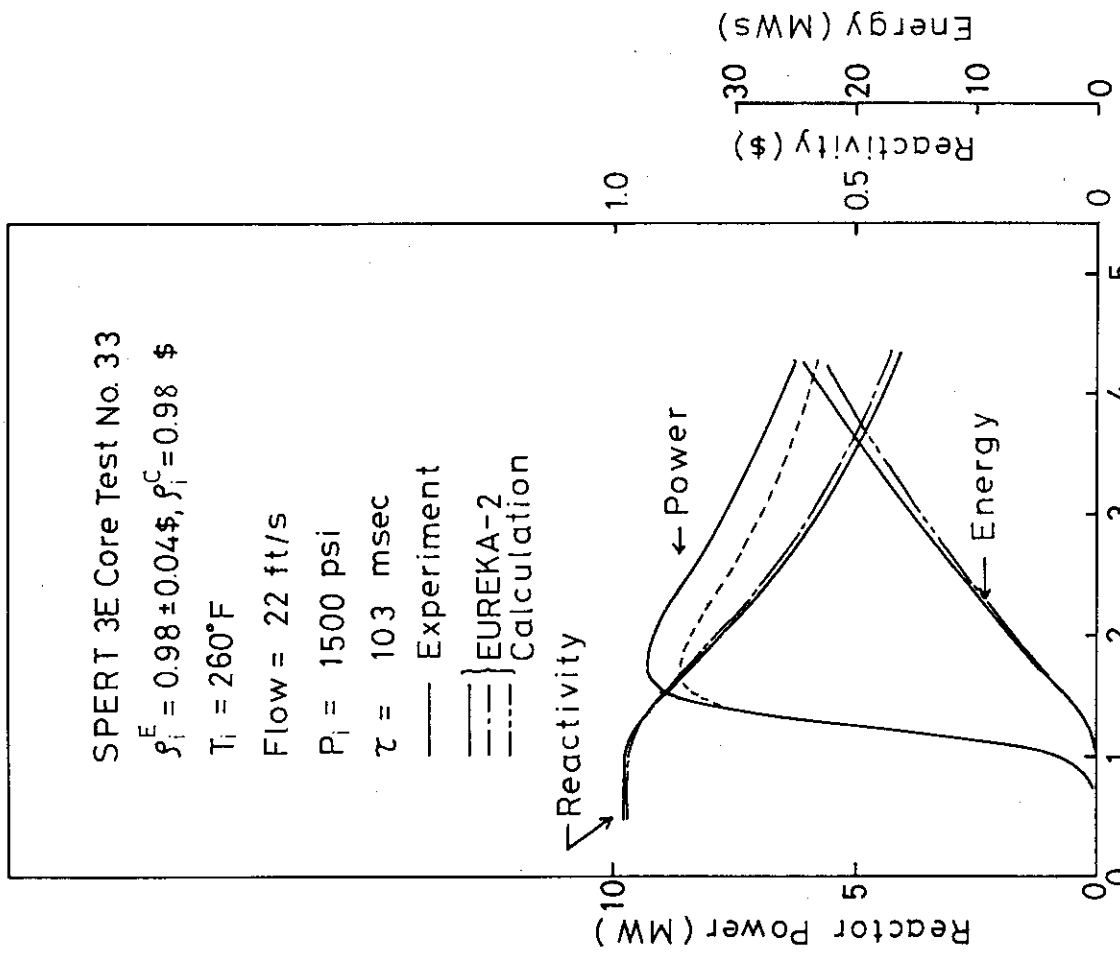

Fig. B.5 SPERT 3E-Core Test No. 33

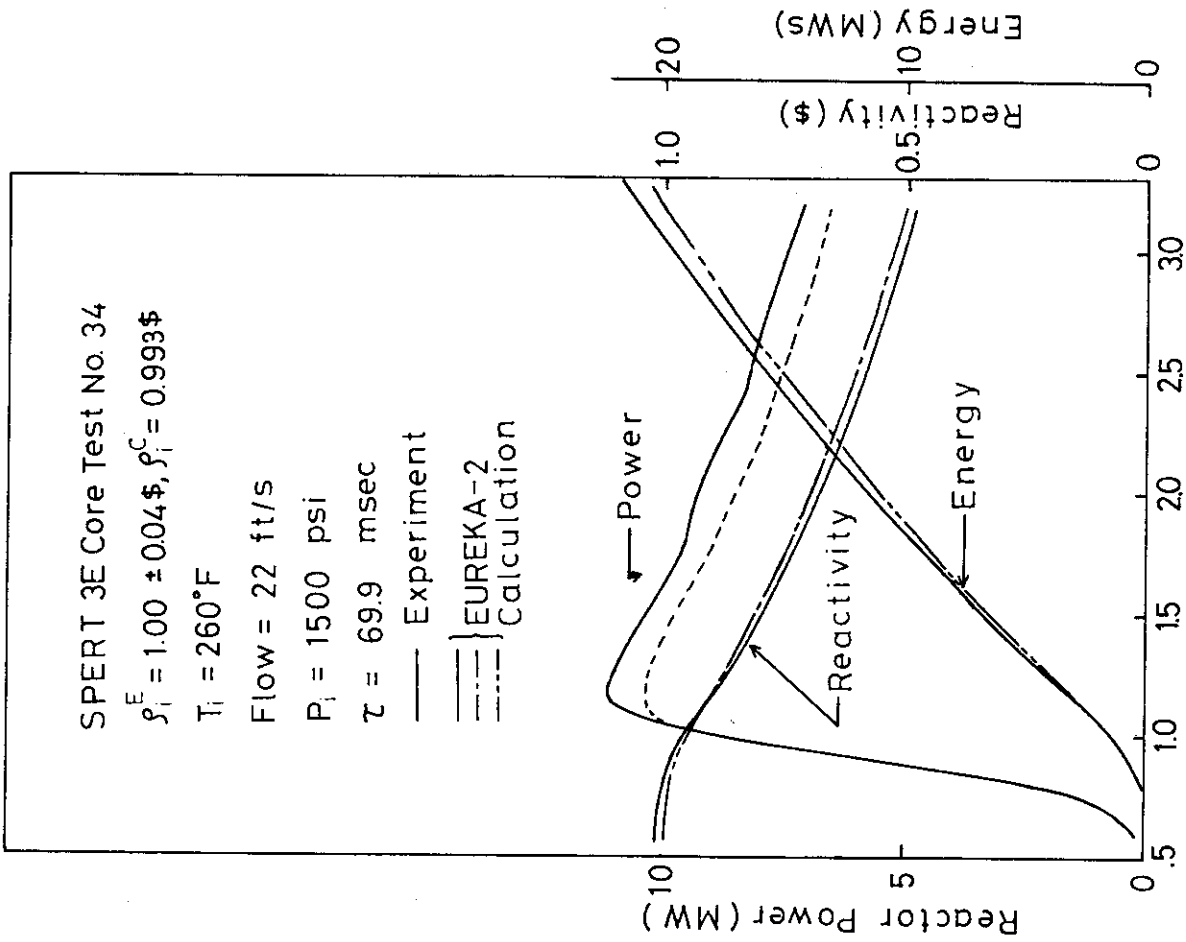

Fig. B.8 SPERT 3E-Core Test No. 34

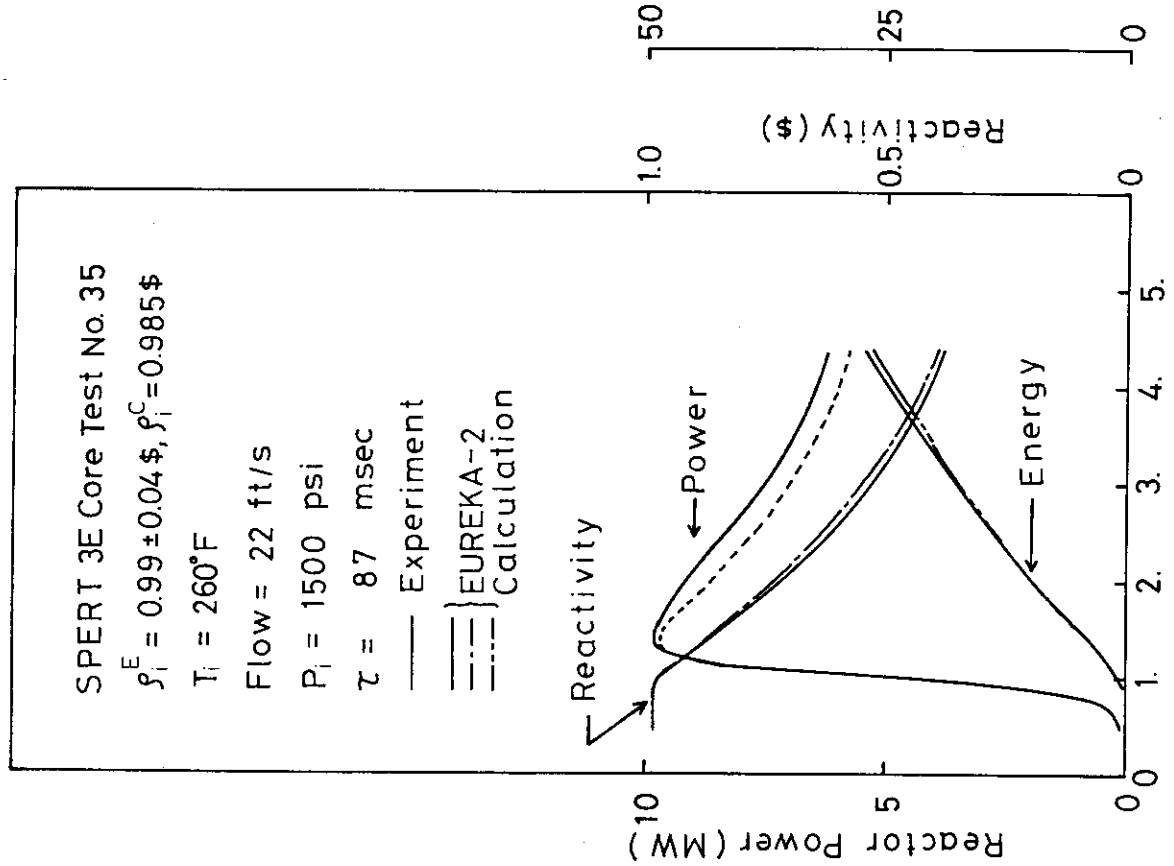

Fig. B.7 SPERT 3E-Core Test No. 35

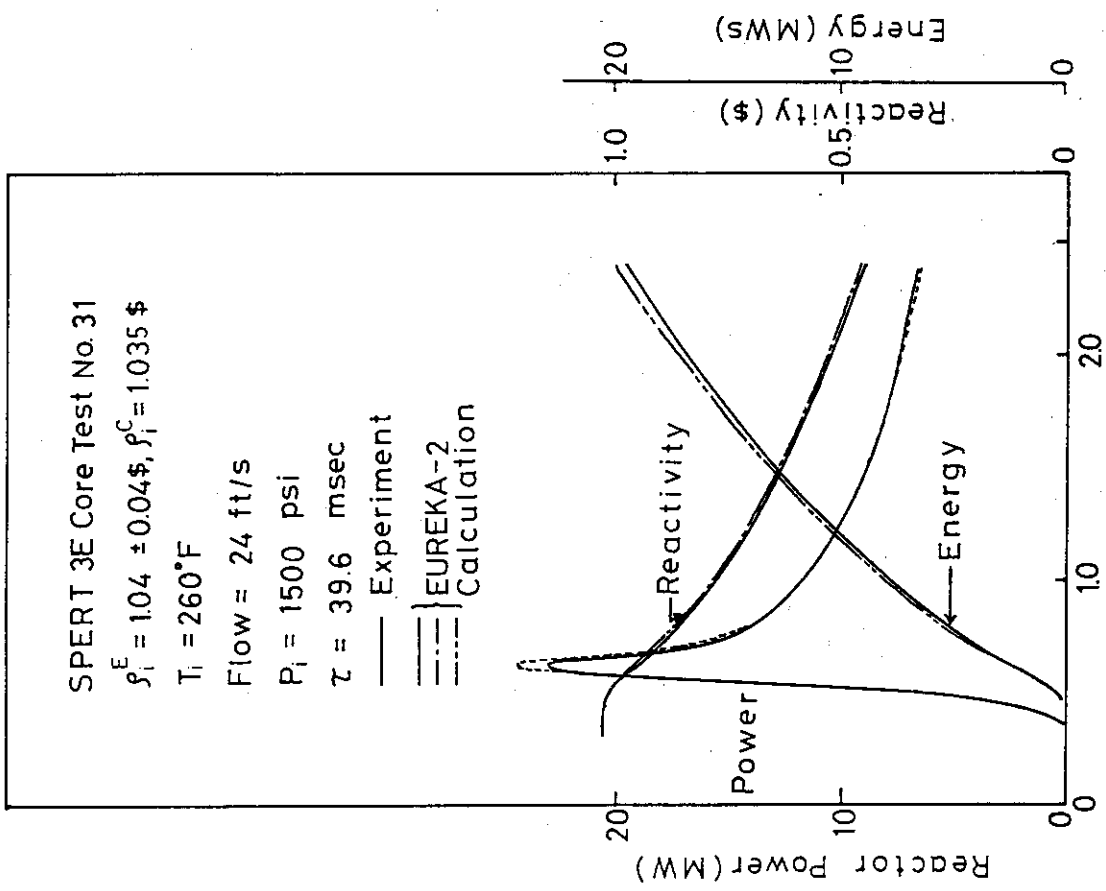

Fig. B.10 SPERT 3E-Core Test No. 31

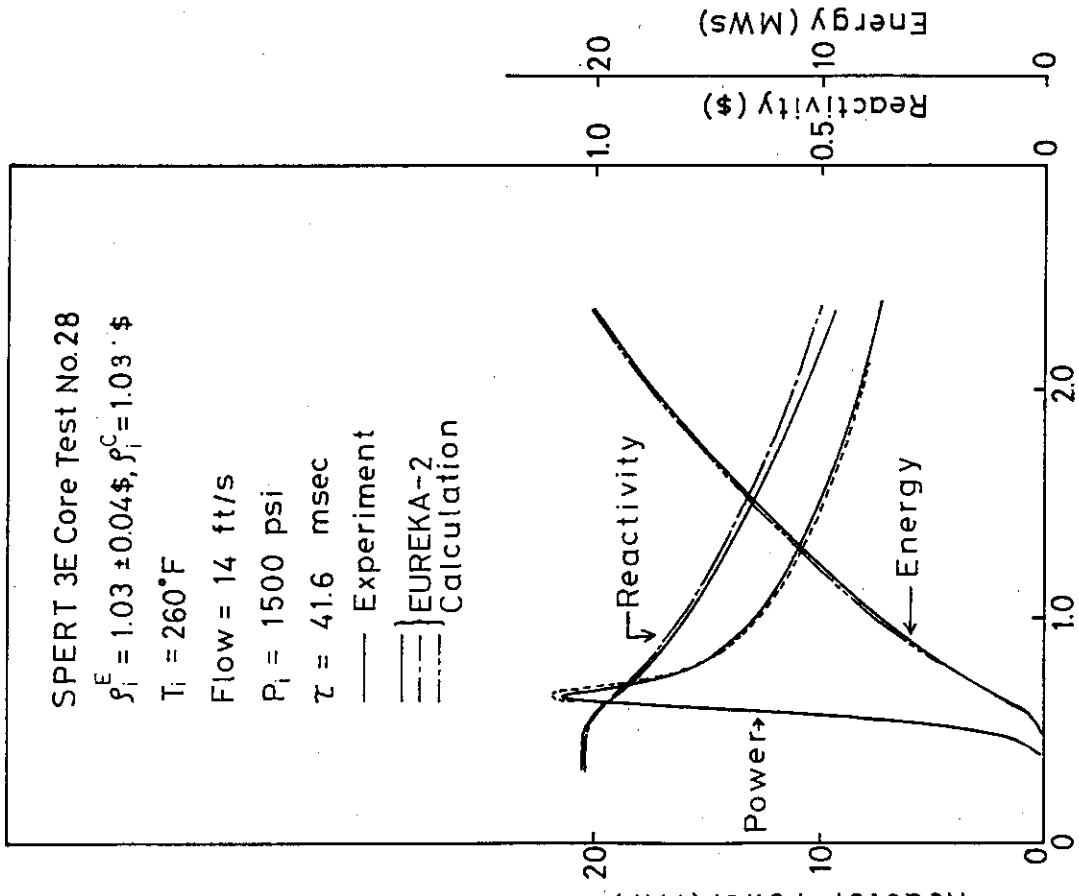

Fig. B.9 SPERT 3E-Core Test No. 28

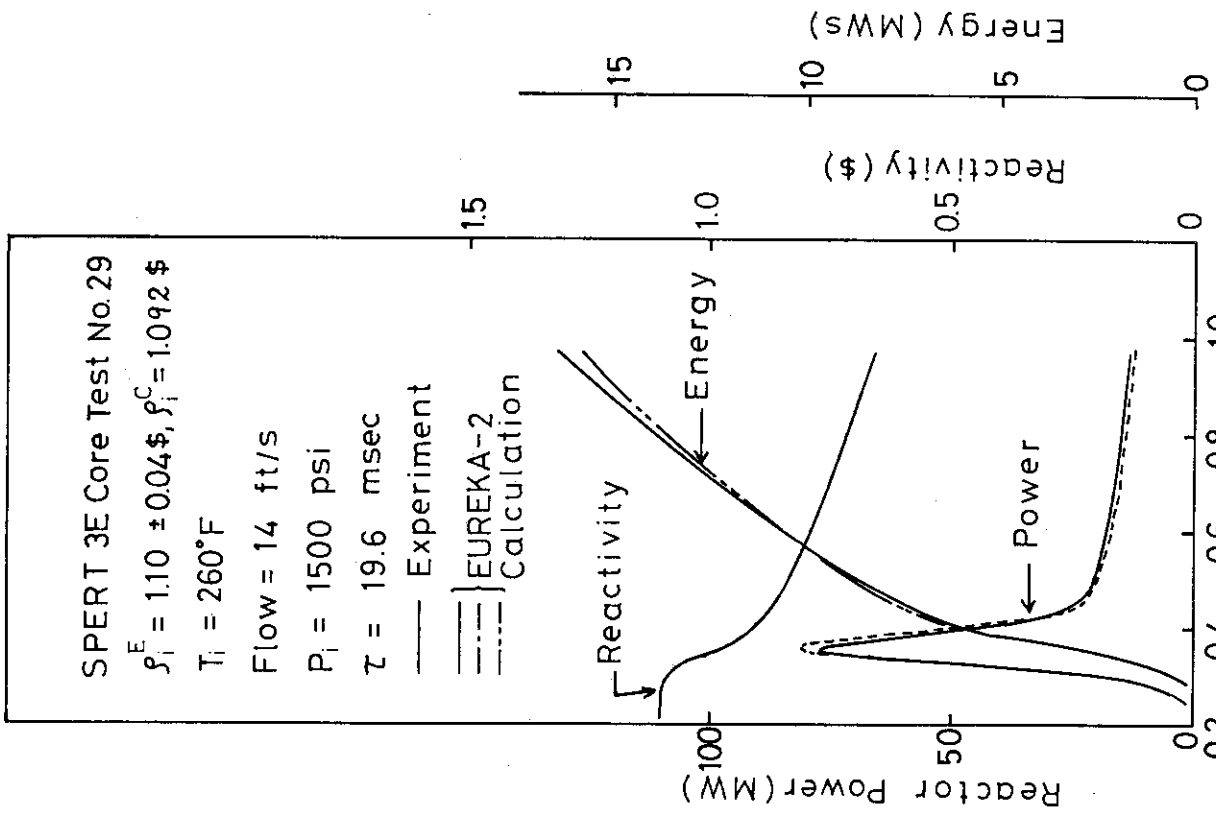

Fig. B.12 SPERT 3E-Core Test No. 29

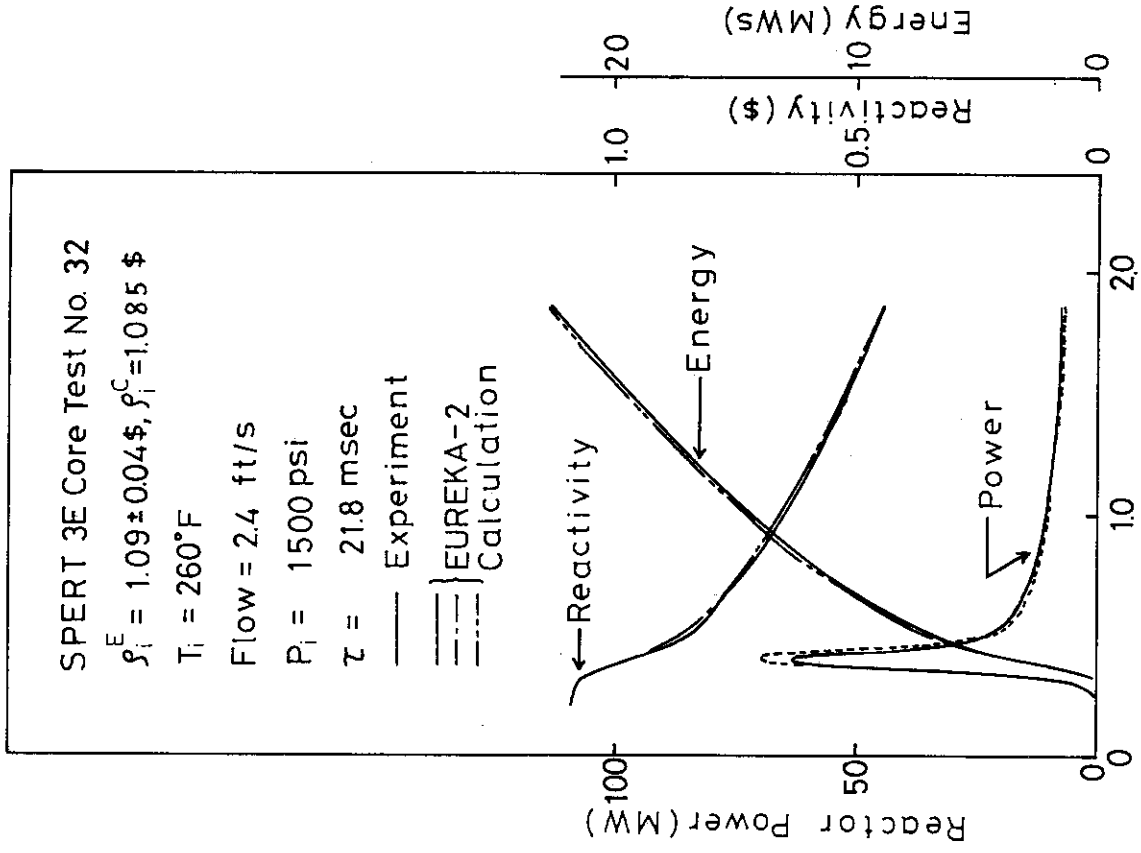

Fig. B.11 SPERT 3E-Core Test No. 32

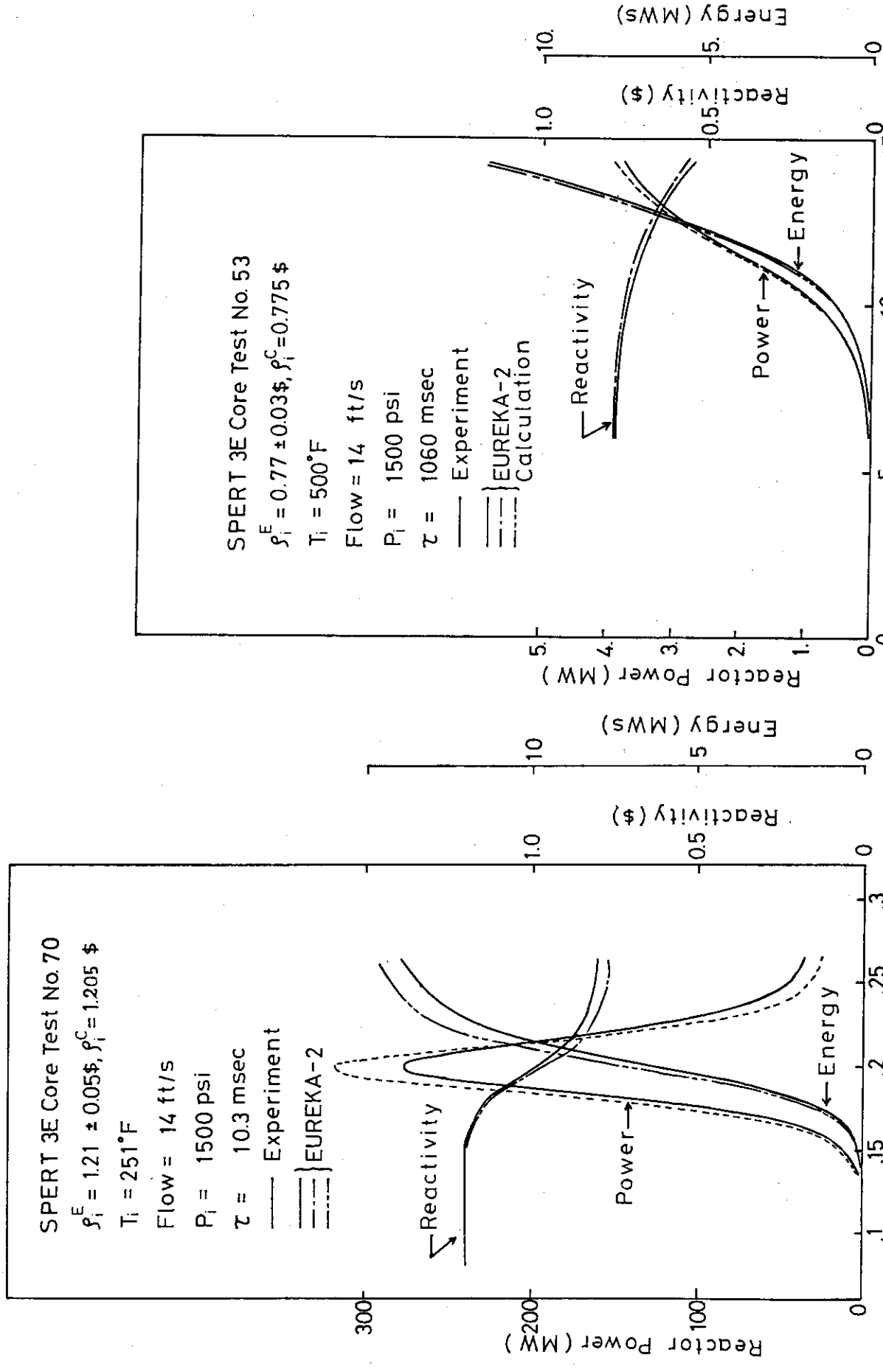

Fig. B.13 SPERT 3E-Core Test No. 70

Fig. B.14 SPERT 3E-Core Test No. 53

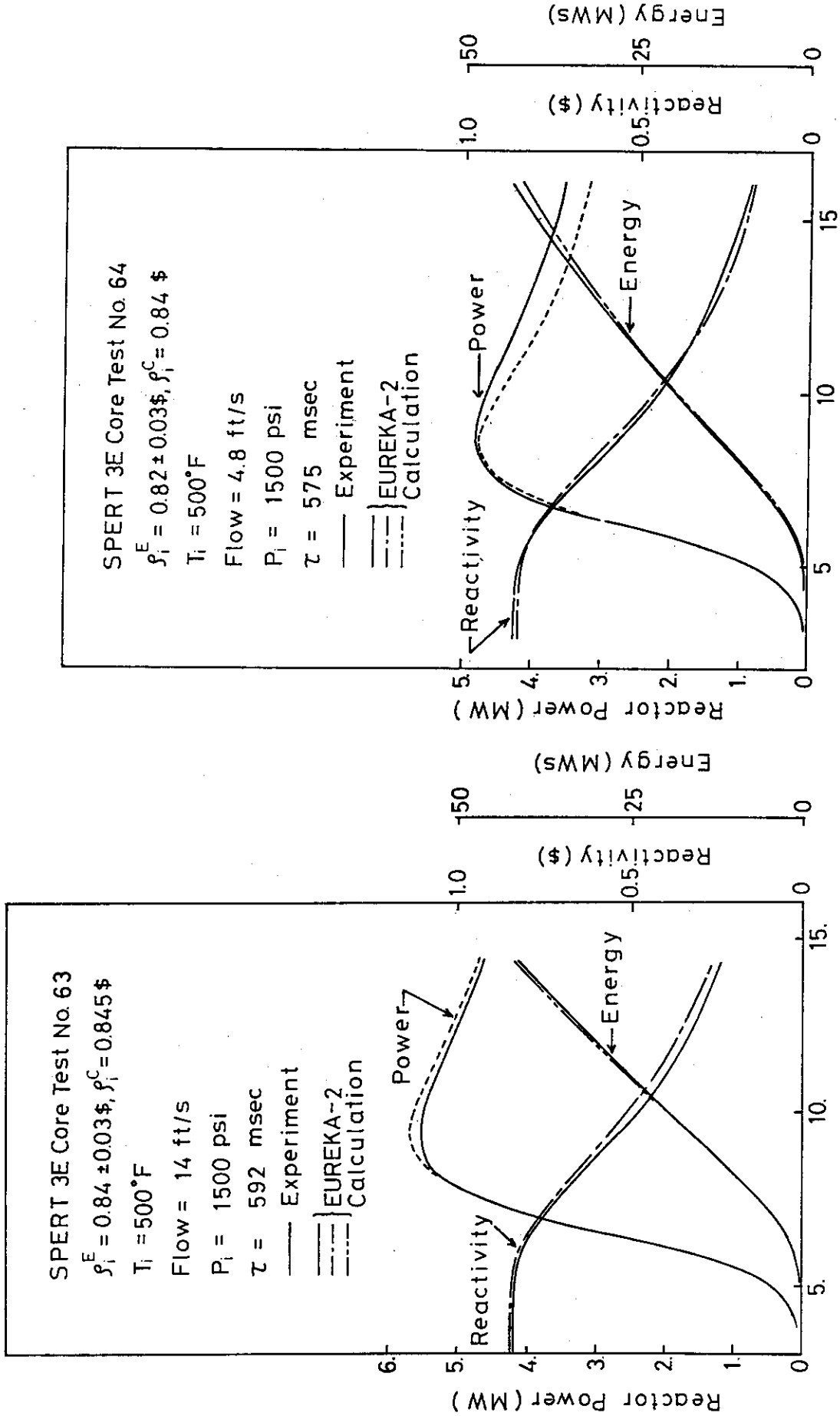

Fig. B.15 SPERT 3E-Core Test No. 63

Fig. B.16 SPERT 3E-Core Test No. 64

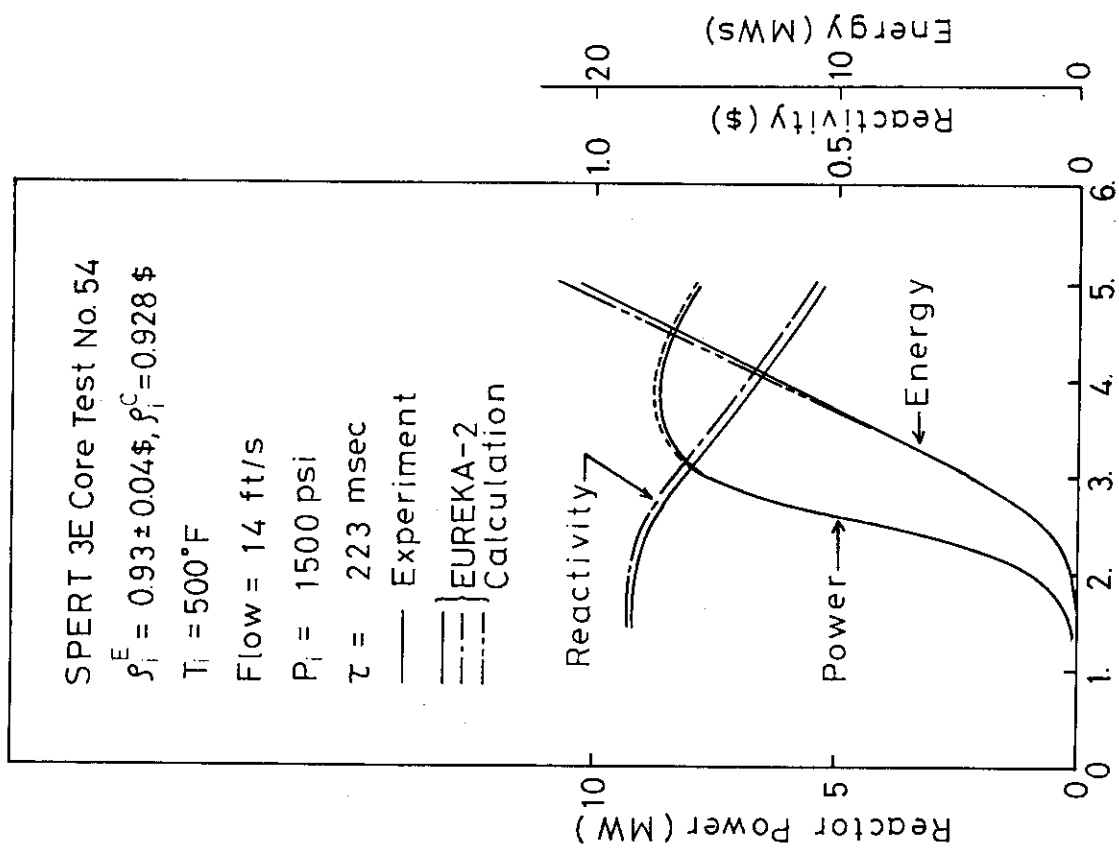

Fig. B.18 SPERT 3E-Core Test No. 54

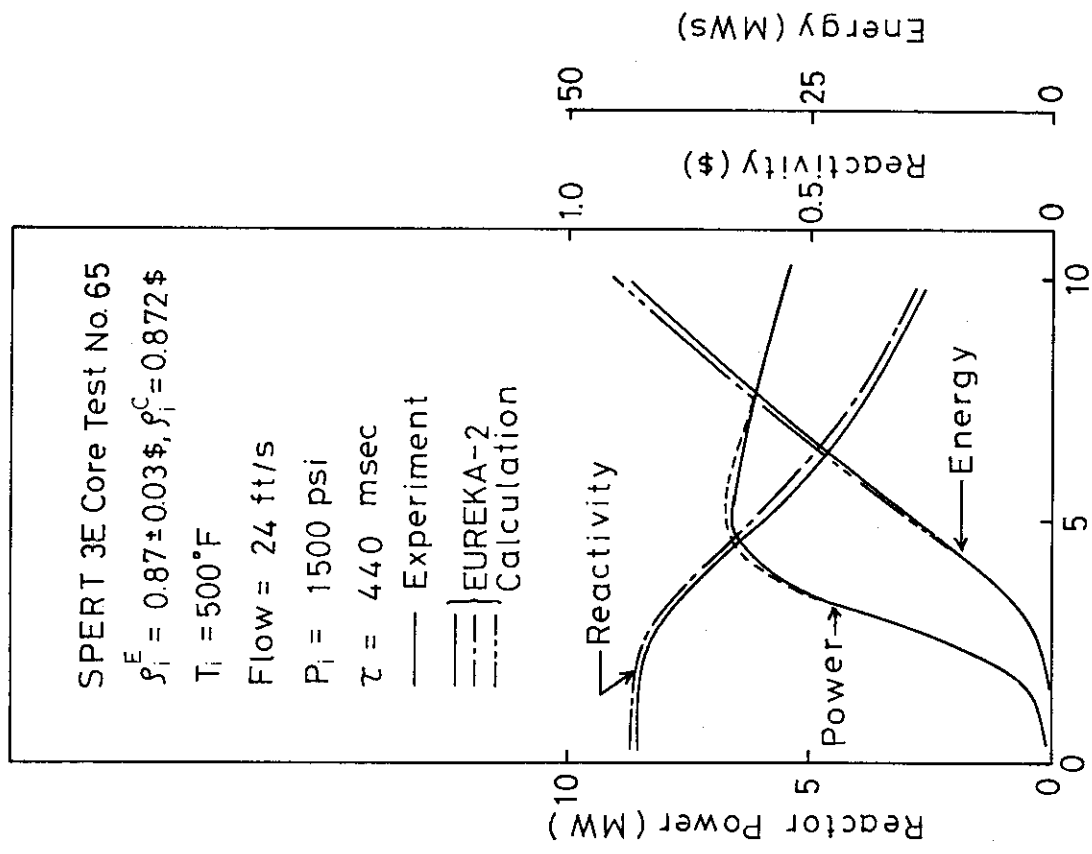

Fig. B.17 SPERT 3E-Core Test No. 65

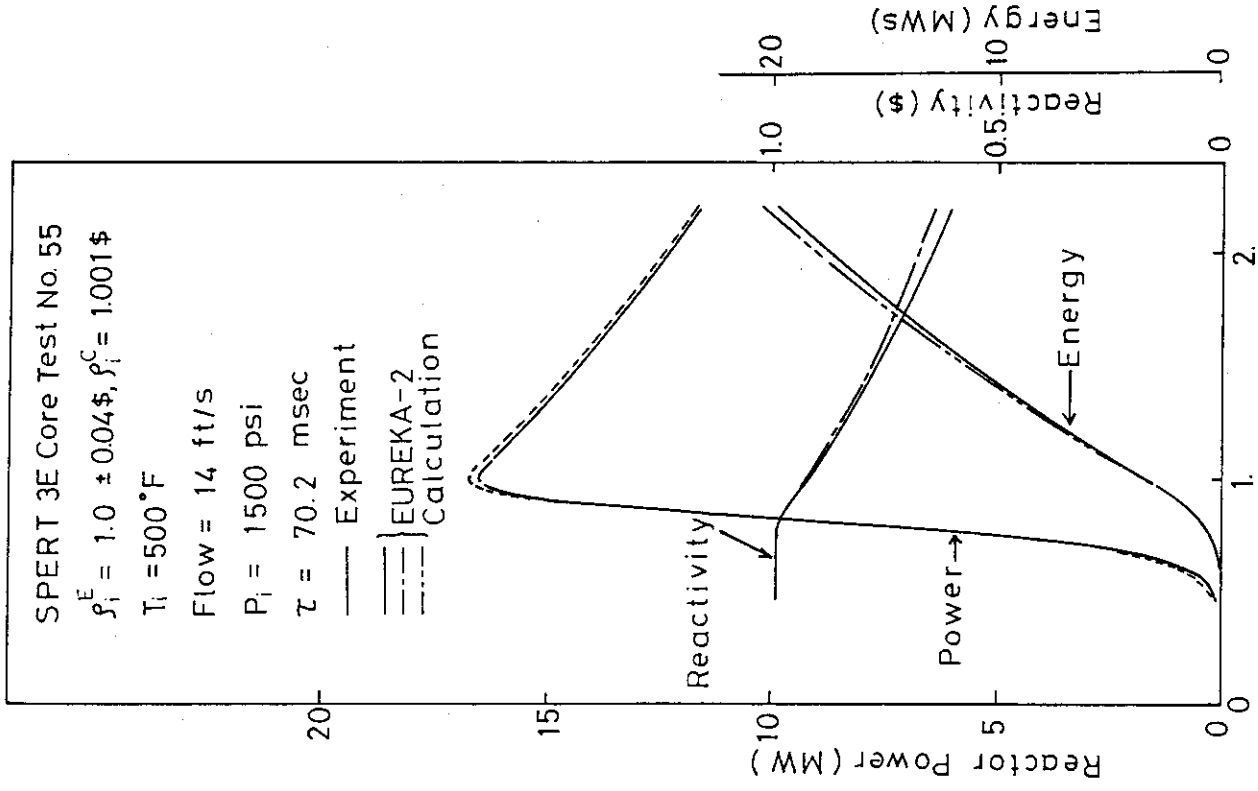

Fig. B.19 SPERT 3E-Core Test No. 55

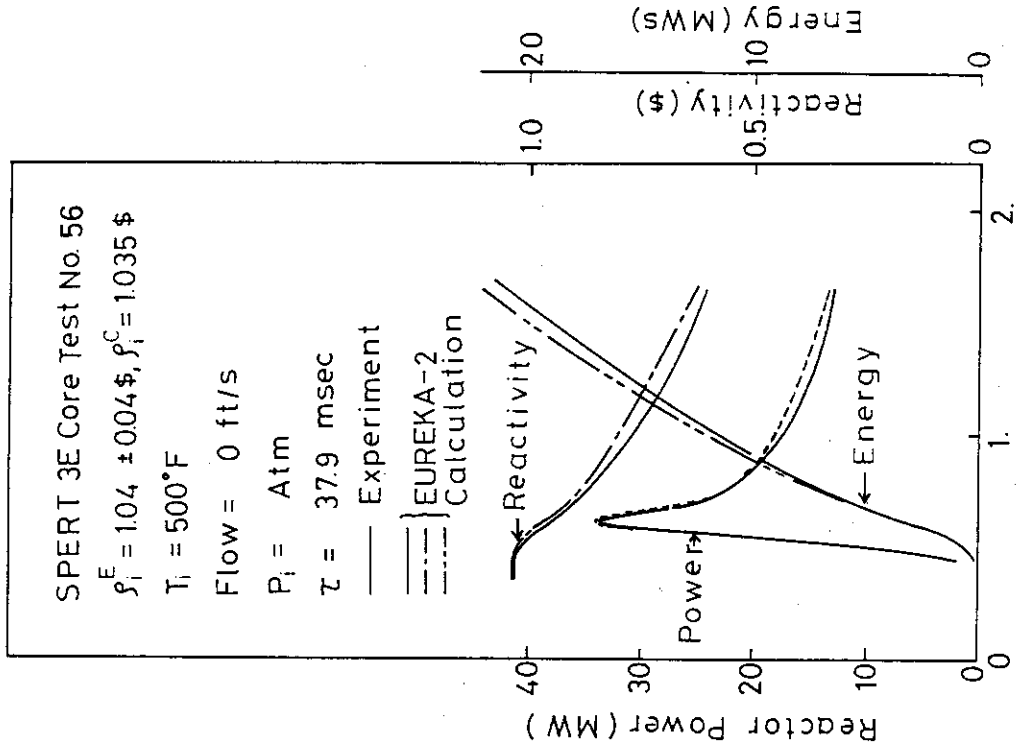

Fig. B.20 SPERT 3E-Core Test No. 56

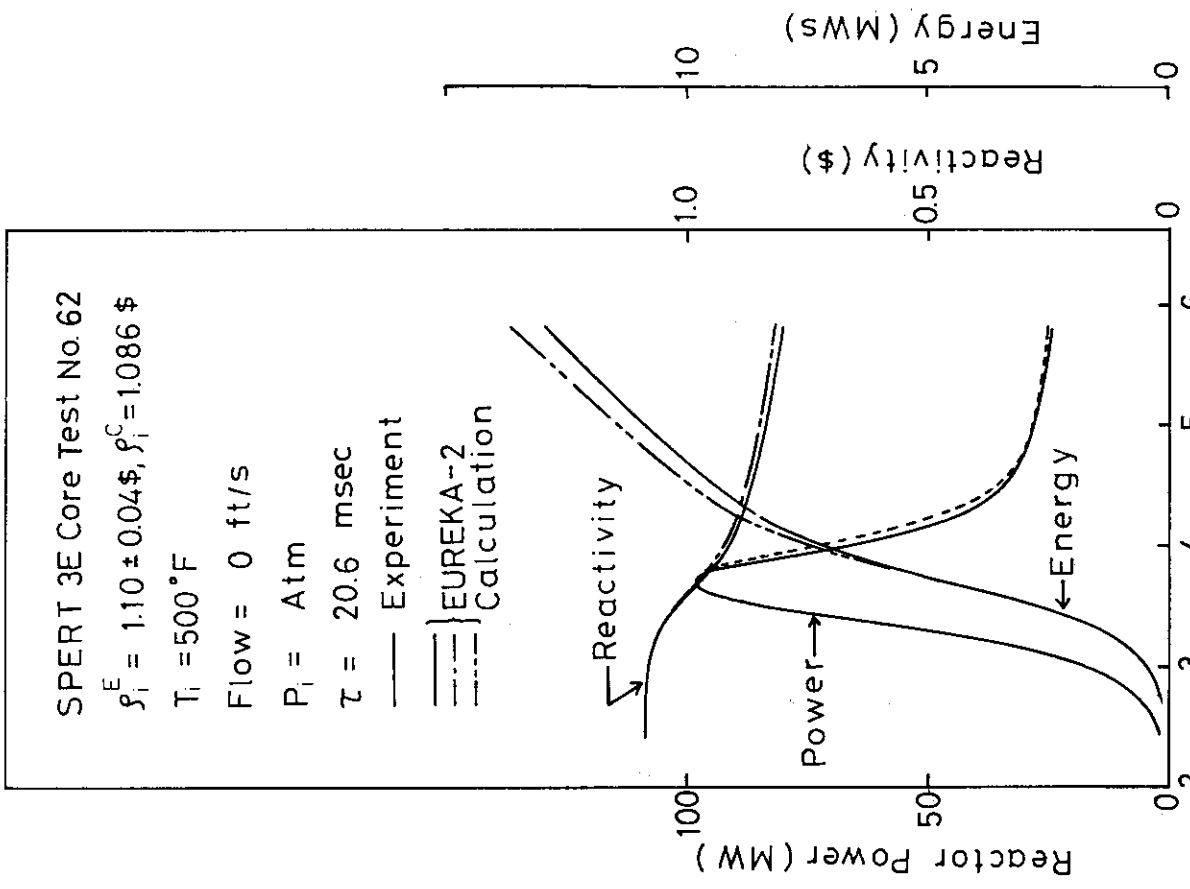

Fig. B.22 SPERT 3E-Core Test No. 62

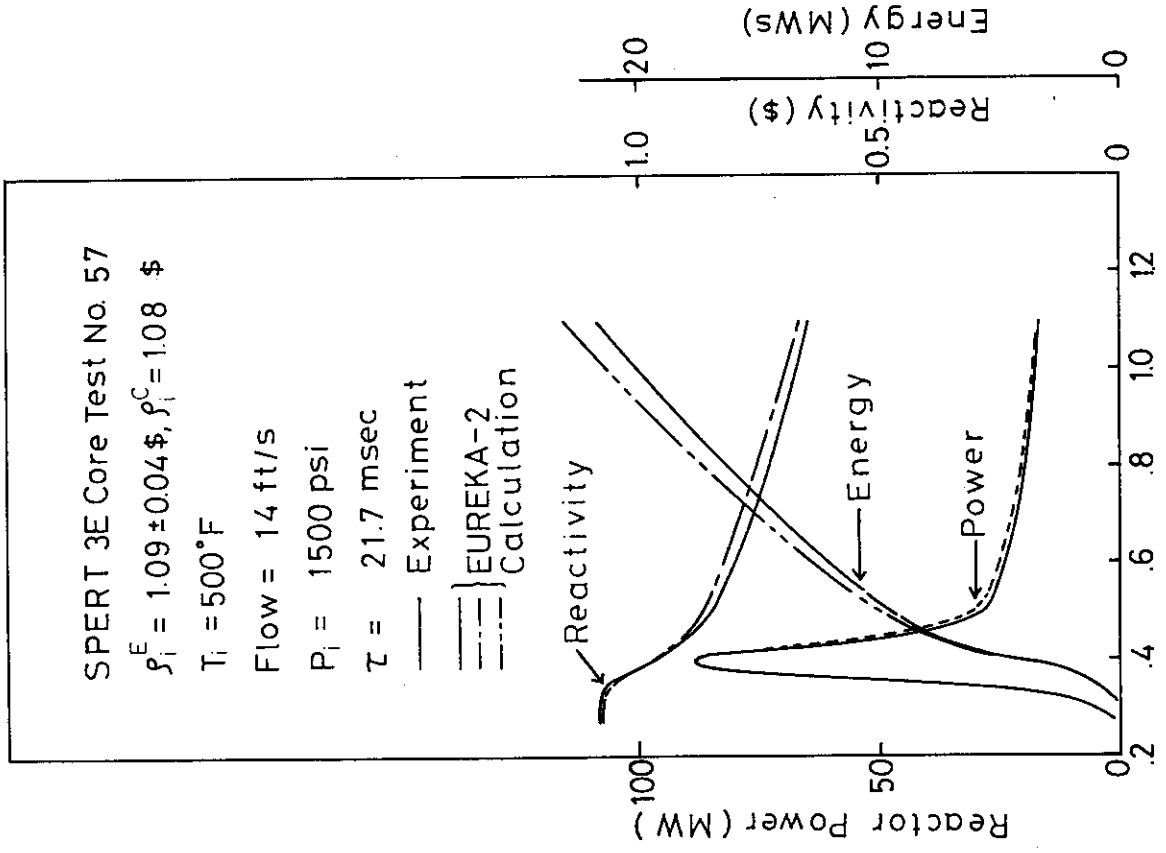

Fig. B.21 SPERT 3E-Core Test No. 57

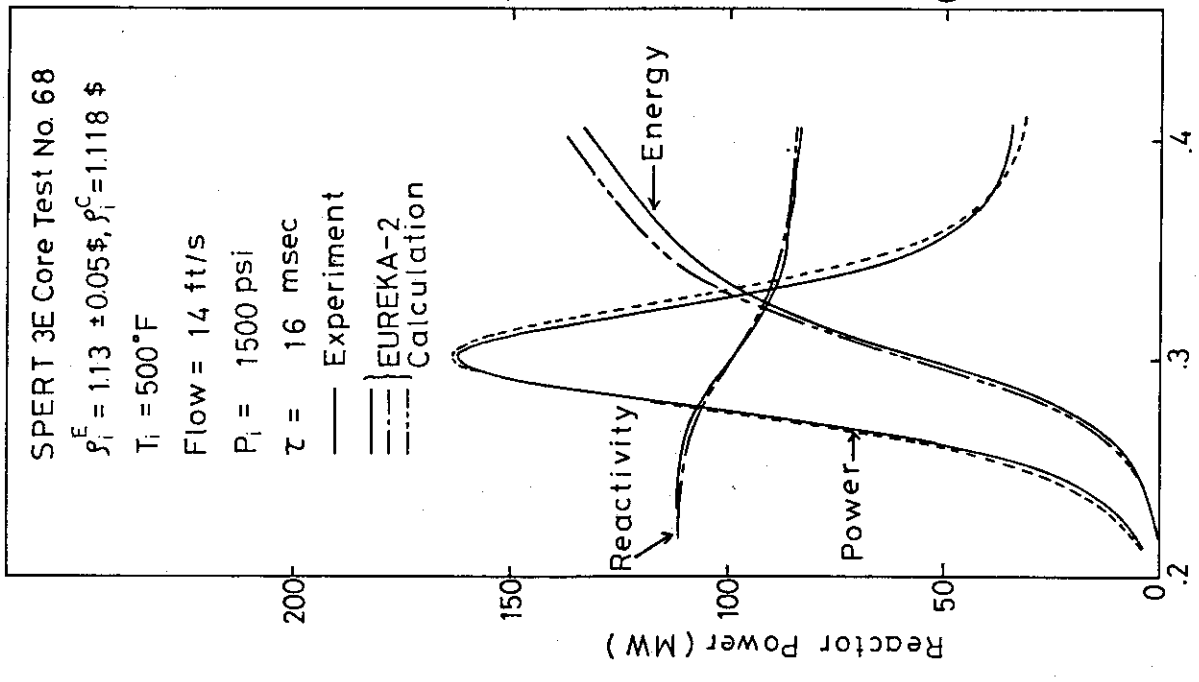

Fig. B.23 SPERT 3E-Core Test No. 68

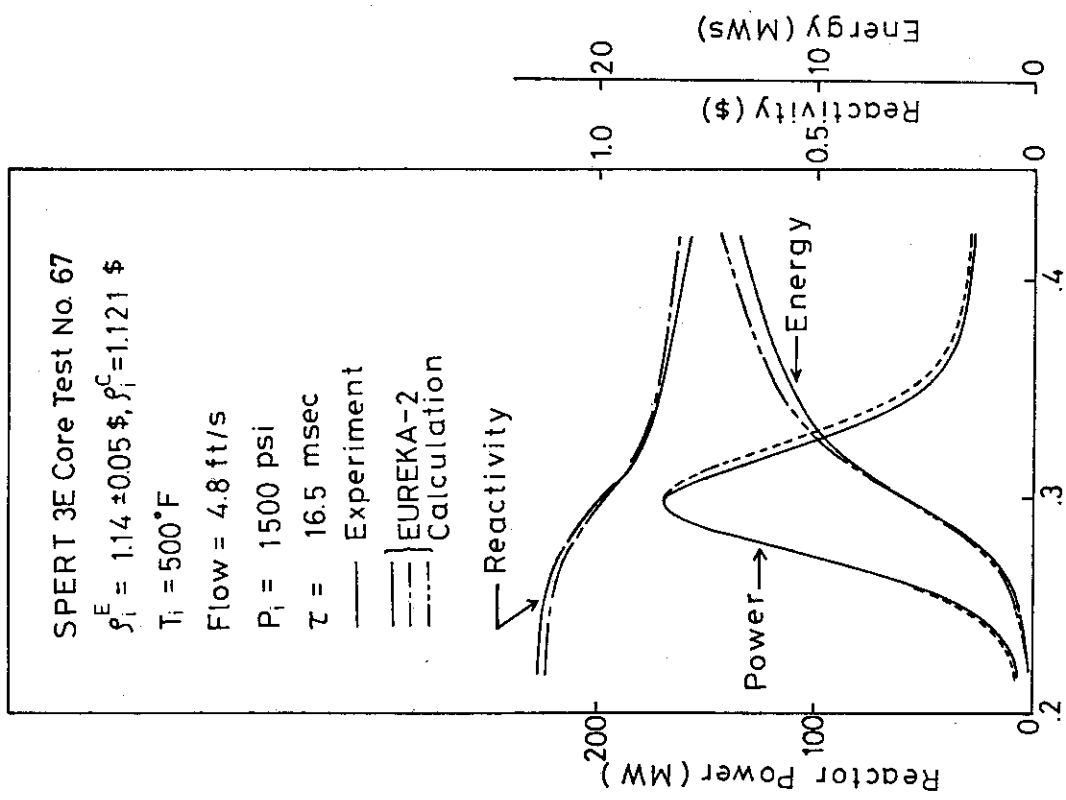

Fig. B.24 SPERT 3E-Core Test No. 67

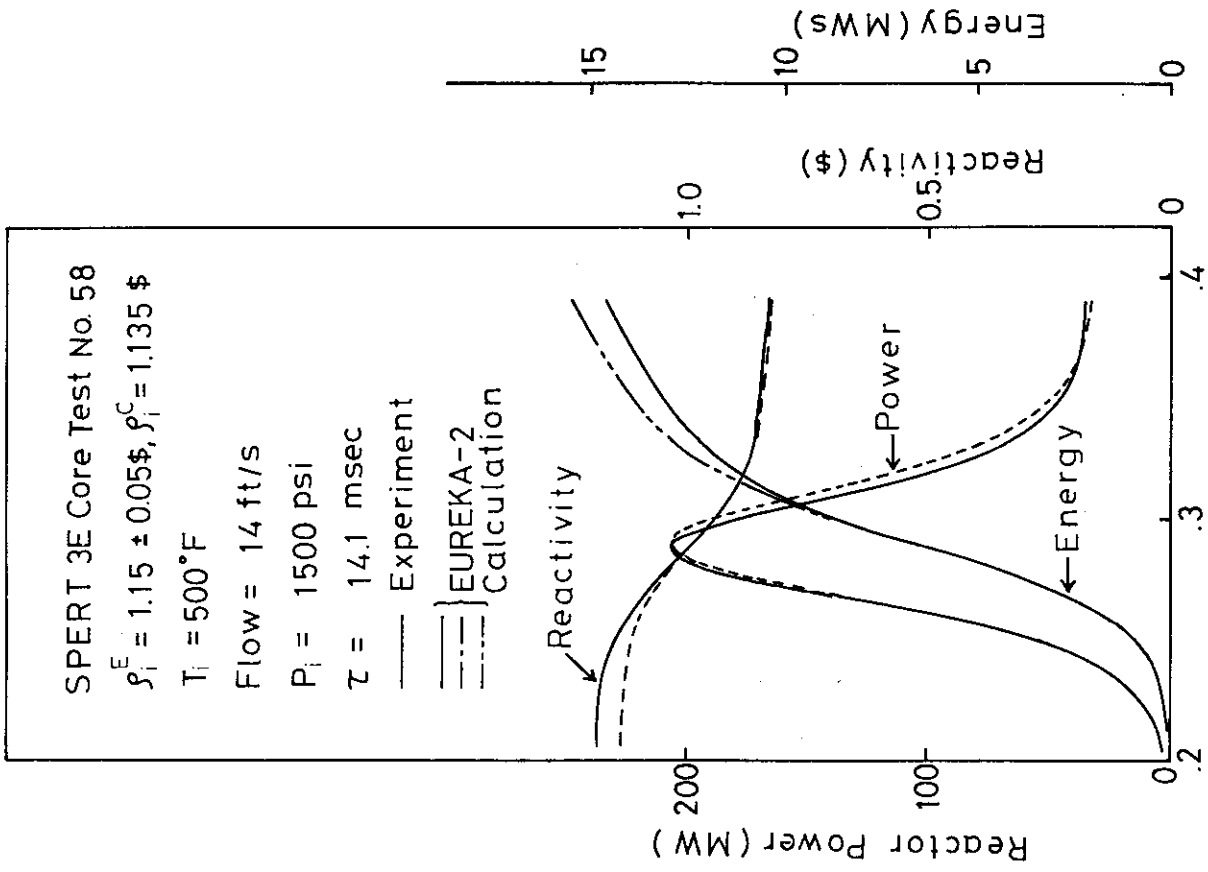

Fig. B.26 SPERT 3E-Core Test No. 58

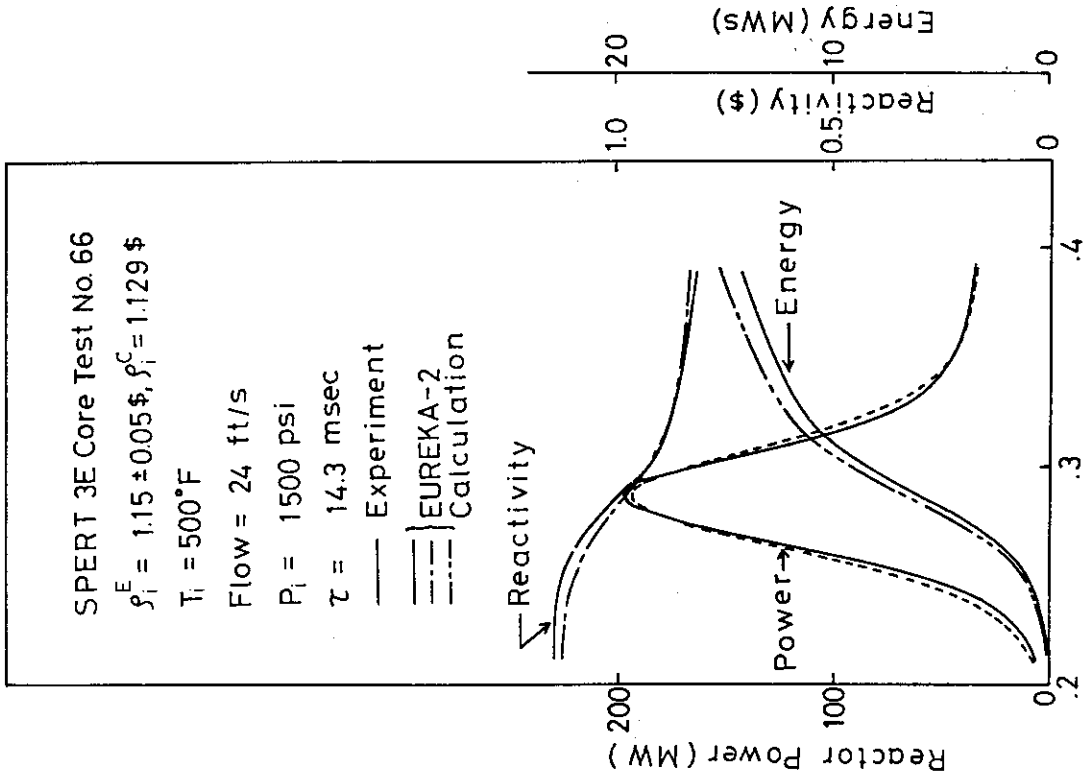

Fig. B.25 SPERT 3E-Core Test No. 66

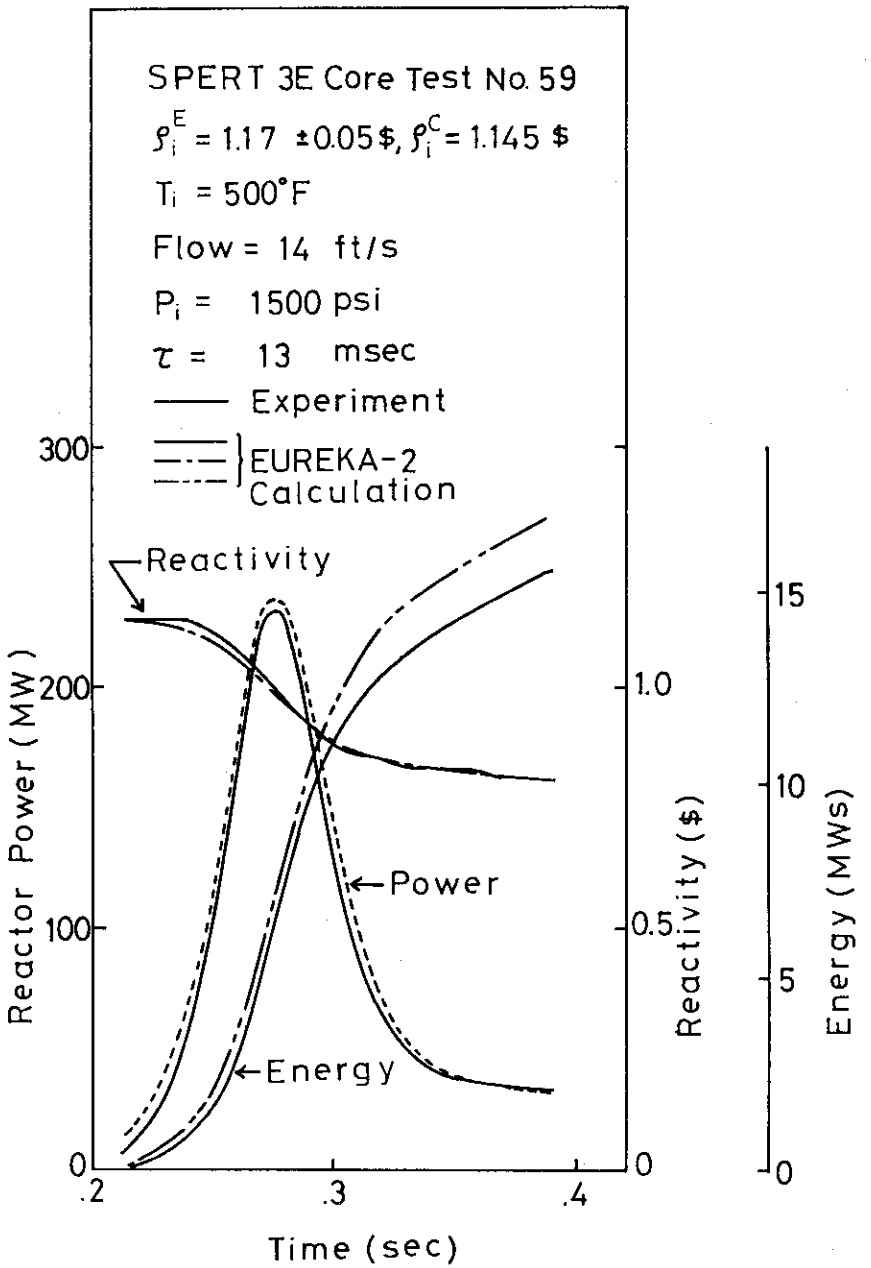

Fig. B.27 SPERT 3E-Core Test No. 59

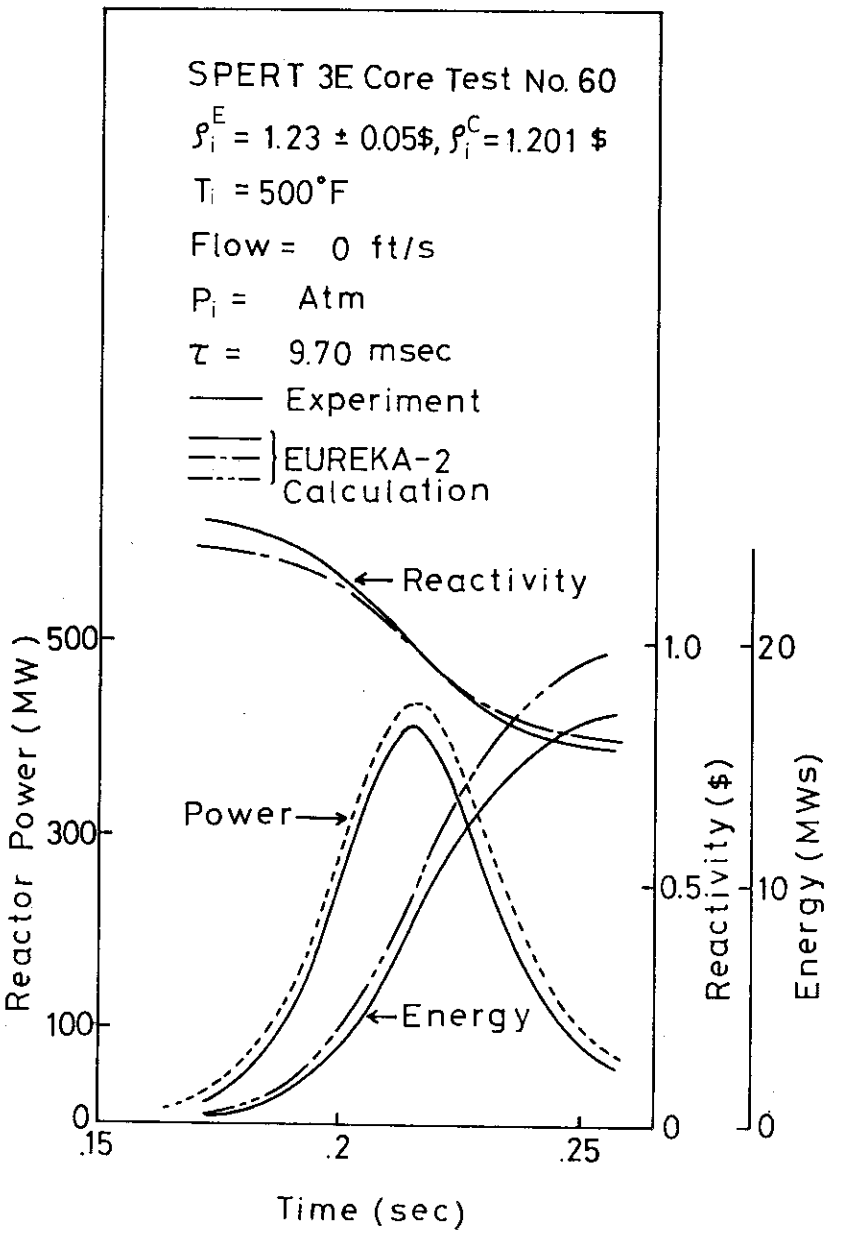

Fig. B.28 SPERT 3E-Core Test No. 60

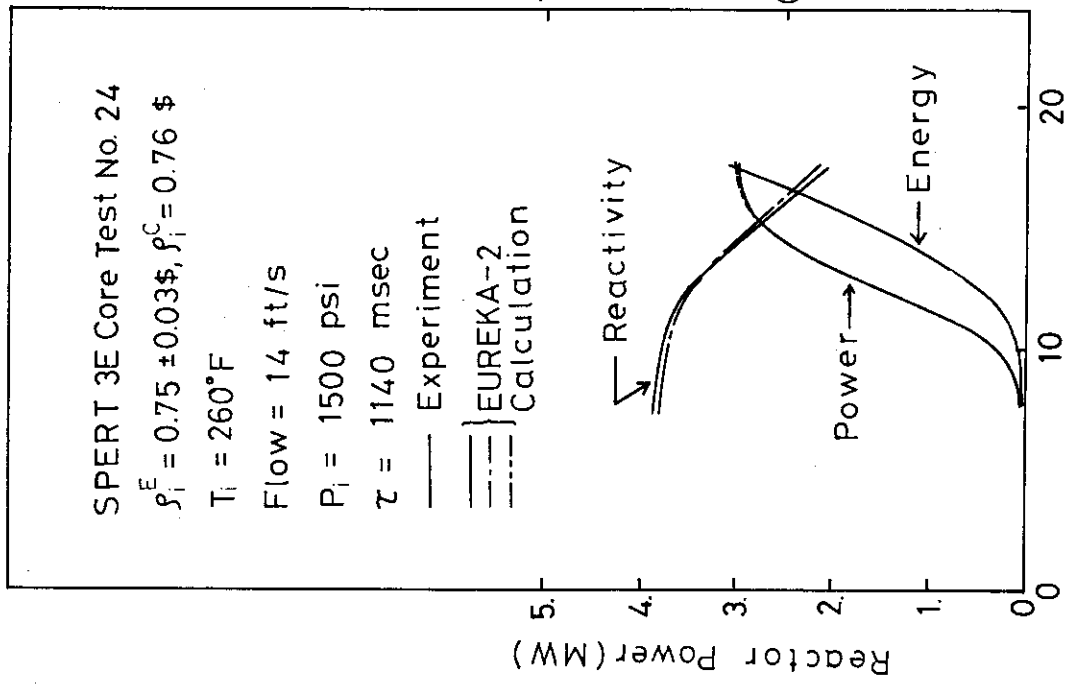

Fig. B.29 SPERT 3E-Core Test No. 24

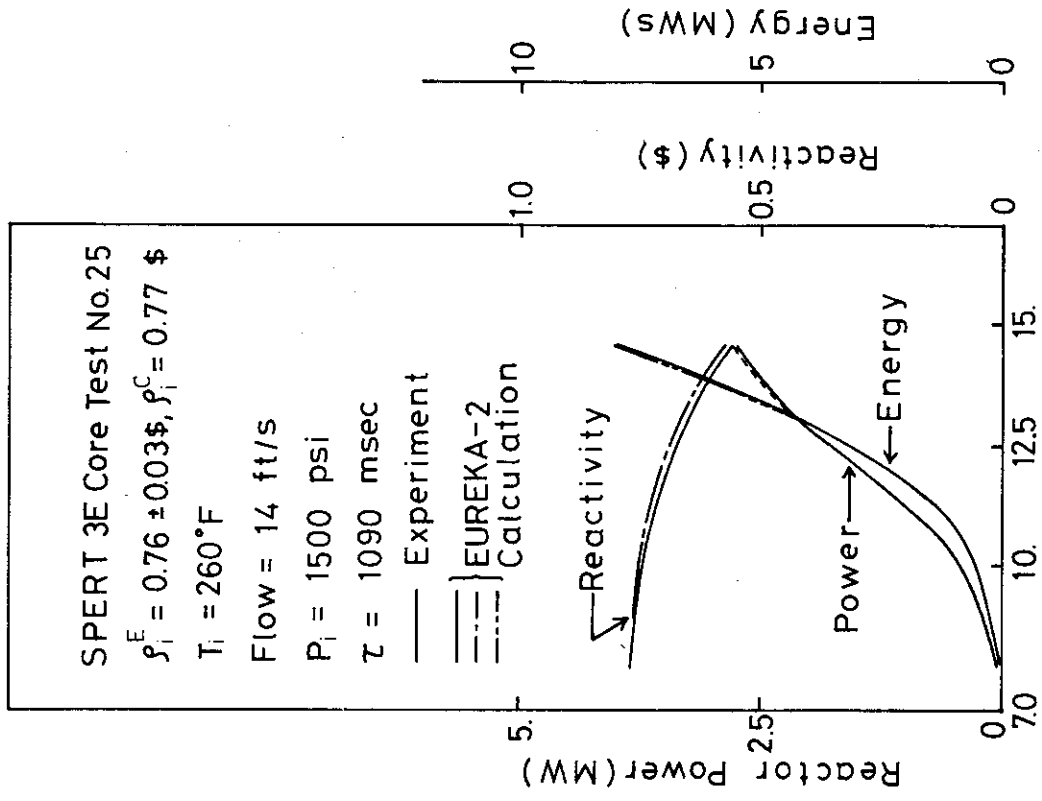

Fig. B.30 SPERT 3E-Core Test No. 25

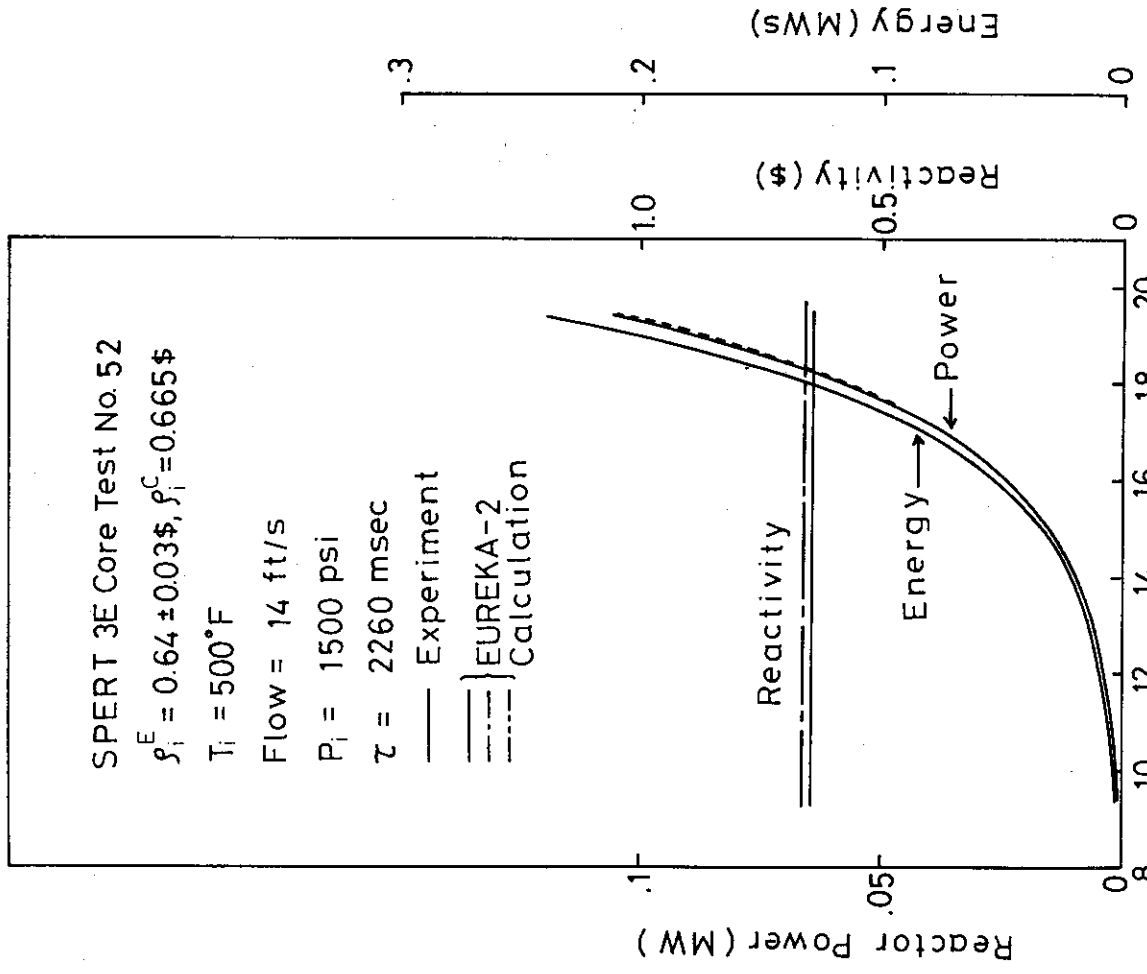

Fig. B.31 SPERT 3E-Core Test No. 52

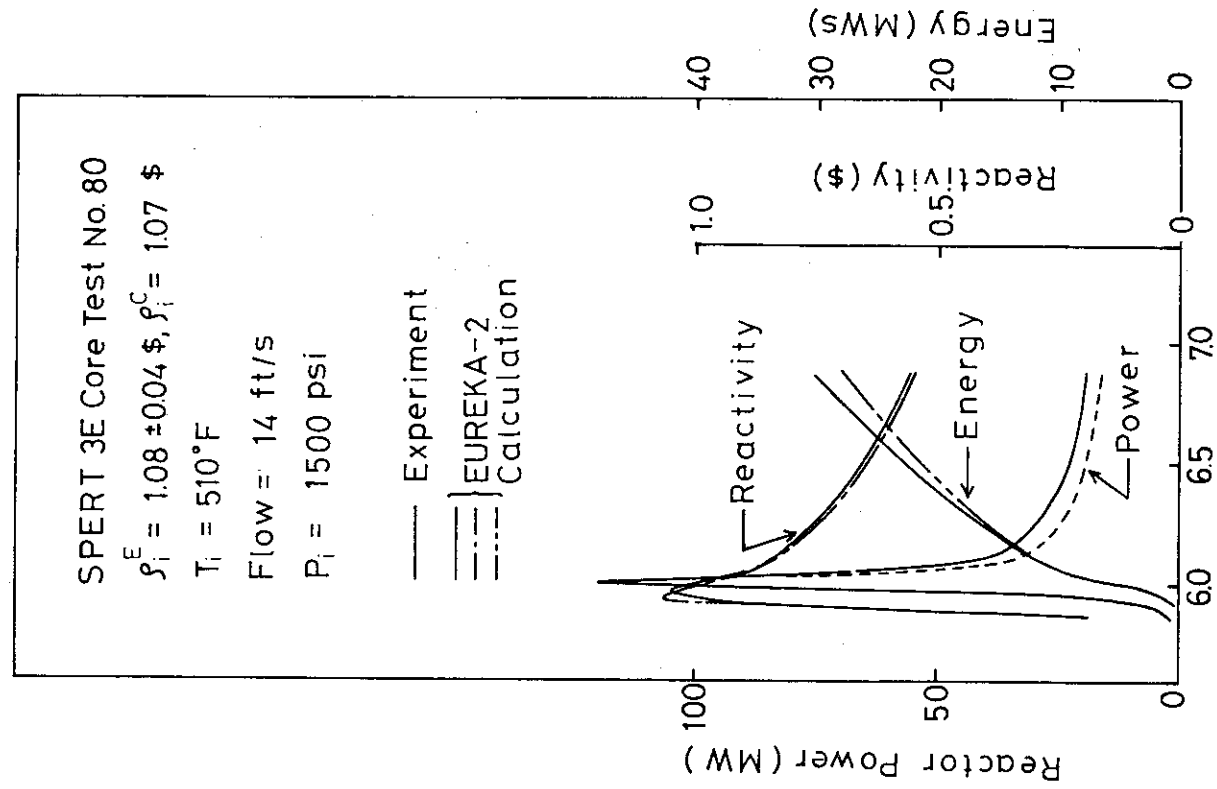

Fig. C.2 SPERT 3E-Core Test No. 80

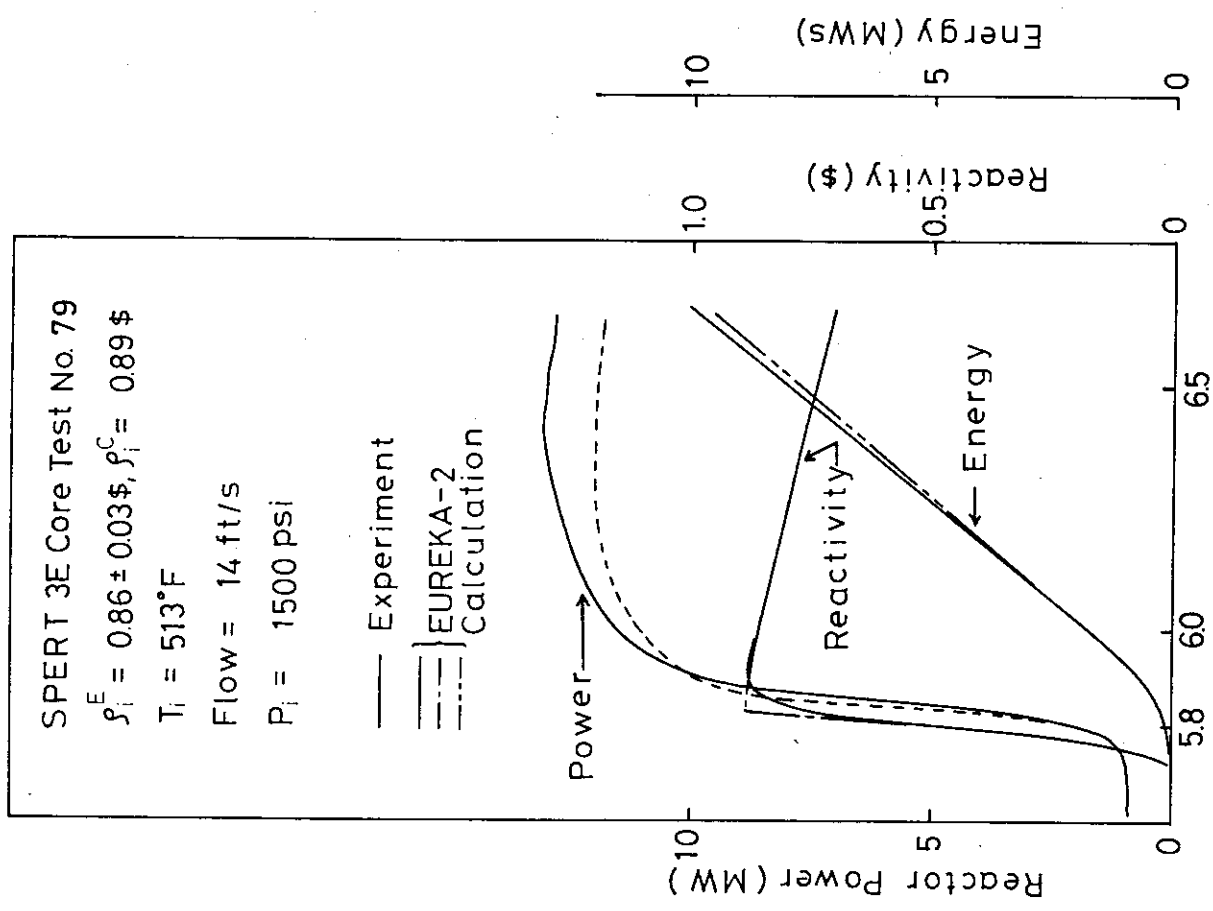

Fig. C.1 SPERT 3E-Core Test No. 79

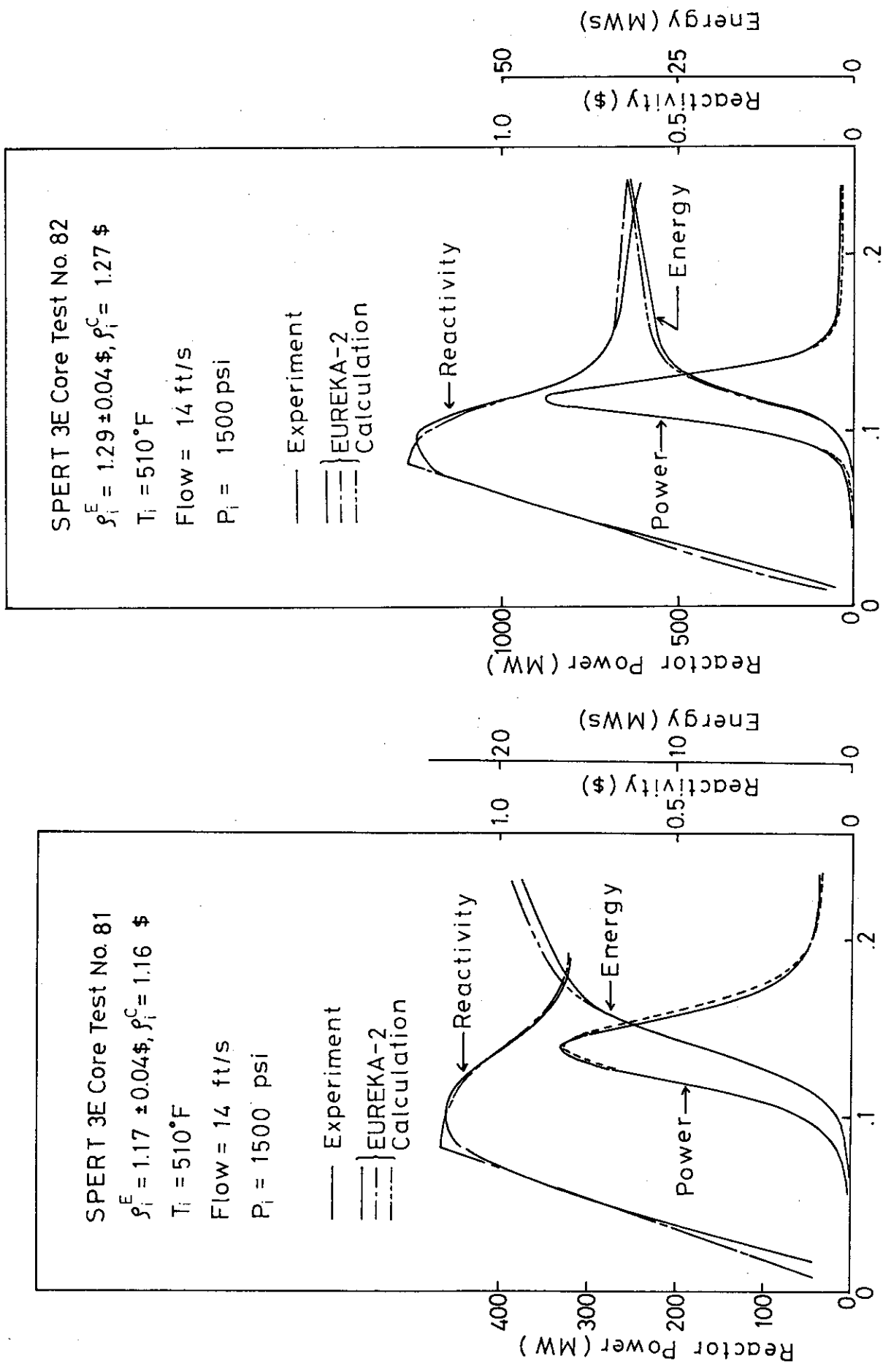

Fig. C.4 SPERT 3E-Core Test No. 82

Fig. C.3 SPERT 3E-Core Test No. 81

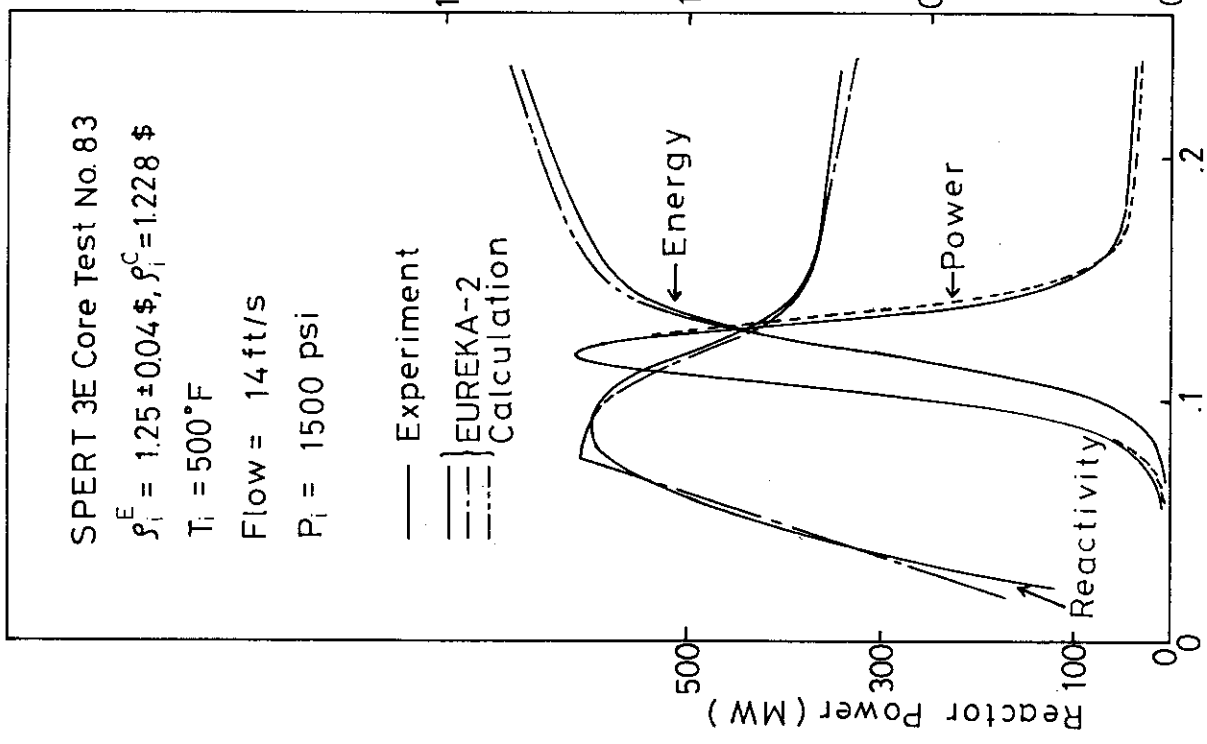

Fig. C.5 SPERT 3E-Core Test No. 83

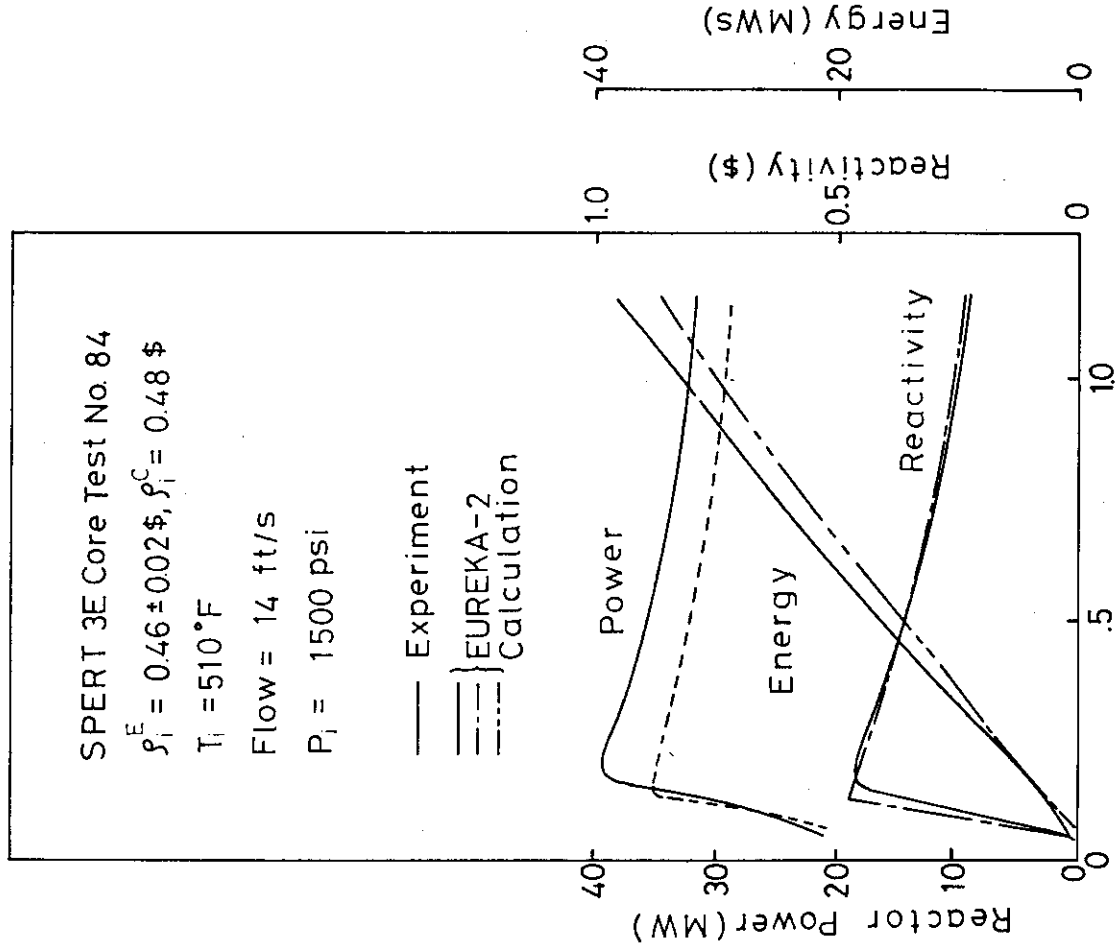

Fig. C.6 SPERT 3E-Core Test No. 84

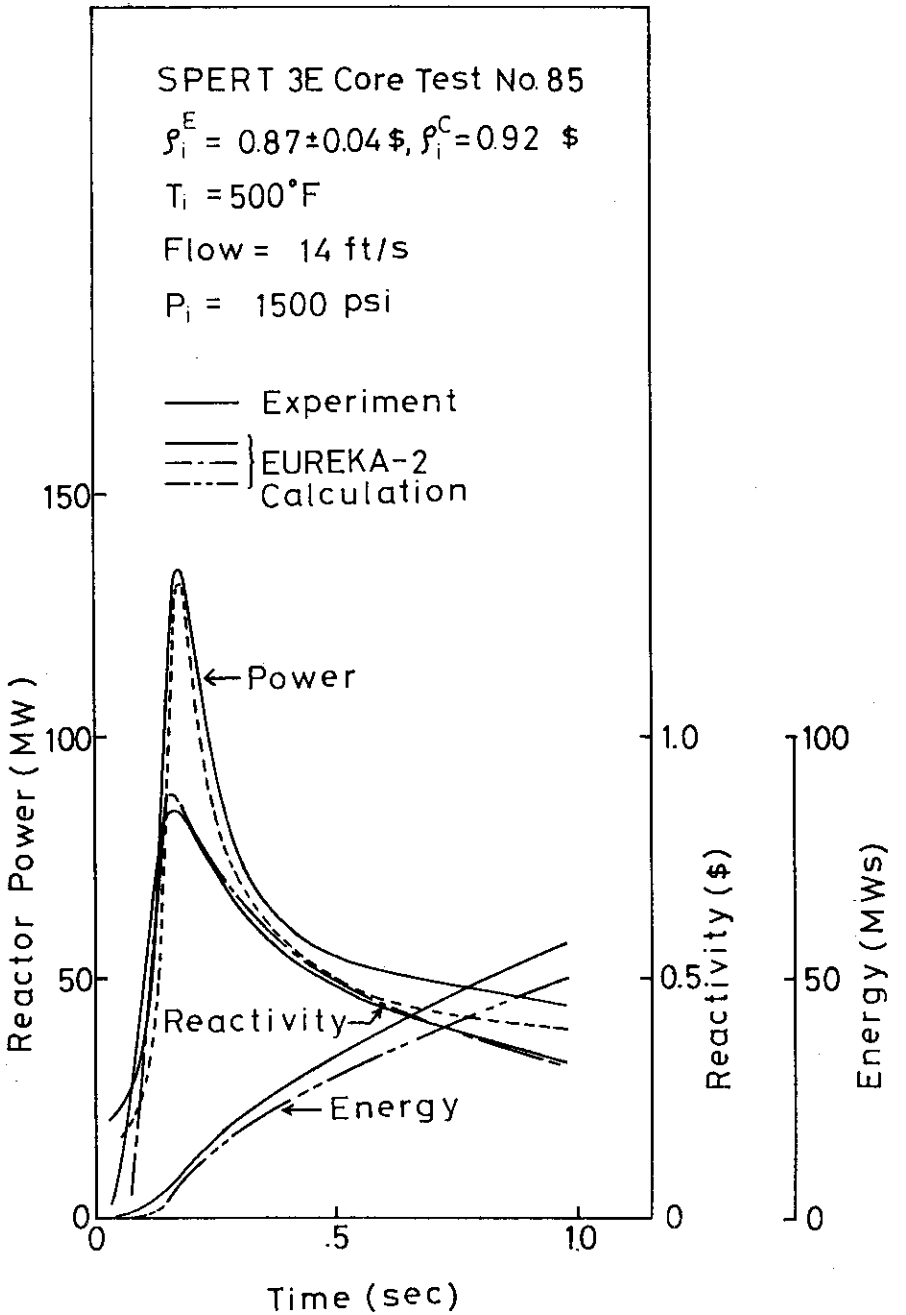

Fig. C.7 SPERT 3E-Core Test No. 85

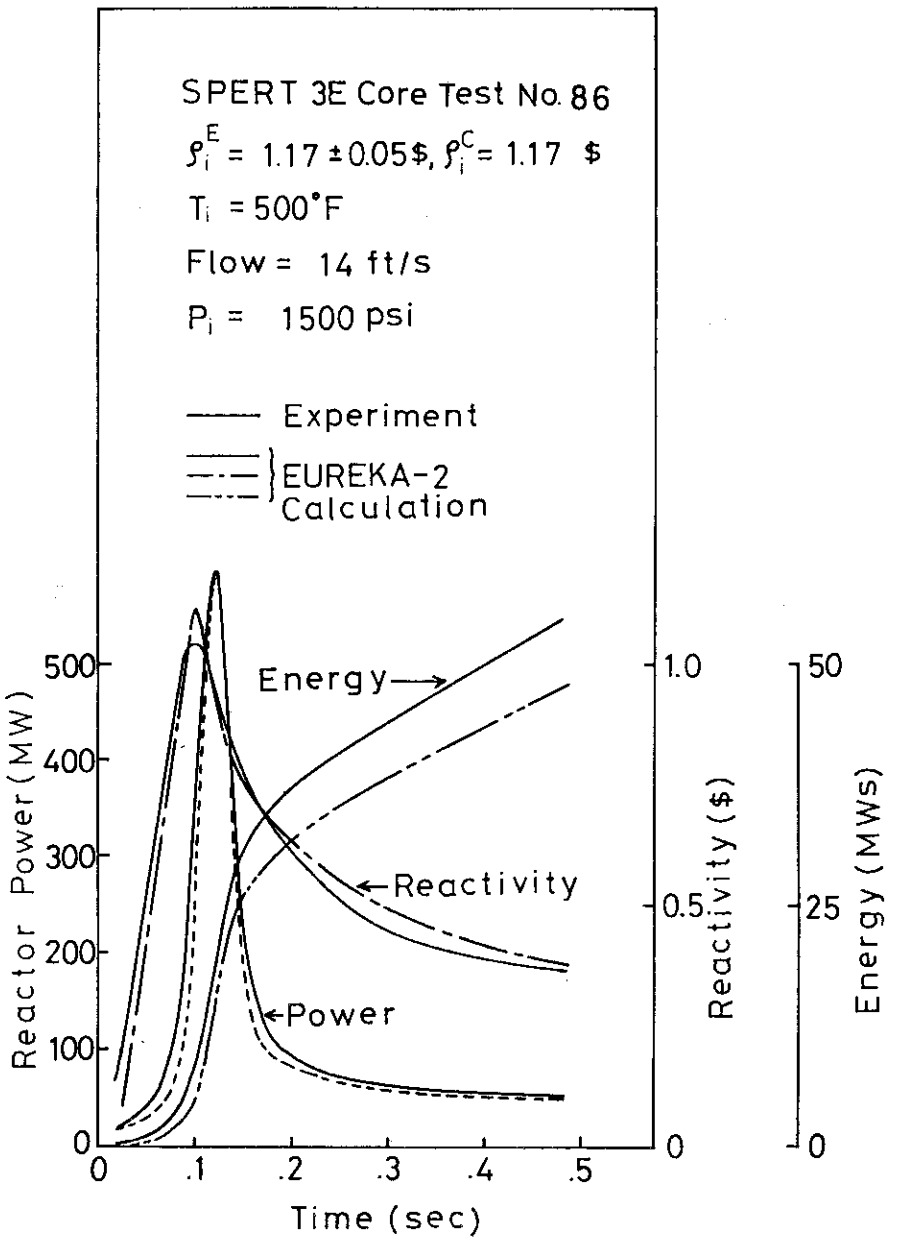

Fig. C.8 SPERT 3E-Core Test No. 86